UNIVERSITY OF CALIFORNIA SAN DIEGO

# Initial stages of olfactory processing and neuromodulation in *Drosophila melanogaster*

A dissertation submitted in partial satisfaction of the
requirements for the degree Doctor of Philosophy

in

Biology

by

Ye Zhang

Committee in charge:

Professor Chih-Ying Su, Chair
Professor Kenta Asahina
Professor William Joiner
Professor Tatyana Sharpee
Professor Jing Wang

2020

The Dissertation of Ye Zhang is approved, and it is acceptable in quality and form for publication on microfilm and electronically:

_____

_____

_____

_____

_____

Chair

University of California San Diego

2020

TABLE OF CONTENTS

LIST OF FIGURES

LIST OF TABLES

ACKNOWLEDGEMENTS

I thank Chih-Ying for her enthusiasm of science and her mentorship. She is a dedicated scientist with great ability, a passionate and selfless mentor, and a caring friend. My PhD career has been such an enjoyable journey in the Su lab, and working with her has always been challenging yet rewarding. I thank Chih-Ying for teaching me the technical skills, enhancing my presentation and writing skills, as well as pushing me to think critically and logically. She has set great examples for me and has motivated me to grow into a better scientist. Most of all, I thank her for providing a home-like work environment in her lab, and allowing me to bring in many of my personalities. I also thank my committee members, Kenta Asahina, Tatyana Sharpee, Jing Wang, and William Joiner for useful discussion and insight. In particular, I want to thank Jing and the Wang lab members, for providing critics and ideas during our joint lab meetings, and for sharing their reagents with me generously.

I thank the Su lab members for supporting me in the past five years. I feel very lucky to have them as my colleagues and my trustworthy friends. I want to thank Angela, for being so kind to me when I interviewed at UCSD. She was the reason why I rotated at the Su lab in the first place, and that was how everything had started. She also worked closely with me for the work presented in Chapter 2, in collaboration with the NCMIR center. I want to thank Wilmer, for supporting me through the difficult periods in my PhD career. I want to thank Renny and Shiuan-Tze, for trusting me so much as a friend, and motivating me to work hard every day. I also want to thank Jürgen Reingruber, our collaborator, for his modeling work presented in Chapter 2.

I thank my friends within and outside UCSD, for their love and support. I cannot image going through my PhD training without them. I am grateful of all the adventures we took together, and of course, all the good food. Things are simply just better when done with them. They make me look forward to meeting with more amazing people like them down the way. Lastly, I also want to thank

my family, for their trust in me. They always encourage me to do the best I can, and not to give up at difficulties.

Chapter 2, in part, is a reprint of the material as it appears in Asymmetric ephaptic inhibition between compartmentalized olfactory receptor neurons 2019. Zhang, Ye; Tsang, Tin Ki; Bushong, Eric A.; Li-An Chu; Ann-Shyn Chiang; Ellisman, Mark H.; Reingruber, Jürgen; Su, Chih-Ying, Nature Communications, 10, 1560, 2019. The dissertation author and Tin Ki Tsang contributed equally to this paper as primary investigators and authors.

Chapter 3, in part, is currently under review for publication of the material. Zhang, Ye; Su, Chih-Ying. The dissertation author was the primary investigator and author of this paper.

VITA

**Education**

2020 Ph.D. in Biology, University of California San Diego
Advisor: Dr. Chih-Ying Su

2015 B.A. in Biochemistry, General Degree Concentration, Colorado State University
Advisor: Dr. James Bamburg

2015 B.A. in Life Sciences, East China Normal University

**Publications**

Zhang, Y.*, Tsang, T. K.*, Bushong, E. A., Chu, L.-A., Chiang, A.-S., Ellisman, M. H., … Su, C.-Y. Asymmetric ephaptic inhibition between compartmentalized olfactory receptor neurons. *Nature Communications*, 2019, *10*(1), 1560. *co-first authors

He, Y., Liu, Y., Lin, Q., Zhu, J., Zhang, Y., Wang, L., Ren, X. and Ye, X. Polydatin suppresses ultraviolet B-induced cycooxygenase-2 expression in vitro and in vivo via reduced production of reactive oxygen species. *British Journal of Dermatology*, 2012, 167: 941-944

**Research Experience**

2015-2020 Doctoral research – UC San Diego, advisor: Chih-Ying Su
Systematic functional survey using *in vivo* single sensillum electrophysiology to reveal the asymmetric lateral inhibition between compartmentalized *Drosophila* olfactory receptor neurons in the same sensillum. Used electrophysiology, immunohistochemistry, and confocal imaging coupled with molecular genetic manipulations to investigate the context-dependent, sex-specific neuromodulation in pheromone sensing olfactory receptor neurons.

2013-2015 Undergraduate thesis research – Colorado State University, advisor: James Bamburg
Research using cultured primary hippocampal neurons on cofilin-actin rod-inducing activity of $A\beta_{42}$ peptides before/after $Cu(II)/H_2O_2$ oxidation to study if tyrosine residue is essential for dimerization of Aβ leading to its enhanced activity.

2011-2013 Undergraduate research assistant – East China Normal University, advisor: Xiyun Ye
*In vitro* drug screening using cell line, accompanied by *in vivo* studies to identify compounds that promote hair growth extracted from Chinese herbal medicines in mice. Assisted a research group to screen active compounds that protect skin from sun damage. Also responsible for general lab care and daily maintenance including media and gel prep, sterilization and lab mice handling.

**Teaching Experience**

2019, winter UCSD, Teaching Assistant, Muticellular Life
2018, winter UCSD, Teaching Assistant, Systems Neurobiology
2017, winter UCSD, Teaching Assistant, Recombinant DNA Techniques

ABSTRACT OF THE DISSERTATION

Initial stages of olfactory processing and neuromodulation in *Drosophila melanogaster*

by

Ye Zhang

Doctor of Philosophy

University of California San Diego, 2020

Professor Chih-Ying Su, Chair

As the first neurons of the olfactory circuit, the olfactory receptor neurons (ORNs) detect environmental volatiles to provide input into the olfactory system. Information processing at the peripheral level can markedly shape the neural code received by the brain, allowing an animal to generate proper behaviors vital for survival in nature. In the *Drosophila* antenna, different ORNs housed in the same sensory hair (sensillum) can inhibit each other non-synaptically. However, the mechanisms underlying this underexplored form of lateral inhibition remain unclear. Here I use recordings from pairs of sensilla impaled by the same tungsten electrode to demonstrate that direct electrical ("ephaptic") interactions mediate lateral inhibition between ORNs. Intriguingly, within individual sensilla, I find that ephaptic lateral inhibition is asymmetric such that one ORN exerts

greater influence onto its neighbor. Serial block-face scanning electron microscopy of genetically identified ORNs and circuit modeling indicate that asymmetric lateral inhibition reflects a surprisingly simple mechanism: the physically larger ORN in a pair corresponds to the dominant neuron in ephaptic interactions. Thus, morphometric differences between compartmentalized ORNs account for highly specialized inhibitory interactions that govern information processing at the earliest stages of olfactory coding (Zhang & Tsang et al., *Nature Communications*, 2019). Besides ephaptic coupling, neuromodulation can also profoundly influence peripheral sensory processing. To elucidate the molecular mechanisms underlying such neuromodulation, I focused on Or47b ORNs, a pheromone-responsive neuronal type that undergoes age-dependent, sexually dimorphic neuromodulation under the regulation of juvenile hormone signaling (JH). Sexual dimorphism in *Drosophila* courtship circuits requires the male-specific transcription factor $Fru^{M}$, which comprises three splice variants — $Fru^{MA}$, $Fru^{MB}$ and $Fru^{MC}$. Multiple $Fru^{M}$ isoforms are typically expressed in the same neuron; however, the functional significance of their co-expression remains underexplored. By focusing on $fru^{M}$-positive olfactory receptor neurons (ORNs), I show that $Fru^{MB}$ and $Fru^{MC}$ are both required for males' age-dependent sensitization to aphrodisiac olfactory cues. Interestingly, $Fru^{MB}$ expression, but not $Fru^{MC}$, is upregulated with age, and overexpression of $Fru^{MB}$ can confer elevated responses in courtship-promoting ORNs. Mechanistically, $Fru^{MB}$ is upstream of PPK25, a DEG/ENaC subunit necessary for response amplification, while $Fru^{MC}$ is upstream of PPK23, which is in turn required for PPK25 function. Together, these results illustrate how male-specific olfactory sensitization is synergistically regulated by different $Fru^{M}$ isoforms — through cooperation of their respective downstream effectors, thus providing critical mechanistic insight into how co-expressed $Fru^{M}$ isoforms jointly coordinate dimorphic neurophysiology (this part of the study is currently under review). Interestingly, besides age-dependent sensitization in males, Or47b ORNs also undergo sex-specific neuromodulation in females, whereby they decrease olfactory sensitivity after mating. Mechanistically, such modulation of Or47b ORN response is regulated by JH signaling, and is independent of sex peptide receptor.

Behaviorally, Or47b neuronal desensitization heightens the selectivity of mate choice for mated females compared to virgins. Taken together, my thesis projects uncover mechanisms which govern peripheral olfactory processing: 1) asymmetric ephaptic interactions between ORNs housed within the same sensillum, which underlies the principle of olfactory information processing at periphery; and 2) context-dependent, sexually dimorphic neuromodulation in pheromone-sensing ORNs, which permits coordination of animals' behaviors with their physiological states. These findings thus highlight the important role of ORNs as the site of neuromodulation which shapes information input to higher-level olfactory circuits.

# Chapter 1: Introduction

Terrestrial animals rely on their sense of smell to detect environmental volatiles, which may signal important information for survival, such as the presence of food, potential mates or dangers, allowing animals to evaluate their surroundings and generate proper behaviors accordingly. In nature, most odors are complex mixtures of volatile chemicals, detected by the olfactory receptor neurons (ORNs) located in the peripheral olfactory organ, and each ORN typically expresses a single type of odorant receptor from a large family of genes (Ache and Young, 2005). The identity of odorant receptor determines an ORN's response profile, and all ORNs that express the same receptor converge onto the same neuropil structure, name glomerulus, where the ORNs synapse onto second order neurons to allow information to be further propagated or processed in higher brain regions (Ache and Young, 2005). As such, meaningful information from complex inputs can be extracted to guide animal behaviors through olfactory processing. So far, much of the effort to understand olfactory processing has focused on the central nervous system, and the contribution of the peripheral olfactory system to information processing is under-explored. This is mainly due to the conventional presumptions that ORNs merely function as passive reporters of environmental volatiles (Wilson, 2013); it is also assumed that no information processing takes place at this level, because ORNs do not have direct synaptic connections with each other (Shanbhag et al., 1999), nor are they stereotypically connected by interneurons. Using *Drosophila Melanogaster* as the model organism, my PhD research revealed that peripheral olfactory processing can be achieved by two mechanisms: through information processing between compartmentalized ORNs, or through cell-type specific neuromodulation. Together, my research suggest that complex information processing can take place at the peripheral in

fly olfactory system, and challenge the conventional views about the circuit functions of ORNs.

### 1.1 Non-synaptic interactions in the first stage of *Drosophila* olfactory information processing

Neural coding of odors in *Drosophila melanogaster* begins in the ORNs, which change spike firing frequency in response to environmental volatiles. The ORN complement in adult flies includes up to 1300 neurons, which are further classified into 50 neuronal classes depending on their expression of unique olfactory receptors (Hallem and Carlson, 2004; Su et al., 2009). *Drosophila* ORNs mostly express odorant receptors of two classes: the odor receptor (Ors) and the ionotropic receptors (Irs) (Su et al., 2009). In most cases, an ORN expresses a single odorant receptor which confers ligand binding specificity and defines the neuron's odor response profile (Couto et al., 2005; Dobritsa et al., 2003; Fishilevich and Vosshall, 2005; van der Goes van Naters and Carlson, 2007; Hallem et al., 2004; Yao et al., 2005). ORNs expressing the same receptor converge onto a single glomerulus in the antennal lobe—a structure in the insect brain equivalent to the vertebrate olfactory bulb—where they synapse onto projection neurons that carry information to higher brain regions (Su et al., 2009). Modulation in the periphery can therefore shape the olfactory inputs that the brain receives.

Typically 2-4 different ORNs are compartmentalized together in sensory hairs. These hairs, also known as sensilla, cover the surfaces of the third segment of antennae which contains 20 known sensillum types, and the maxillary palps which contain three sensillum types (Shanbhag et al., 1999, 2000; Su et al., 2009). Depending on their morphology, these sensory hairs are classified as 1) basiconic sensilla, which mainly respond to food odors (Dobritsa et al., 2003; Hallem and Carlson, 2006; Hallem et al., 2004); 2) trichoid sensilla, which largely respond to pheromones (van der Goes van Naters and Carlson, 2007; Ha and Smith, 2006; Kurtovic et al., 2007; Lin et al., 2013); or 3) coeloconic sensilla that house ORNs which, unlike the Or-expressing neurons from the previous two

sensillum classes, typically express Irs responding to amines and acids (Benton et al., 2009; Yao et al., 2005).

Within the sensilla, ORNs are compartmentalized in stereotyped combinations, in that the grouping of ORN types follow strict pairing rules (de Bruyne et al., 2001). Furthermore, the group-housed ORNs exhibit characteristic differences in extracellular spike amplitudes; ORNs are thus named “A”, “B”, “C”, or “D” based on their relative spike amplitudes in descending order (de Bruyne et al., 2001). Curiously, neighboring ORNs neither detect similar odors (Hallem and Carlson, 2006), nor do they necessarily project to neighboring glomeruli (Couto et al., 2005). Do these stereotyped compartmentalization schemes affect neuronal function?

Despite such stereotyped grouping of ORNs, their responses were assumed to be determined solely by their expressed receptor (Hallem et al., 2004). However, using a two-odor stimulus paradigm to simultaneously activate neighboring ORNs, my mentor Dr. Su discovered that the activation of an ORN can inhibit the firing of its neighbor (Su et al., 2012). This novel form of neuronal communication between grouped ORNs is observed broadly across sensillum types, and in principle enables odor mixture information to be integrated in a sensillum. What then is the mechanism for this inhibition?

Surprisingly, lateral inhibition between ORNs does not depend on a synapse or a gap junction. Given that the outer dendrites of ORNs are in close proximity (Shanbhag et al., 1999, 2000), and that the confined compartmental sensillum environment gives rise to high extracellular resistivity (De Kramer, 1985; Redkozubov, 1995), it was proposed that lateral inhibition between neighboring ORNs is mediated by direct electrical interactions, named ephaptic coupling (Su et al., 2012). Unlike a typical sensory neuron whose transduction current is driven by transmembrane ionic gradients, an ORN’s transduction current is primarily driven instead by the transepithelial potential (Vermeulen and Rospars, 2004). Therefore, ORNs in the same sensillum share the same driving force (Kaissling, 1986; Vermeulen and Rospars, 2004), and activation of one neuron can thus deprive the available driving

force for its neighbor, thereby affecting its neighbor's activity. As the ionic current is shunted away, the activity of an ORN can be inhibited by strong activation of its neighbor. These features can in principle enable grouped ORNs to interact through direct electrical interactions. However, direct experimental evidence for inhibition between neighboring ORNs via ephaptic interactions is lacking. Furthermore, the published circuit model assumed that neighboring ORNs have identical electrotonic properties, such that ephaptic interaction between the two neurons should be symmetrical. Is this assumption true, or can compartmentalized ORNs laterally inhibit each other in an asymmetric manner? Addressing this question would further our understanding towards the principle of peripheral olfactory information processing, as well as the impact of ephaptic interaction on circuit functions.

Beyond insect olfactory sensilla, ephaptic interactions are also observed in several vertebrate nervous systems. The most extensively studied example is found in fish teleost medulla, in which ephaptic interactions between interneurons and Mauthner cell were implicated in mediating the tail flip escape reaction (Faber and Korn, 1989; Jefferys, 1995; Weiss et al., 2008). Similar electrical interactions were also reported in the vertebrate cerebellum (Blot and Barbour, 2014; Korn and Axelrad, 1980), though their functional significance remains unclear due to the technical difficulties in manipulating these interactions *in vivo*. If neighboring ORNs indeed interact via ephaptic coupling, the *Drosophila* peripheral olfactory system can provide an excellent opportunity to examine the functional impacts of this underexplored form of neuronal interaction.

### 1.2 Sexually dimorphic neuromodulation in pheromone-sensing ORNs

Upon encountering a potential mate, male flies perform a series of sophisticated courtship behaviors, including orienting towards the female target, following, wing extensions, generating courtship song, tapping the abdomen with forelegs, licking genitalia, and attempting to copulate (Yamamoto and Koganezawa, 2013). In response, females will either accept or reject male courtship depending on their receptivity, which is primarily determined by their mating status (Ellendersen and

von Philipsborn, 2017). These examples illustrate the clear distinctions between the sexually-dimorphic mating behaviors between males and females.

To increase the probability of successful mating and to ensure fitness of offspring, both males and females rely on multimodal sensory cues to evaluate the suitability of their potential mates. Among them, pheromone cues detected by the olfactory system play a particularly central role by broadcasting information regarding a candidate's sex, species, and mating status (Rings and Goodwin, 2019; Yew and Chung, 2017). Modulation in ORNs can therefore significantly affect flies' sexual behavior. Are ORNs modulated in a sexually-dimorphic manner to mediate male and female-specific behaviors? If so, what could be the underlying molecular mechanisms for such differential neuromodulation?

The male and female sexual characteristics and sex-specific behaviors of *Drosophila* are determined by a cascade of splicing events in sex-determining genes (Auer and Benton, 2016; Billeter et al., 2006a; Christiansen et al., 2002; MacDougall et al., 1995; Pavlou and Goodwin, 2013). The primary sex-determination gene is *Sex lethal* (Sxl), which is transcribed only when the X chromosome to autosome ratio (X/A ratio) equals to or exceeds 1. As a result, *sxl* is transcribed only in females. Sxl binds to the primary RNA of the *transformer* (*tra*) gene, yielding a protein-coding *tra* mRNA only in females. The Tra protein then binds to the primary RNA *doublesex* (*dsx*), to mediate sex-specific splicing (Auer and Benton, 2016). While Dsx determines somatic sexual differentiation, and is also a transcription factor important for sexual dimorphism (Auer and Benton, 2016; Billeter et al., 2006a; Pavlou and Goodwin, 2013), it is not expressed in adult ORNs (Rideout et al., 2010).

The Tra protein also regulate splicing of transcript produced from the P1 promoter of *fruitless* (*fru*) (Ryner et al., 1996a). In females, Tra promote splicing near its binding site, introducing a premature stop codon that renders the transcript nonfunctional. In males, due to the absence of Tra, an alternative splice site is used for splicing *fruitless*, yielding a functional protein ($Fru^M$) (Auer and Benton, 2016), which functions as transcription regulators and orchestrates the neural circuits for

*Drosophila* male courtship behaviors (Hall, 1994; Kimura et al., 2005; Manoli et al., 2005; Ryner et al., 1996a; Stockinger et al., 2005). Importantly, $Fru^M$ is expressed in three types of adult ORNs: the Or47b, Ir84a, and Or67d ORNs, which project to VA1v, VL2a and DA1 glomeruli in the antennal lobe, respectively (Stockinger et al., 2005). Among these three neuronal types, Or47b and Ir84a ORNs promote male courtship behaviors (Dweck et al., 2015; Grosjean et al., 2011; Lin et al., 2016), while Or67d ORNs inhibit courtship (Kurtovic et al., 2007). Intriguingly, of the ~50 glomeruli in the antennal lobe, only the three glomeruli innervated by the $Fru^M$ positive ORNs show sexually dimorphic volumetric enlargement in males (Kondoh et al., 2003; Stockinger et al., 2005), and such sexual dimorphism is dependent on the expression of $Fru^M$ (Stockinger et al., 2005).

Beyond regulating sexually dimorphic anatomy during development, $Fru^M$ also mediates dimorphic neurophysiology in the adult nervous system. Recent studies report male-specific modulations in the sensitivity of courtship-promoting ORNs (Lin et al., 2016; Ng et al., 2019). Responding to an aphrodisiac pheromone that enhances male mating drive, Or47b ORN responses are upregulated with age in male but not female flies (Lin et al., 2016). This heightened Or47b sensitivity is regulated by juvenile hormone (JH) (Lin et al., 2016), whose level also increases with age in males (Lee et al., 2017). Mechanistically, Or47b ORN age-dependent sensitization requires a DEG/ENaC sodium channel, Pickpocket 25 (PPK25) (Ng et al., 2019). Similarly Ir84a ORNs, which respond to aphrodisiac food odors, also show male-specific, age-dependent sensitization (Ng et al., 2019). A previous study, which focused on the role of $Fru^M$ in how social experience influences courtship behavior, has shown that male Or47b ORN responses are regulated by $Fru^M$ in a dose-dependent manner (Sethi et al., 2019). This evidence, along with the finding that Dsx is not expressed in adult ORNs (Rideout et al., 2010; Sethi et al., 2019), raises the possibility that $Fru^M$ can function as a key factor for male-specific neurophysiological modulation.

Notably, the *fru* gene is further subject to alternative splicing at its 3' end, resulting in at least three functional variants: $Fru^{MA}$, $Fru^{MB}$, $Fru^{MC}$ (based on Demir and Dickson, 2005; Song et al., 2002).

The $Fru^{MA-C}$ isoforms each contain a common N-terminal BTB dimerization domain and a distinct zinc-finger DNA-binding domain (Billeter et al., 2006b; Rezával et al., 2014; Ryner et al., 1996b; von Philipsborn et al., 2014). In both pupal and adult males, $Fru^{MA-C}$ show high but incomplete overlapping expression patterns in the brain and ventral nerve cord, with $Fru^{MA}$ expressed in the smallest subset of $Fru^{M}$ positive neurons (Rezával et al., 2014; von Philipsborn et al., 2014). Is $Fru^{M}$ necessary for the male-specific, age-dependent regulation of olfactory neurophysiology in Or47b ORNs? If so, which $Fru^{M}$ isoform(s) are required? Furthermore, if multiple isoforms are involved, it remains unclear how co-expressed $Fru^{M}$ variants regulate sexually dimorphic neuromodulation within the same neuron. Do each of them directly function together to regulate downstream targets; or do they individually regulate their respective targets, which act cooperatively instead?

**1.3 Mating status dependent modulation in females**

After mating, female flies show many post-mating behavioral and physiological changes (Isaac et al., 2010; Kubli, 2003, 2010), most of which require sex peptide (SP), which is found in the seminal fluid from males, and are transferred to females during insemination (Kubli, 2003). Once transferred to females, SP acts on sex peptide receptors (SPRs) expressed in genital tract neurons (Häsemeyer et al., 2009), which ascend and transmit mating information to the central nervous system (Feng et al., 2014). Interestingly, subsets of female chemosensory neurons also undergo post-mating neurophysiological modulations to increase their preference towards nutrients important for egg-development and oviposition. Mechanistically, the neurons change their responses through neuropeptide-mediated modulation (Hussain et al., 2016). However, it remains unclear if other classes of chemosensory neurons in females also undergo post-mating neuromodulation, and if they are modulated through the same mechanism.

Intriguingly, the male-specific sensitization in Or47b ORNs is regulated by the upregulation of JH signaling (Lin et al., 2016), suggesting that post-mating neuromodulation in the periphery may not

be induced by SPR ligands alone. Furthermore, the JH level increases in females after mating (Reiff et al., 2015), is it possible that the same form of hormonal regulation also mediates female Or47b neurons in a context-dependent manner? If so, would these neurons' olfactory response be sensitized or desensitized, and how does a shift in neuronal sensitivity affect females' behavioral output?

### 1.4 Summary of key findings

My dissertation contains two focuses. The first focus aimed to systematically characterize ephaptic interactions between grouped ORNs housed across different sensillum types. Specifically, I hypothesized that ephaptic interaction is asymmetric between grouped neurons in most sensillum types. Before testing this hypothesis, I first conducted electrophysiological recordings by using tungsten electrodes to electrically connect two sensilla of different types. Through this experiment, I provided experimental evidence that direct electrical interaction is sufficient to drive lateral inhibition between ORNs. This finding supports the previously proposed model that group-housed ORNs may inhibit their neighbors through ephaptic interactions (Su et al., 2012), and that the electrotonic properties of an ORN would directly determine the degree of lateral inhibition it can exert on its neighbors.

To characterize the electrotonic properties of paired ORNs, I next performed *in vivo* single-sensillum recordings on grouped ORNs, using private odorants that selectively activate one of the cells for each sensillum type. In support of my hypothesis, I found that grouped ORNs have different maximal field responses, suggest that they can exert ephaptic inhibition on their neighbors at different strengths, as the ORNs housed in the same sensillum share the same driving force. Next, I examined the susceptibility of an ORN to a neighboring neuron's ephaptic influence, measured by the ORN's tendency to change spike frequency towards a reduction of field potential, by comparing the spiking properties of grouped neurons. Using odor or optogenetic stimulation paradigms, I found that at the same reduction in external field potential, most grouped ORNs have different tendencies to change their spike rates compared to their neighbors, and consistent with the LFP analysis, the large-spike

"A" neurons are less susceptible to ephaptic influence. Taken together, these results indicate that ephaptic interactions are asymmetric between grouped neurons. What then could be the mechanism underlying the differences in the electrotonic properties of paired ORNs?

I hypothesized that the "A" neurons are physically larger than the smaller-spiked neurons in the same sensillum, as a greater dendritic and somatic surface area and volume leads to a smaller input resistance, resulting in a larger maximal LFP response; less somatic input resistance also results in a reduced tendency to generate action potentials at a given change in LFP. To test whether "A" neurons indeed have larger volumes, we required a method to faithfully generate models of each ORN within the same sensillum. I therefore collaborated with Tin Ki Tsang, a former member of the lab, to generate 3D volumetric reconstructions of grouped ORNs using a novel electron microscopy method (Tsang et al., 2018). In support of my hypothesis, we observed distinct morphometric differences between grouped ORNs which correlate with their distinct electrotonic properties. Specifically, the dominant "A" neurons with larger extracellular spike amplitudes are physically larger than their compartmentalized partners. Combining the electrophysiological results with the morphometric analyses, we revised the published electric circuit model of a sensillum (Vermeulen and Rospars, 2004), which assumed that the two compartmentalized ORNs have identical electrotonic properties. Our revised model of the sensillum reflects the morphometric differences between neighboring neurons, and demonstrates that the size of a neuron is a key factor in determining the strength of ephaptic interactions. Together, our findings reveal a fundamental principle by which ephaptic interactions modulate *Drosophila* olfactory circuit in the periphery, and may pave the way for further study on ephaptic interactions in other model systems (this part of the study is published in *Nature Communications*, 2019).

The second focus of my thesis sought to uncover the molecular mechanisms underlying sexually dimorphic neuromodulation of ORNs. In males, I focused on the transcription factor $Fru^{M}$, and asked if it is required for the age-dependent sensitization in subtypes of the $Fru^{M}$-positive ORNs.

Via single-sensillum recording, I found that $Fru^{M}$ is required for the elevated response in courtship-promoting Or47b and Ir84a neurons, but not in courtship-inhibiting Or67d neurons. By focusing on Or47b neurons, I systematically analyzed the expression patterns of all three $Fru^{M}$ isoforms, and found that both $Fru^{MB}$ and $Fru^{MC}$ are required for the elevated Or47b responses of older males, and that $Fru^{MB}$ expression is upregulated with age. Consistent with this finding, $Fru^{MB}$ overexpression can mimic the effects of age in sensitizing Or47b neuronal responses. Furthermore, through a series of epistasis experiments, I found that juvenile hormone signaling operates upstream of $Fru^{MB}$, which further regulates PPK25 expression. $Fru^{MC}$, while not upregulated with age, is required for the expression of PPK23, which is further involved in forming functional PPK25 channels. Together, these results provide insights into how co-expressed $Fru^{M}$ isoforms each regulate unique downstream targets, which coordinate and function together to modulation neurophysiology in males (this part of the study is currently under review).

Although female Or47b ORNs do not exhibit age-dependent sensitization, it is unclear whether these neurons can be modulated in a different sex-specific context. Through collaboration with Dr. Jean-Christophe Billeter, a neuroethologist specializing in female *Drosophila*, I found that the mating status of females can profoundly modulate their Or47b olfactory sensitivity: the pheromone responses of mated females are markedly lower than those of virgins. Via single-sensillum recordings of Or47b neurons from virgin and mated females, I observed reduced Or47b ORN responses in females mated for 16hr or longer prior to recording. To further understand the mechanism underlying this neuromodulation, I treated virgin females with methoprene, a JH analogue, to mimic the upregulation of JH signaling post-mating. I found that the JH analogue treatment is sufficient to reduce Or47b neuronal response in virgins. In a reciprocal experiment, I knocked down Methoprene tolerant (Met), a JH receptor, specifically in Or47b ORNs, and found that Or47b neurons no longer undergo post-mating desensitization. To test whether sex peptide transferred during copulation also plays a role in the neuromodulation I observed, I knocked down SPR in the Or47b ORNs, and found that this

manipulation does not affect Or47b neuronal response in either virgin and mated females. I therefore concluded that mechanistically, this neuromodulation is mediated by JH signaling, and is independent of SPR.

How does JH differentially regulate the olfactory response in Or47b neurons in a sexually dimorphic manner? I hypothesized that in the absence of $Fru^M$ isoforms in females, JH upregulation leads to Or47b ORN desensitization. To test this hypothesis, I specifically feminized Or47b neurons in males by expressing Tra using the Gal4-UAS system, followed by treating these males with methoprene to mimic the mating-induced upregulation of JH signaling. In the absence of $Fru^M$, methoprene treatment desensitizes feminized Or47b ORNs, while the same treatment sensitizes wildtype, FruM-positive Or47b neurons. Similar results were also observed in Or47b neurons from $fru^F$ males that do not express any functional $Fru^M$ proteins, further supporting my hypothesis that JH upregulation desensitizes Or47b ORNs in the absence of $Fru^M$ isoforms (a manuscript is currently in preparation).

Taken together, my experiments have unveiled key mechanisms for the sexually dimorphic, neurophysiological modulation in Or47b neurons; shown that such modulation heavily depends on the physiological conditions; and demonstrated that such modulation serves important roles in regulating sex-specific behaviors.

### 1.5 References


Ache, B.W., and Young, J.M. (2005). Olfaction: Diverse species, conserved principles. Neuron *48*, 417–430.

Auer, T.O., and Benton, R. (2016). Sexual circuitry in Drosophila. Curr. Opin. Neurobiol. *38*, 18–26.

Benton, R., Vannice, K.S., Gomez-Diaz, C., and Vosshall, L.B. (2009). Variant Ionotropic Glutamate Receptors as Chemosensory Receptors in Drosophila. Cell *136*, 149–162.

Billeter, J.-C., Rideout, E.J., Dornan, A.J., and Goodwin, S.F. (2006a). Control of Male Sexual Behavior in Drosophila by the Sex Determination Pathway. Curr. Biol. *16*, R766–R776.

Billeter, J.C., Villella, A., Allendorfer, J.B., Dornan, A.J., Richardson, M., Gailey, D.A., and Goodwin, S.F. (2006b). Isoform-Specific Control of Male Neuronal Differentiation and Behavior in Drosophila

by the fruitless Gene. Curr. Biol. *16*, 1063–1076.

Blot, A., and Barbour, B. (2014). Ultra-rapid axon-axon ephaptic inhibition of cerebellar Purkinje cells by the pinceau. Nat. Neurosci. *17*, 289–295.

de Bruyne, M., Foster, K., and Carlson, J.R. (2001). Odor Coding in the Drosophila Antenna. Neuron *30*, 537–552.

Christiansen, A.E., Keisman, E.L., Ahmad, S.M., and Baker, B.S. (2002). Sex comes in from the cold: the integration of sex and pattern. Trends Genet. *18*, 510–516.

Couto, A., Alenius, M., and Dickson, B.J. (2005). Molecular, Anatomical, and Functional Organization of the Drosophila Olfactory System. Curr. Biol. *15*, 1535–1547.

Demir, E., and Dickson, B.J. (2005). fruitless splicing specifies male courtship behavior in Drosophila. Cell *121*, 785–794.

Dobritsa, A.A., van der Goes van Naters, W., Warr, C.G., Steinbrecht, R.A., and Carlson, J.R. (2003). Integrating the Molecular and Cellular Basis of Odor Coding in the Drosophila Antenna. Neuron *37*, 827–841.

Dweck, H.K.M., Ebrahim, S.A.M., Thoma, M., Mohamed, A.A.M., Keesey, I.W., Trona, F., Lavista-Llanos, S., Svatoš, A., Sachse, S., Knaden, M., et al. (2015). Pheromones mediating copulation and attraction in Drosophila. Proc. Natl. Acad. Sci. U. S. A. *112*, E2829-35.

Ellendersen, B.E., and von Philipsborn, A.C. (2017). Neuronal modulation of D. melanogaster sexual behaviour. Curr. Opin. Insect Sci. *24*, 21–28.

Faber, D.S., and Korn, H. (1989). Electrical field effects: their relevance in central neural networks. Physiol. Rev. *69*, 821–863.

Feng, K., Palfreyman, M.T., Häsemeyer, M., Talsma, A., and Dickson, B.J. (2014). Ascending SAG neurons control sexual receptivity of Drosophila females. Neuron *83*, 135–148.

Fishilevich, E., and Vosshall, L.B. (2005). Genetic and Functional Subdivision of the Drosophila Antennal Lobe. Curr. Biol. *15*, 1548–1553.

van der Goes van Naters, W., and Carlson, J.R. (2007). Receptors and Neurons for Fly Odors in Drosophila.

Grosjean, Y., Rytz, R., Farine, J.-P., Abuin, L., Cortot, J., Jefferis, G.S.X.E., and Benton, R. (2011). An olfactory receptor for food-derived odours promotes male courtship in Drosophila. Nature *478*, 236–240.

Ha, T.S., and Smith, D.P. (2006). A Pheromone Receptor Mediates 11-cis-Vaccenyl Acetate-Induced Responses in Drosophila. J. Neurosci. *26*.

Hall, J.C. (1994). The mating of a fly. Science *264*, 1702–1714.

Hallem, E.A., and Carlson, J.R. (2004). The odor coding system of Drosophila. Trends Genet. *20*, 453–459.

Hallem, E.A., and Carlson, J.R. (2006). Coding of Odors by a Receptor Repertoire. Cell *125*, 143–160.

Hallem, E.A., Ho, M.G., and Carlson, J.R. (2004). The Molecular Basis of Odor Coding in the Drosophila Antenna. Cell *117*, 965–979.

Häsemeyer, M., Yapici, N., Heberlein, U., and Dickson, B.J. (2009). Sensory Neurons in the Drosophila Genital Tract Regulate Female Reproductive Behavior. Neuron *61*, 511–518.

Hussain, A., Üçpunar, H.K., Zhang, M., Loschek, L.F., and Grunwald Kadow, I.C. (2016). Neuropeptides Modulate Female Chemosensory Processing upon Mating in Drosophila. PLOS Biol. *14*, e1002455.

Isaac, R.E., Li, C., Leedale, A.E., and Shirras, A.D. (2010). *Drosophila* male sex peptide inhibits siesta sleep and promotes locomotor activity in the post-mated female. Proc. R. Soc. B Biol. Sci. *277*, 65–70.

Jefferys, J.G. (1995). Nonsynaptic modulation of neuronal activity in the brain: electric currents and extracellular ions. Physiol. Rev. *75*, 689–723.

Kaissling, K. (1986). Chemo-Electrical Transduction in Insect Olfactory Receptors. Annu. Rev. Neurosci. *9*, 121–145.

Kimura, K.-I., Ote, M., Tazawa, T., and Yamamoto, D. (2005). Fruitless specifies sexually dimorphic neural circuitry in the Drosophila brain. Nature *438*, 229–233.

Kondoh, Y., Kaneshiro, K.Y., Kimura, K.I., and Yamamoto, D. (2003). Evolution of sexual dimorphism in the olfactory brain of Hawaiian Drosophila. Proc. R. Soc. B Biol. Sci. *270*, 1005–1013.

Korn, H., and Axelrad, H. (1980). Electrical inhibition of Purkinje cells in the cerebellum of the rat. Proc. Natl. Acad. Sci. U. S. A. *77*, 6244–6247.

De Kramer, J.J. (1985). The Electrical Circuitry of an Olfactory Sensillum in Antheraea polyphemus'. J. Neurosci. *5*, 2484–2493.

Kubli, E. (2003). Sex-peptides: Seminal peptides of the Drosophila male. Cell. Mol. Life Sci. *60*, 1689–1704.

Kubli, E. (2010). Sexual behavior: Dietary food switch induced by sex. Curr. Biol. *20*, R474–R476.

Kurtovic, A., Widmer, A., and Dickson, B.J. (2007). A single class of olfactory neurons mediates behavioural responses to a Drosophila sex pheromone. Nature *446*, 542–546.

Lee, S.S., Ding, Y., Karapetians, N., Rivera-Perez, C., Noriega, F.G., and Adams, M.E. (2017). Hormonal Signaling Cascade during an Early-Adult Critical Period Required for Courtship Memory Retention in Drosophila. Curr. Biol. *27*, 2798-2809.e3.

Lin, H.-H., Chu, L.-A., Fu, T.-F., Dickson, B.J., and Chiang, A.-S. (2013). Parallel Neural Pathways Mediate CO2 Avoidance Responses in Drosophila. Science (80-. ). *340*.

Lin, H.-H., Cao, D.-S., Sethi, S., Zeng, Z., Chin, J.S.R., Chakraborty, T.S., Shepherd, A.K., Nguyen, C.A., Yew, J.Y., Su, C.-Y., et al. (2016). Hormonal Modulation of Pheromone Detection Enhances Male Courtship Success. Neuron *90*, 1272–1285.

MacDougall, C., Harbison, D., and Bownes, M. (1995). The developmental consequences of alternate splicing in sex determination and differentiation in Drosophila. Dev. Biol. *172*, 353–376.

Manoli, D.S., Foss, M., Villella, A., Taylor, B.J., Hall, J.C., and Baker, B.S. (2005). Male-specific fruitless specifies the neural substrates of Drosophila courtship behaviour. Nature *436*, 395.

Ng, R., Salem, S.S., Wu, S.T., Wu, M., Lin, H.H., Shepherd, A.K., Joiner, W.J., Wang, J.W., and Su, C.Y. (2019). Amplification of Drosophila Olfactory Responses by a DEG/ENaC Channel. Neuron *104*,

947-959.e5.

Pavlou, H.J., and Goodwin, S.F. (2013). Courtship behavior in Drosophila melanogaster: towards a "courtship connectome". Curr. Opin. Neurobiol. *23*, 76–83.

Redkozubov, A. (1995). High electrical resistance of the bombykol cell in an olfactory sensillum of Bombyx mori: Voltage- and current-clamp analysis. J. Insect Physiol. *41*, 451–455.

Reiff, T., Jacobson, J., Cognigni, P., Antonello, Z., Ballesta, E., Tan, K.J., Yew, J.Y., Dominguez, M., and Miguel-Aliaga, I. (2015). Endocrine remodelling of the adult intestine sustains reproduction in Drosophila. Elife *4*, e06930.

Rezával, C., Nojima, T., Neville, M.C., Lin, A.C., and Goodwin, S.F. (2014). Sexually Dimorphic Octopaminergic Neurons Modulate Female Postmating Behaviors in Drosophila. Curr. Biol. *24*, 725–730.

Rideout, E.J., Dornan, A.J., Neville, M.C., Eadie, S., and Goodwin, S.F. (2010). Control of sexual differentiation and behavior by the doublesex gene in Drosophila melanogaster. Nat. Neurosci. *13*, 458–466.

Rings, A., and Goodwin, S.F. (2019). To court or not to court – a multimodal sensory decision in Drosophila males. Curr. Opin. Insect Sci. *35*, 48–53.

Ryner, L.C., Goodwin, S.F., Castrillon, D.H., Anand, A., Villella, A., Baker, B.S., Hall, J.C., Taylor, B.J., and Wasserman, S.A. (1996a). Control of male sexual behavior and sexual orientation in Drosophila by the fruitless gene. Cell *87*, 1079–1089.

Ryner, L.C., Goodwin, S.F., Castrillon, D.H., Anand, A., Villella, A., Baker, B.S., Hall, J.C., Taylor, B.J., and Wasserman, S.A. (1996b). Control of Male Sexual Behavior and Sexual Orientation in Drosophila by the fruitless Gene. Cell *87*, 1079–1089.

Sethi, S., Lin, H.H., Shepherd, A.K., Volkan, P.C., Su, C.Y., and Wang, J.W. (2019). Social Context Enhances Hormonal Modulation of Pheromone Detection in Drosophila. Curr. Biol. *29*, 3887-3898.e4.

Shanbhag, S.., Müller, B., and Steinbrecht, R.. (1999). Atlas of olfactory organs of Drosophila melanogaster: 1. Types, external organization, innervation and distribution of olfactory sensilla. Int. J. Insect Morphol. Embryol. *28*, 377–397.

Shanbhag, S.., Müller, B., and Steinbrecht, R.. (2000). Atlas of olfactory organs of Drosophila melanogaster: 2. Internal organization and cellular architecture of olfactory sensilla. Arthropod Struct. Dev. *29*, 211–229.

Song, H.J., Billeter, J.C., Reynaud, E., Carlo, T., Spana, E.P., Perrimon, N., Goodwin, S.F., Baker, B.S., and Taylor, B.J. (2002). The fruitless gene is required for the proper formation of axonal tracts in the embryonic central nervous system of Drosophila. Genetics *162*, 1703–1724.

Stockinger, P., Kvitsiani, D., Rotkopf, S., Tirián, L., and Dickson, B.J. (2005). Neural Circuitry that Governs Drosophila Male Courtship Behavior. Cell *121*, 795–807.

Su, C.-Y., Menuz, K., and Carlson, J.R. (2009). Olfactory Perception: Receptors, Cells, and Circuits. Cell *139*, 45–59.

Su, C.-Y., Menuz, K., Reisert, J., and Carlson, J.R. (2012). Non-synaptic inhibition between grouped neurons in an olfactory circuit.

Tsang, T.K., Bushong, E.A., Boassa, D., Hu, J., Romoli, B., Phan, S., Dulcis, D., Su, C.-Y., and Ellisman, M.H. (2018). High-quality ultrastructural preservation using cryofixation for 3D electron microscopy of genetically labeled tissues. Elife *7*, e35524.

Vermeulen, A., and Rospars, J.-P. (2004). Why are insect olfactory receptor neurons grouped into sensilla? The teachings of a model investigating the effects of the electrical interaction between neurons on the transepithelial potential and the neuronal transmembrane potential. Eur. Biophys. J. *33*, 633–643.

von Philipsborn, A.C., Jörchel, S., Tirian, L., Demir, E., Morita, T., Stern, D.L., and Dickson, B.J. (2014). Cellular and Behavioral Functions of fruitless Isoforms in Drosophila Courtship. Curr. Biol. *24*, 242–251.

Weiss, S.A., Preuss, T., and Faber, D.S. (2008). A role of electrical inhibition in sensorimotor integration. Proc. Natl. Acad. Sci. U. S. A. *105*, 18047–18052.

Wilson, R.I. (2013). Early olfactory processing in Drosophila: mechanisms and principles. Annu. Rev. Neurosci. *36*, 217–241.

Yamamoto, D., and Koganezawa, M. (2013). Genes and circuits of courtship behaviour in drosophila males. Nat. Rev. Neurosci. *14*, 681–692.

Yao, C.A., Ignell, R., and Carlson, J.R. (2005). Chemosensory Coding by Neurons in the Coeloconic Sensilla of the Drosophila Antenna. J. Neurosci *25*, 8359–8367.

Yew, J.Y., and Chung, H. (2017). Drosophila as a holistic model for insect pheromone signaling and processing. Curr. Opin. Insect Sci. *24*, 15–20.

# Chapter 2: Asymmetric ephaptic inhibition between compartmentalized olfactory receptor neurons

## 2.1 Abstract

In the *Drosophila* antenna, different subtypes of olfactory receptor neurons (ORNs) housed in the same sensory hair (sensillum) can inhibit each other non-synaptically. However, the mechanisms underlying this underexplored form of lateral inhibition remain unclear. Here I use recordings from pairs of sensilla impaled by the same tungsten electrode to demonstrate that direct electrical ("ephaptic") interactions mediate lateral inhibition between ORNs. Intriguingly, within individual sensilla, I find that ephaptic lateral inhibition is asymmetric such that one ORN exerts greater influence onto its neighbor. Serial block-face scanning electron microscopy of genetically identified ORNs and circuit modeling indicate that asymmetric lateral inhibition reflects a surprisingly simple mechanism: the physically larger ORN in a pair corresponds to the dominant neuron in ephaptic interactions. Thus, morphometric differences between compartmentalized ORNs account for highly specialized inhibitory interactions that govern information processing at the earliest stages of olfactory coding.

## 2.2 Introduction

Ionic fluxes from neuronal activity lead to changes in the extracellular potential (Buzsáki et al., 2012), which can influence the excitability of adjacent neurons by electrical field effects, known as ephaptic interaction (Faber and Korn, 1989; Jefferys, 1995). First observed between two axons brought together experimentally (Arvanitaki; Katz and Schmitt, 1940), ephaptic interaction takes place between uninsulated neuronal processes packed into an electrically isolated microenvironment (Faber and Korn, 1989; Jefferys, 1995). Such an arrangement commonly occurs in fascicles containing bundles of unmyelinated axons, such as the mammalian olfactory nerve (Bokil et al., 2001) and the interoceptive sensory system (Damasio and Carvalho, 2013), as well as in regions of the nervous system including the fish hindbrain, mammalian cerebellum, hippocampus, and retina (Buzsáki et al., 2012; Faber and Korn, 1989; Han et al.; Jefferys, 1995; Kamermans et al., 2001). Despite their likely

prevalence, field effects have long been considered nebulous (Hubel, 1982), as most neurons that are known to interact ephaptically also communicate via chemical synapses or gap junctions (Faber and Korn, 1989; Jefferys, 1995; Kamermans et al., 2001). In addition, ephaptic interaction is notoriously difficult to study because it is enabled by high extracellular resistance and density of neural membranes (Faber and Korn, 1989; Jefferys, 1995), none of which are amenable to in vivo experimental manipulation. Therefore, it remains unclear whether and how ephaptic interaction by itself is sufficient to influence circuit function.

Taking advantage of the powerful genetic toolkit of *Drosophila melanogaster*, I showed that olfactory receptor neurons (ORNs) housed in the same sensory hair, or sensillum, can inhibit each other, and that such lateral inhibition can modulate odor-guided behavior (Su et al., 2012). Despite the lack of direct synaptic connections, transient activation of one ORN rapidly suppresses the ongoing activity of its neighbor (Su et al., 2012). Electric circuit modeling suggested a potential mechanism for this nonsynaptic signaling (Su et al., 2012; Vermeulen and Rospars, 2004): in the restrictive space of a sensillum lumen, the high resistance of the lymph (Redkozubov, 1995) favors the generation of field effects between compartmentalized ORNs (Faber and Korn, 1989; Jefferys, 1995). However, whether ephaptic interaction underlies the inhibition between ORNs has not been directly demonstrated.

In addition, outstanding questions remain about the peripheral organization of ORNs. Most insect ORNs housed in the same sensillum exhibit distinct and characteristic extracellular spike amplitudes. Grouped ORNs are thus named “A”, “B” or “C” based on their relative spike amplitudes in descending order (de Bruyne et al., 1999). In fruitflies, olfactory sensilla contain up to four neurons, with the majority of them housing two ORNs (de Bruyne et al., 1999, 2001). Intriguingly, certain odorant receptors are exclusively expressed in the large-spike “A” neurons, whereas others in the small-spike ORNs. For instance, in *D. melanogaster*, the Or22a receptor is expressed in the large-spike “A” neuron in the antennal basiconic sensilla of type 3 (ab3A), which is paired with a small-spike neighbor expressing Or85b (ab3B) (Couto et al., 2005; Fishilevich and Vosshall, 2005; Hallem

et al., 2004). The ab3A(Or22a)-ab3B(Or85b) arrangement is also observed in other *Drosophila* species (Linz et al., 2013; Stensmyr et al., 2003). These evolutionarily conserved patterns of ORN arrangement point to functional constraints in neuronal organization. They also imply that grouped ORNs have distinguishable functional characteristics. However, beyond ligand specificity (Hallem and Carlson, 2006), little is known about whether and how the large-spike "A" ORN functionally differs from its small-spike neighbor.

In this study, I use a novel experimental approach to provide direct experimental evidence that ephaptic coupling alone is sufficient to drive lateral inhibition between ORNs. In addition, the other primary author of the study, Tin Ki Sang, conducted morphometric analysis based on serial block-face scanning electron microscopy (SBEM) (Denk and Horstmann, 2004) and found that the dominant large-spike "A" ORNs are physically larger than their respective small-spike neighbors. Using the morphometric data, our co-author, Professor Jürgen Reingruber, further conducted circuit modeling of the sensillum. Together, we uncover a surprising functional disparity between compartmentalized ORNs in ephaptic inhibition and elucidate the underlying mechanism. Our study thus establishes the peripheral olfactory system of *Drosophila* as an ideal model to illuminate the impact of ephaptic interaction on circuit function and to determine its general operating principle.

## 2.3 Results

### 2.3.1 Direct evidence of ephaptic inhibition between ORNs

How does one prove that ORNs inhibit each other ephaptically if the inhibition is not mediated by any manipulatable target? I addressed this question by testing whether direct electrical interaction is sufficient to cause inhibition between ORNs. If lateral inhibition proceeds electrically in a sensillum, by means of experimental manipulation, I expect to observe similar cross inhibition between ORNs housed in different yet electrically coupled sensilla. I therefore performed extracellular recordings using a metal electrode to connect the electric fields of two adjacent sensilla, a

manipulation that allows for direct demonstration of the impact of electrical interaction (Van der Goes van Naters, 2013).

In the control experiment examining an individual ab1 sensillum, the sustained spike responses of ab1A and ab1B to a prolonged dose of vinegar (large spikes in Figure 2.1A), top panel, ab1A and ab1B spikes could not be sorted reliably and were thus grouped) were markedly reduced by a pulse of superimposed $CO_2$ that activated ab1C (small spikes). The inhibition of ab1A/B by $CO_2$ was abolished in mutant flies lacking functional $CO_2$ receptors (Jones et al., 2007) (Figure 2.1A, bottom panel), indicating that the inhibition of ab1A/B depends on the excitation of ab1C, consistent with our earlier results by genetic ablation of ab1C (Su et al., 2012).

Next I used a tungsten electrode to impale two adjacent sensilla, ab1 and ab3, in order to connect their electric fields so that the field changes in one sensillum can be detected by ORNs in the other sensillum (Van der Goes van Naters, 2013). This approach eliminates the influence of other possible nonsynaptic mechanisms, such as inhibition mediated by shared odorant binding proteins (Jeong et al., 2013). Using this paradigm, I recorded ORN activity from both ab1 and ab3 sensilla simultaneously (Figure 2.1B, top panel). As predicted, the sustained responses of ab1A/B were similarly inhibited by a superimposed pulse of E2-hexenol that excited the electrically coupled ab3B. The cross-inhibition depended on the electric coupling because withdrawing the tungsten electrode from the ab3 sensillum also abolished the inhibition of ab1A/B by E2-hexenol (Figure 2.1B, middle panel, from the same group of ab1A/B neurons). I note that vinegar did not elicit significant sustained responses in ab3A (Figure 2.1B, bottom panel). Therefore, the inhibition observed in the bridged configuration (Figure 2.1B, top panel) was driven by the activation of electrically coupled ab3B. In control experiments, I showed that the bridged configuration did not cause any change in the responses of individual ORNs (Figure 2.2).

Furthermore, when ab3A was chronically activated by optogenetic stimulation, the sustained response could also be inhibited by a pulse of $CO_2$, which excited ab1C housed in the electrically coupled

sensillum (Figure 2.1C). Together, these results provide direct evidence that the sustained response of one ORN was cross-inhibited by the excitation of another ORN via the interconnected electric fields. In other words, direct

electrical interaction, or ephaptic coupling, is sufficient to drive lateral inhibition between ORNs that share the same electric field.

### 2.3.2 Field response and ephaptic inhibition

I next asked whether the large-spike "A" ORNs are functionally distinguishable from their small-spike neighbors in ephaptic interaction. In earlier work, I showed that lateral inhibition between ORNs is bidirectional: Transient activation of the "B" ORN inhibits the sustained response of the "A" neuron and vice versa (Su et al., 2012). However, it is unclear whether the bidirectional inhibition is equal in strength. To compare directly the strength of A-to-B and B-to-A inhibition is technically challenging because high frequency firing of the large-spike "A" neuron occludes spike activity of the "B" neuron. In addition, the degree of inhibition is influenced by the activity level of both ORNs (Su et al., 2012). To overcome these limitations, I sought to define the strength of ephaptic inhibition by other means.

According to an electric circuit model, neighboring ORNs shared the same electric field, also known as the transepithelial potential, which provides the driving force for odor-induced transduction currents (Vermeulen and Rospars, 2004). As such, activation of one ORN reduces the transepithelial potential, thereby shunting currents away from its neighbor to cause ephaptic inhibition (Su et al., 2012). Thus, the degree to which activation of one ORN reduces the transepithelial potential, which can be measured as a change in the local field potential (LFP), indicates the magnitude of its ephaptic influence. The larger the LFP responses of one ORN, the more it can inhibit its neighbor.

To determine the relationship between ephaptic inhibition and LFP responses, I first identified odorants that strongly and selectively activate only one of the grouped ORNs (henceforth referred to as

"private odorants", Figure. 2.3 and Table 2.1). Using private odorants for the ab2 ORNs (ab2A: methyl acetate; ab2B: ethyl 3-hydroxy butyrate), I recorded LFP responses to 0.5-s pulses of the private odorants, delivered either as individuals or as concurrent binary odor mixtures (Figure 2.4A). If there is no ephaptic inhibition, the LFP response to a binary odor mixture is expected to be the linear sum of the responses to its constituents. Thus, the difference between the linear sum and the measured LFP response indicates the magnitude of ephaptic inhibition.

As expected, I observed bidirectional inhibition using binary odor mixtures. Concurrent activation of ab2B by ethyl 3-hydroxy butyrate attenuated the LFP responses of ab2A to methyl acetate, and so did activation of ab2A to ab2B responses (Figure. 2.4B). Importantly, the degree of inhibition increased with higher LFP responses (Figure. 2.4C). Henceforth, I measured the LFP responses of an ORN to evaluate its ephaptic influence on its neighbor.

### 2.3.3 Grouped ORNs have different maximal field responses

To compare the LFP responses, I first focused on the ab2 ORNs, for which multiple private odorants are available (Table 2.1). When ab2A was stimulated by increasing concentrations of methyl acetate, its LFP responses plateaued at ~23 mV. In comparison, the near-saturated LFP responses elicited by ethyl 3-hydroxy butyrate, a private odorant for ab2B, were markedly smaller, only ~10 mV (Figure 2.5A, top panel). Importantly, the LFP amplitudes were characteristics of the ORNs, regardless of the position of the electrode along the sensillum. I note that ethyl 3-hydroxy butyrate activates ab2B strongly and effectively; at $3\times10^{-4}$ dilution, the odorant elicited a high spike response in ab2B (~250 spikes $s^{-1}$), comparable to the spike responses of ab2A to methyl acetate (Figure 2.6 and Table 2.1). Thus, the difference in the ab2A and ab2B LFP responses is unlikely to have originated from different efficacies of the odorants. To verify this interpretation, I tested another pair of private odorants for the ab2 ORNs (ab2A: ethyl acetate; ab2B: E3-hexenol). I found that the near-saturated LFP response of ab2A remained markedly larger than that of ab2B (Fig. 2.5a, bottom panel).

These results indicate that strong activation of ab2A can reduce the shared electric field more than that of ab2B. In this context, ab2A is the dominant ORN in the pair.

To test whether other large-spike "A" neurons also exert greater ephaptic influence upon their neighbors, I extended our analysis to additional sensillum types, selected on the basis of whether private odorants are available (Table 2.1). In total, our analysis included eight sensilla covering the major sensillum

classes in the antenna and maxillary palp: large basiconic (ab2 and ab3), small basiconic (ab4 and ab5), coeloconic (ac3I and ac3II), trichoid (at4), and palp basiconic (pb1) (de Bruyne et al., 1999; Prieto-Godino et al., 2017; Su et al., 2009).

In five out of the eight sensillum types examined, grouped ORNs exhibited notably different maximal LFP responses, including ORNs housed in the ab2, ab3, ab4, pb1, and ac3II sensilla. In each case where near-saturated responses were observed, the "A" neuron showed greater maximal LFP responses than its small-spike neighbor (Figure 2.5A-E). Analysis of the at4 ORNs could not be completed because their private odorants failed to elicit near-saturated LFP responses even at a high concentration ($10^{-1}$) (Figure 2.5F; see Methods for details).

I note that a small minority of *Drosophila* olfactory sensilla contain ORNs of similar spike amplitudes, such as the ab5 and ac3I sensilla (Figure 2.7). In both cases, the near-saturated LFP responses of the grouped ORNs were nearly indistinguishable (Figure 2.5G, H), suggesting that these neurons exert comparable ephaptic influence upon each other.

Overall, our results indicate that grouped ORNs exhibiting markedly different spike amplitudes likely exert unequal ephaptic influence upon each other, and most large-spike "A" neurons are the dominant neurons in this context. The relative spike amplitudes of grouped ORNs thus indicate the rank order of their ephaptic influence. In agreement with this notion, I found that transient activation of ab1C was more effective than ab1D in inhibiting the sustained response of ab1A ORNs (Figure 2.8).

### 2.3.4 Grouped ORNs have different tendencies to change spike rates

Next I compared the susceptibility of grouped ORNs to ephaptic influence. Using single-sensillum recordings, I simultaneously recorded the LFP responses, which originate in the sensory cilia and reflect transduction currents (Guillet and Bernard, 1972; Nagel and Wilson, 2011), as well as the spike responses, which result from depolarization of the ORN soma. I used the spike/LFP ratio to evaluate the degree to which the neuron alters its spiking rate in relation to changes in its LFP response. For an ORN with a higher spike/LFP ratio, the neuron will experience a greater reduction in its spike response when the shared driving force is diminished by the activation of its neighbor. The ORN will therefore be more susceptible to ephaptic influence.

Upon stimulation, the frequency of ORN spiking is determined by depolarization of the soma, which is the product of the transduction current and somatic input resistance (see Methods). Although the transduction current cannot be measured directly in an in vivo preparation, it is thought to give rise to the LFP responses (Guillet and Bernard, 1972; Kaissling and Thorson, 1980; Nagel and Wilson, 2011). Hence, I used the LFP responses as a proxy for transduction currents in the following analysis.

I first stimulated ab3A and ab3B with 0.5-s pulses of their respective private odorants at increasing concentrations (Figure 2.9A). By plotting the peak spike rate as a function of the peak LFP amplitude (absolute value), I found that the spike/LFP ratio was significantly higher for ab3B (Figure 2.9B), indicating that ab3B is more susceptible to ephaptic influence than ab3A. However, the spiking rate of an insect ORN is determined not only by the amplitude but also by the kinetics of the LFP (Nagel and Wilson, 2011). Thus, the variability in LFP kinetics introduced by differing transduction kinetics or odorant dynamics (Martelli et al., 2013; Nagel and Wilson, 2011) may confound our spike/LFP analysis.

To address this concern, I used an optogenetics approach so that identical stimuli can be used to activate grouped ORNs. When light activated either ab3A or ab3B expressing Channelrhodopsin2

(H134R-ChR2) (Pulver et al., 2009), the LFP responses increased with stimulus intensity (Figure 2.9C). Consistent with our earlier analysis with odor stimulation, the spike/LFP ratio was also significantly higher for ab3B in the optogenetic assay (Figure 2.9D). Of note, a similar spike/LFP relationship was observed even with a lower level of functional H134R-ChR2, achieved by lowering the concentration of retinal fed to flies (Figure 2.10). Therefore, the difference in the spike/LFP ratios between ab3A and ab3B was unlikely to have been affected by the exact expression level of H134R-ChR2.

I note that direct activation of H134R-ChR2 in the soma could in principle also contribute to ORN spike responses. To evaluate the impact of this possibility, I performed additional control experiments. I ectopically expressed Or83c, an odorant receptor tuned to farnesol (Ronderos et al., 2014), in either ab3A or ab3B to allow for direct comparison of their responses to identical odor stimuli. Farnesol ($\leq 2\times10^{-2}$ dilutions) did not activate the cognate receptors of the ab3 ORNs (Figure 2.11A). Analyses of farnesol-induced responses in the Or83c-expressing ab3 ORNs indicated that the spike/LFP ratio was also significantly higher for ab3B (Figure 2.11B, C). This result suggests that somatic activation of H134R-ChR2, if any, is unlikely to have altered the relative spike/LFP relationship between neighboring ORNs.

I then extended the optogenetic analysis to five additional sensillum types, including ab1, ab2, ab4, pb1, and at4. In each case, the small-spike ORNs exhibited significantly higher spike/LFP ratios than the neighboring "A" ORNs (Figure 2.9E), except for the at4 ORNs of which the spike amplitudes were the least distinct (Figure 2.7G). Notably, even in the ab1 sensillum that houses four ORNs, the relative spike amplitudes of the neurons (ab1A $\geq$ ab1B > ab1C > ab1D) remained indicative of the rank order of the spike/LFP ratios (ab1A $\leq$ ab1B < ab1C < ab1D) (Figure 2.9E).

To test whether grouped ORNs with similar spike amplitudes have similar spike/LFP ratios, I examined ab5 and ac3I, the two sensilla which house ORNs of similar spike amplitudes (Figure 2.7H, I). For technical reasons, I could not perform the optogenetic analysis in these sensilla (see Methods

for details). Therefore, I ectopically expressed Or83c in either ab5A or ab5B to compare their responses to the same odorant, farnesol. Analyses of farnesol-induced responses indicated that ab5A and ab5B indeed have similar spike/LFP relationships (Figure 2.12A, B). Consistent with this result, analyses with private odorants for ab5 and ac3I ORNs also suggested that these neighboring neurons exhibit similar spike/LFP relationships (Figure 2.12C-F).

Taken together, our odorant and optogenetic analyses show that in most sensilla, ephaptic interactions are asymmetric in that the large-spike "A" neuron is dominant. This dominance is due to (1) the "A" neuron's greater ability to reduce the shared driving force (measured as LFP responses, Figure 2.5), and (2) its lower susceptibility to ephaptic influence, evaluated by its lower propensity to change spiking rate in response to changes in LFP (Figure 2.9).

### 2.3.5 Overexpression of odorant receptors

What determines the difference in the maximal LFP responses of the "A" and "B" ORNs? One possibility is that the density of odorant receptors expressed in the "B" ORNs is typically lower than in the "A" ORNs. As such, fewer receptors in the "B" neuron can be activated by odor stimulation, resulting in a smaller increase in conductance and subsequently a smaller LFP response. To test this possibility, I overexpressed the cognate receptor, Or85a, together with its obligatory coreceptor Orco (Larsson et al., 2004), in the ab2B ORNs.

In the wild-type control, strong activation of ab2A resulted in a large LFP response (~28 mV), markedly higher than the near-saturated LFP response of ab2B (~12 mV) (Figure 2.13A, left panel). Interestingly, in the ab2B overexpressing Or85a, the maximal LFP response remained similar to that of the control, well below the ab2A counterpart (Figure 2.13A, right panel). That is, overexpression of Or85a did not increase the LFP responses of ab2B. A plausible scenario is that the expression level of endogenous Or85a is already high, likely close to saturation, such that overexpressed Or85a only

replaces the endogenous receptor in the sensory dendrite without further increasing its receptor density. Thus, the smaller LFP response of a "B" ORN is unlikely to have arisen from a lower receptor density.

### 2.3.6 Swapping odorant receptors does not alter the LFP response

Next, I examined the contribution of receptor identity to the maximal LFP responses. In a sensillum, neighboring ORNs express different odorant receptors (Benton et al., 2009; Couto et al., 2005; Fishilevich and Vosshall, 2005). Given that *Drosophila* odorant receptors are ligand-gated cation channels (Butterwick et al., 2018; Sato et al., 2008; Wicher et al., 2008), it is possible that the conductance of the receptors expressed in the "A" ORNs is typically larger than in the "B" neurons. If so, when the cognate receptor of an "A" ORN is replaced by a "B" neuron receptor, one would expect a marked reduction in the maximal LFP response of the neuron.

To test this possibility, I performed receptor-swap experiments in ab4A, of which the cognate receptor is Or7a (Hallem et al., 2004). I chose ab4A because Or7a receptor mutants ($\Delta Or7a^{GAL4}$) are readily available (Lin et al., 2015), and because its small-spike neighbor, ab4B, is narrowly tuned to geosmin (Stensmyr et al., 2012). In $\Delta Or7a^{GAL4}$ mutants, the response of ab4A (Δab4A) to an Or7a ligand, E2-hexenol, is completely abolished. Genetic rescue of Or7a in Δab4A (Δab4A:Or7a) restored the response; the restored LFP dosage curve was similar to that of the wild-type ab4A (Figures 2.14B and 2.5C). When a "B" neuron receptor (Or85a/ab2B) was expressed in ab4A instead (Δab4A:Or85a), the LFP dosage curve to an Or85a ligand, ethyl 3-hydroxy butyrate (Figure 2.13B, left panel), was remarkably similar to that of Δab4A:Or7a to E2-hexenol (Figure 2.13B, right panel). These results suggest that the characteristic near-saturated LFP responses of an ORN are not influenced by receptor density or identity but likely by other ORN features.

What then underlies the asymmetry in ephaptic interactions? The size difference between grouped ORNs is likely a key. In most sensilla, grouped ORNs have differing sizes (Shanbhag et al., 2000), and the large-spike "A" neurons were postulated to have larger dendritic calibers (Gnatzy et al.,

1984; Hansson et al., 1994; Keil, 1984). However, without a genetically encode EM marker, it was impossible to assign ORN identity. Notably, the ORN with a larger soma would have a smaller input resistance, which could account for the smaller spike/LFP ratio of the "A" neurons. In addition, a larger surface area of the sensory dendrites could give rise to a larger maximal LFP response, also characteristic of the "A" neurons. Therefore, we hypothesized that the dominant "A" neuron is larger than its neighbor.

To test this hypothesis, former graduate student from our lab, Tin Ki Tsang, measured the morphometric features of genetically identified ORNs using electron microscopy (EM), and found that morphometric disparity between grouped ORNs underlies their asymmetrical ephaptic interactions. Professor Jürgen Reingruber further used mathematical modeling to explain how the morphometric disparity between ORNs contributes to their asymmetric interactions.

**2.4 Discussion**

I demonstrate here that ephaptic interaction alone is sufficient to influence circuit function by driving lateral inhibition between compartmentalized ORNs. What benefits might this form of direct neuronal interaction provide for olfactory coding? Ephaptic interaction between ORNs shapes timing of spiking in ORNs (Su et al., 2012), thereby allowing for a more elaborately patterned neural code in higher processing centers (Shimizu and Stopfer, 2012). In addition, the rapid kinetics afforded by ephaptic interaction likely permits fast processing of odor-mixture information in the pheriphery (Su et al., 2012).

Surprisingly, I find that across sensillum types, most large-spike "A" neurons can exert greater ephaptic influence onto their neighbors and are also less susceptible to ephaptic influence. Mechanistically, the functional disparity arises from morphometric differences between compartmentalized ORNs. Together, this study describes a highly specialized inhibitory interaction that governs information processing at the earliest stages of olfactory coding. It also establishes the

peripheral olfactory system of *Drosophila* as a model to understand the impact of electric field effects on neural circuit function.

Ephaptic interactions are asymmetric between grouped ORNs with distinct spike amplitudes. Conversely, grouped ORNs exhibiting similar spike amplitudes exert similar ephaptic influence on each other (Figures 2.5G, H and 2.12). This relationship suggests that the extracellular spike amplitude of an ORN and its ephaptic influence are regulated by a common factor. Indeed, as with ephaptic influence, the extracellular spike amplitude of a neuron also negatively correlates with its input resistance (Pettersen and Einevoll, 2008). Thus, the larger ORN in a pair, which has the smaller input resistance, is expected to have larger spike amplitude as well as ephaptic dominance over its neighbor.

In addition to fly ORNs, there are reports of asymmetric inhibition between other primary sensory neurons. For example, in fly vision, R7 and R8 photoreceptors of the same ommatidium inhibit each other synaptically. Interestingly, the mutual inhibition between R7 and R8 is also asymmetric (Schnaitmann et al., 2018). The asymmetry may have arisen from the unequal numbers of reciprocal synapses (Takemura et al., 2015). In the bumblebee galea sensilla, gap junction-mediated inhibitory coupling is unequal between compartmentalized gustatory receptor neurons (Miriyala et al., 2018). Therefore, although the precise mechanisms may vary, asymmetric lateral inhibition between adjacent primary sensory neurons may represent a conserved computational motif whereby sensory inputs are unequally processed at the periphery before being transmitted to higher brain centers.

Ephaptic interactions between ORNs allow odor-mixture information to be processed by the first neurons of an olfactory circuit (Su et al., 2012). To evaluate the extent to which natural odors activate grouped ORNs simultaneously, I surveyed volatile compounds from several food sources for fruitflies (Table 2.2). From 16 fruits and fermented foods, I identified 51 odorants that can excite at least one ORN with responses $\geq$50 spike $s^{-1}$, based on published datasets (de Bruyne et al., 2001; Hallem and Carlson, 2006; Stensmyr et al., 2012). Among them, 30 individual odorants were capable of coactivating neighboring ORNs. For instance, ethyl hexanoate elicited significant responses in both

ab3A and ab3B ORNs (Table 2.2). Strikingly, all of the analyzed odor sources contained volatiles that excited at least one pair of the grouped ORNs, suggesting that grouped fly ORNs are commonly coactivated by natural odors.

What then is the significance of asymmetric lateral inhibition between grouped ORNs? In such a situation, this operation may provide a peripheral mechanism for evaluating countervailing signals and favoring the propagation of the input carried by the large-spike ORNs. In a mixture, odorants that excite the small-spike ORNs are more likely to be masked by odorants activating their large-spike neighbors. In support of this idea, my advisor, Professor Chih-Ying Su, previously found that this coupling effect is powerful enough to influence animal behavior and that activation of ab1A by vinegar odors attenuated the aversiveness of $CO_2$ detected by ab1C (Su et al., 2012). In future studies, it will be important to determine how odorants that excite the large-spike ORNs qualitatively differ from those that excite the small-spike neurons.

## 2.5 Materials and methods

### *Drosophila* stocks

Flies were raised on standard cornmeal medium at 25 °C, ~60% relative humidity in an incubator with a 12-h light/dark cycle. Female CS flies 5–7 days post eclosion were used in all experiments unless noted otherwise. For the ablation (*UAS-rpr*) and optogenetic (*UAS-H134R-ChR2*) experiments, 5-day-old females were used; for the SBEM (*UAS-APEX2*) experiments, 6–8-day-old females were used.

### Single-sensillum recordings

A fly was wedged into the narrow end of a truncated plastic 200-μl pipette tip to expose the antenna, which was subsequently stabilized between a tapered glass microcapillary tube and a coverslip covered with double-sided type (Ng et al., 2017). Single-unit recordings were performed as

follows. Briefly, electrical activity of the ORNs was recorded extracellularly by placing a sharp electrode filled with 0.6× sensillum lymph Ringer solution (Kaissling and Thorson, 1980) into a sensillum and the reference electrode filled with the same Ringer solution was placed in the eye or the clypeus (for at4 recordings). For recordings performed with a tungsten electrode, a tungsten rod (0.01 × 3 inch, 717000, A-M Systems) secured in an electrode holder (ST50-BNC, Syskiyou) was sharpened in 0.5 N NaOH with a microelectrode etcher (EE-1D, Bak Electronics) at 24 V for nine cycles. No more than three sensilla from the same antenna were recorded. All measurements were taken from distinct neurons except for recordings performed using the bridged configuration shown in Figure 2.1B (top and middle panels) and Fig 2.2.

AC signals (100–20k Hz) and DC signals were simultaneously recorded on an NPI EXT-02F amplifier (ALA Scientific Instruments) and digitized at 5 kHz with Digidata 1550 (Molecular Devices). ORN spikes were detected and sorted using threshold search under Event Detection in Clampfit 10 (Molecular Devices). Spike timing data were exported and analyzed in Igor Pro 6.3 (Wavemetrics). Peri-stimulus time histograms were obtained by averaging spike activities in 50-ms bins and smoothed using a binomial filter (Igor Pro 6.3, Wavemetrics).

Sensillum types were identified based on their locations on the antenna or maxillary palp, and their characteristic odor response profiles (de Bruyne et al., 2001; Hallem and Carlson, 2006). For ac3I and ac3II sensilla, sensillum types were determined according to ORN-specific fluorescent labeling (ac3I: *Ir75b-GAL4*; ac3II: *Ir75c-GAL4*) because the response profiles for ac3I and ac3II in *D. melanogaster* are virtually indistinguishable (Prieto-Godino et al., 2017). Based on the location of the fluorescence signals, I recorded from ac3I with a medial mounting position and ac3II with a posterior mounting position (Lin and Potter, 2015).

**Odor stimuli**

Chemicals were >99% pure or of the highest purity available at Sigma-Aldrich unless otherwise specified. Odorants were diluted in paraffin oil unless otherwise noted. Apple cider vinegar (Spectrum, naturals filtered apple cider vinegar) and geosmin were diluted in water, and *trans*-palmitoleic acid (Cayman Chemical) was diluted in ethanol. For odor mixture experiments, individual odorants (2× stock solutions) were mixed either with paraffin oil or with another odorant at 1:1 (v/v) ratio prior to experiments. For short odor pulses, odor stimuli (100 µl applied to a filter disc) were delivered from a Pasteur pipette via a pulse of air (200 ml $min^{-1}$) into the main air stream (2000 ml $min^{-1}$). A Pasteur pipette filled with pure (Figure 2.1 and Figure 2.2) or diluted $CO_2$ ($5\times10^{-2}$, v/v in air, Figure 2.8) was used to deliver $CO_2$ stimuli into the main air stream. Background odor stimuli were delivered from a 125-ml flask containing 3 ml of odor dilutions directly downstream of the main air stream (2000 ml $min^{-1}$).

For palmitoleic acid, 4.5 µl of the freshly diluted odorant was applied to filter paper inserted inside a truncated 200-µl pipette tip. Ethanol was allowed to evaporate for 1 h in a vacuum desiccator prior to experiments. The odor cartridge was positioned around 4 mm away from the antenna as described (Ng et al., 2017). Odor stimulus was delivered via a 500-ms pulse of air (500 ml $min^{-1}$) directly at the antenna in the presence of humidified air flow at 2000 ml$min^{-1}$ from a different direction. Of note, female at4A does not respond to palmitoleic acid as strongly as male at4A in 7-day-old flies (Ng et al., 2019).

**Optogenetic stimulation**

Newly eclosed female flies expressing the H134R-ChR2 transgene in target ORNs were reared in constant darkness for 5 days on fly food supplemented with 100 µM all *trans*-retinal (Sigma) unless otherwise specified. Flies were transferred to fresh retinal food 1 day prior to experiments. A light stimulus was generated via a blue LED (470 nm, Universal LED Illumination System, pE-4000, Cool LED). Light pulses (500-ms duration) were controlled by a shutter (Vincent Associates) driven

by Clampex 10.4 (Molecular Devices). Light output around the position of the recorded antenna was measured with an optical power meter (PMKIT-05-01, Newport Corporation) via a slim profile wand detector (818-ST2/DB, Newport Corporation).

The LFP light responses in the ac3 neurons expressing H134R-ChR2 were too small to be reliably analyzed. Attempts to express H134R-ChR2 in ab5A (Or82a-GAL4) or ab5B (Or47a-GAL4) failed to yield any light responses, despite the observation that the fluorescence of mCherry tag on H134-ChR2 was visible in the target ORNs. Aging the transgenic flies to 14 days old or increasing retinal concentrations in the food did not improve the situation.

**Statistics**

All data presented as mean ± s.e.m. were analyzed using Igor Pro 6.3 or SigmaPlot 13.0. Coefficients and the standard deviations of the linear fits were generated in Igor Pro 6.3. Unpaired two-tailed *t* test was performed in Figure 2.11 for single variable comparison between two groups. Data are presented as mean ± s.e.m. $P < 0.05$ was considered to be statistically significant and is presented as $^{*}P < 0.05$, $^{**}P < 0.01$, or $^{***}P < 0.001$. Statistical significance for linear coefficients was determined by analysis of covariance (ANCOVA) in RStudio using functions within the car package (version3.0-0). Data are presented as coefficient ± s.d. $P < 0.05$ was considered to be statistically significant and the differences are denoted by different letters.

Chapter 2, in part, is a reprint of the material as it appears in Asymmetric ephaptic inhibition between compartmentalized olfactory receptor neurons 2019. Zhang, Ye; Tsang, Tin Ki; Bushong, Eric A.; Li-An Chu; Ann-Shyn Chiang; Ellisman, Mark H.; Reingruber, Jürgen; Su, Chih-Ying, *Nature Communications*, 10, 1560, 2019. The dissertation author and Tin Ki Tsang contributed equally to this paper as primary investigators and authors.

**Figure 2.1. Direct electrical interaction drives lateral inhibition between ORNs.**

**(A)** The sustained response of ab1A and ab1B was cross-inhibited by the transient activation of ab1C. Top: ab1A/B responded (large spikes in trace) to a sustained stimulus of apple cider vinegar ($3x10^{-3}$ dilution, v/v in water, long blue bar). A 500-ms pulse of carbon dioxide ($CO_2$, orange bar above trace) activated ab1C (small spikes). The responses of ab1A and ab1B were inhibited by the $CO_2$ stimulus (decreased frequency of large spikes). In the average spike responses on the right, the orange trace represents the response of ab1C to $CO_2$, and the blue trace represents the response of the large-spike neurons. ab1A and ab1B spikes could not be sorted reliably and were grouped. The sustained responses of the large-spike ORNs (blue traces) are indicated in the parentheses (spikes $sec^{-1}$). Line width indicates s.e.m. Bottom: in the $CO_2$ receptor mutant flies, $CO_2$ did not activate ab1C or inhibit the sustained response of ab1A/B to vinegar. **(B)** Cross inhibition between electrically coupled ORNs. Top: a tungsten electrode was used to electrically couple two adjacent sensilla: ab3 (distal) and ab1 (proximal). Activation of ab1A/B by a sustained stimulus of vinegar ($3x10^{-3}$ dilution) was inhibited by the excitation of ab3B housed in the electrically coupled sensillum by a pulse of E2- hexenol ($10^{-3}$). Middle: when the same two sensilla were no longer electrically coupled, E2- hexenol ceased to inhibit the sustained response of ab1A/B to vinegar. Bottom: when ab3 sensillum was recorded alone, no cross inhibition was observed between ab3A and ab3B by the same odor stimuli. **(C)** A tungsten electrode was used to electrically couple two adjacent sensilla: ab1 (distal) and ab3 (proximal). The sustained ab3A activity in response to optogenetic activation was inhibited by a pulse of $CO_2$, which excited ab1C housed in the electrically coupled sensillum. Light stimulation: 470 nm, 2.66 $\mu W\ mm^{-2}$. Of note, in the bridged configuration, spike amplitudes of the ORNs housed in the distal sensillum are typically smaller than those in the proximal sensillum. $n$=9 for all recordings.

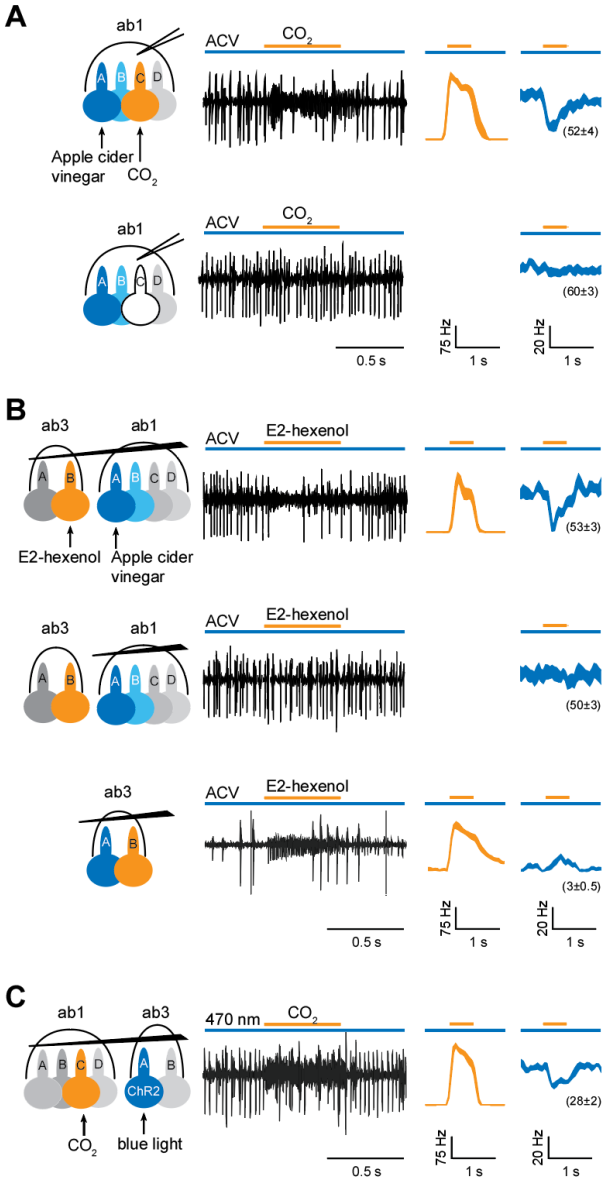
A
ab1
A B C D
Apple cider vinegar
CO2
ACV
CO2
(52±4)
ab1
A B C D
ACV
CO2
(60±3)
0.5 s
75 Hz
1 s
20 Hz
1 s
B
ab3
ab1
A B
A B C D
E2-hexenol
Apple cider vinegar
ACV
E2-hexenol
(53±3)
ab3
ab1
A B
A B C D
ACV
E2-hexenol
(50±3)
ab3
A B
ACV
E2-hexenol
(3±0.5)
0.5 s
75 Hz
1 s
20 Hz
1 s
C
ab1
ab3
A B C D
A B
ChR2
CO2
blue light
470 nm
CO2
(28±2)
0.5 s
75 Hz
1 s
20 Hz
1 s

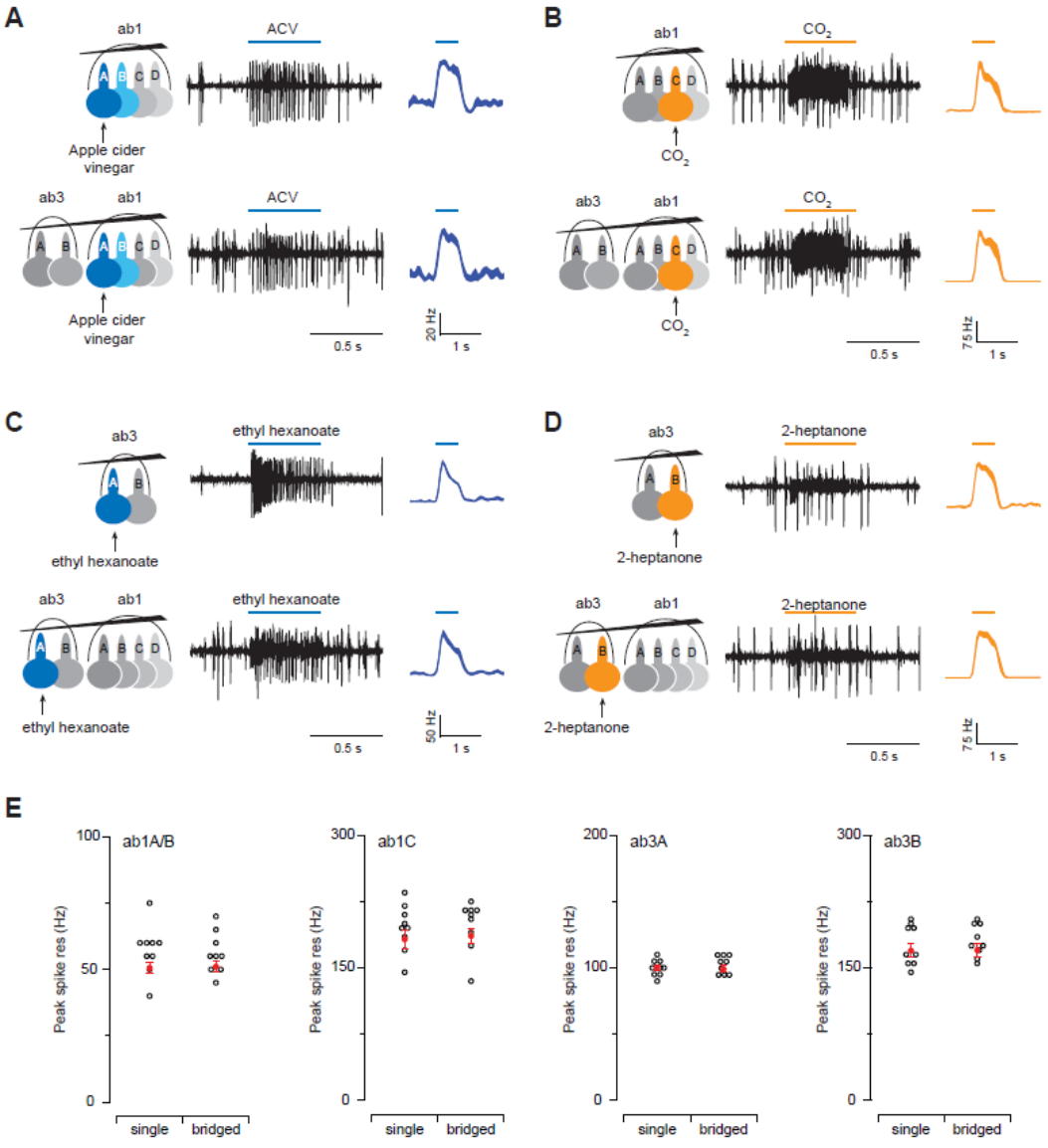


**Figure 2.2. Bridged recording configuration does not change ORN responses.**

**(A)** ab1A/B responses to a pulse of apple cider vinegar (ACV, 3x10-6) were recorded using single-sensillum (top panel) or bridged two-sensillum recording configuration (bottom panel). ab1A and ab1B spikes could not be sorted reliably and were grouped. Distal sensillum: ab3; proximal sensillum: ab1. **(B)** As in **(A)**, except that a pulse of CO2 (~1%) was used to activate ab1C. **(C-D)** As in **(A-B)**, except that a pulse of ethyl hexanoate (3x10-6) was used to activate ab3A **(c)** and a pulse of 2-heptanone (3x10-6) was used to activate ab3B **(D)**. Of note, the spike amplitudes of ab3 ORNs were smaller when recorded using the bridged configuration in the distal sensillum than when recorded in the single-sensillum configuration. **(e)** Quantification of the peak responses, mean ± s.e.m., paired *t*-test.

**Figure 2.3. Identification of private odorants for grouped ORNs.**

Odorants from published datasets were selected to screen for private odorants1-7. **(A)** Top panels: ab2A is strongly activated by methyl acetate (3x10-4 dilution). Sample trace for the spike response (top), ab2A raster plots (middle), and the average ab2A peri-stimulus time histogram (bottom) are shown. Upper right panel: the corresponding LFP response. Line width indicates s.e.m. Bottom panels: a cell death gene, reaper (rpr) is expressed in ab2A to selectively ablate the neuron. In the absence of ab2A, methyl acetate (3x10-4) scarcely elicits any LFP response in the ab2 sensillum, indicating that methyl acetate-elicited LFP responses originate mainly from ab2A activation. $n=9$, mean ± s.e.m., parallel experiments. **(B)** As in **(B)**, except that ab2B responses are shown. Ethyl 3-hydroxy butyrate is a private odorant for ab2B. Genetic ablation of ab2B abolishes the LFP response elicited by ethyl 3-hydroxy butyrate (3x10-4 dilution) in the ab2 sensillum. **(C-D)** Identification of private odorants for ab3A **(C)** and ab3B **(D)**. Single-sensillum recordings and genetic ablation experiments were carried out as described in **(A)**. Private odorants do not elicit significant LFP responses in the absence of the target ORNs. The odorants are not considered "private" above the indicated concentrations because they will also activate the neighboring neurons. $n=9$, mean ± s.e.m., parallel experiments. Similar genetic ablation experiments were conducted to identify private odorants for 7 additional pairs of grouped ORNs (see **Table 2.1** for summary).

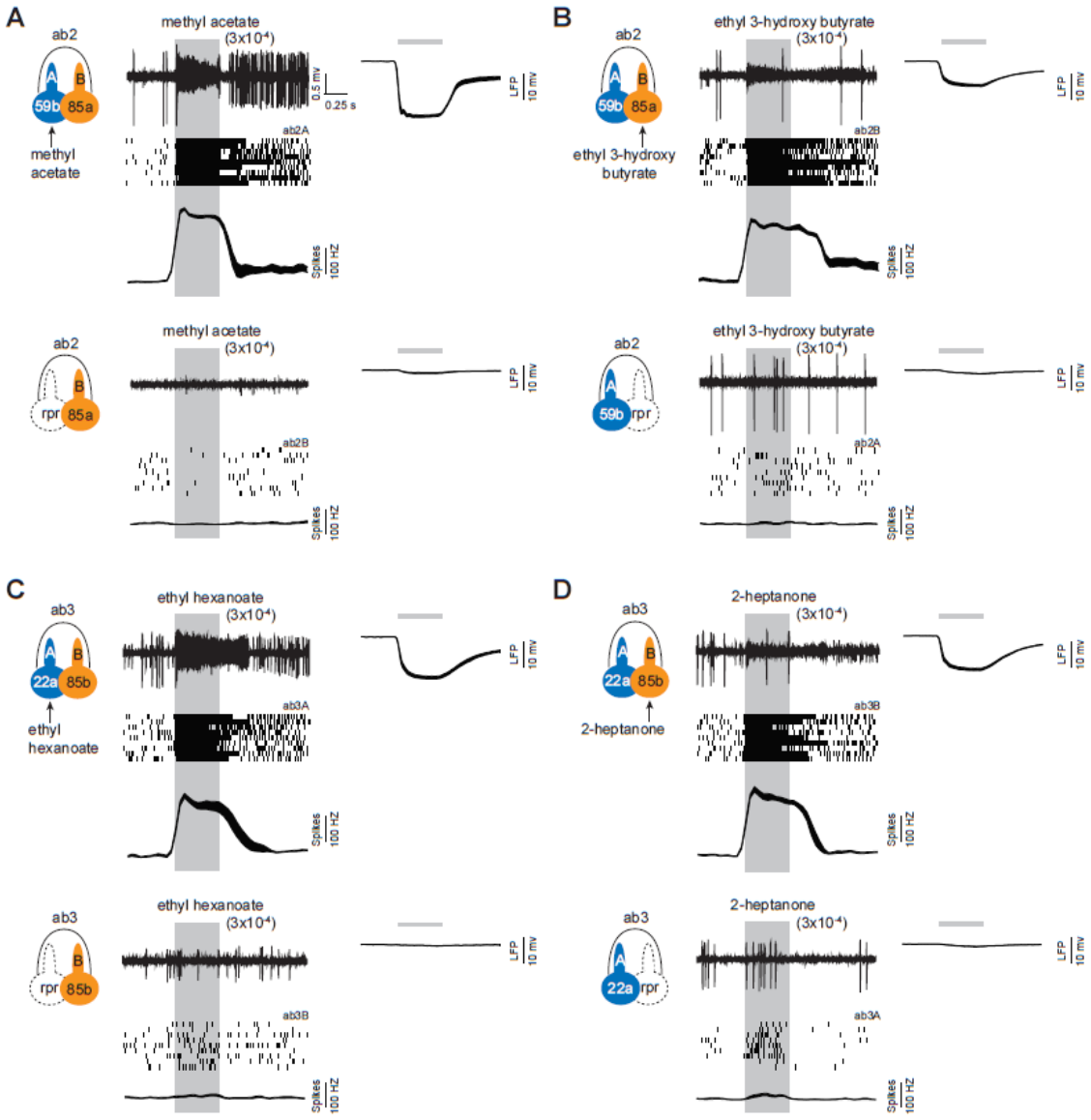
A
ab2
methyl acetate
(3x10⁻⁴)
59b
85a
methyl acetate
ab2A
ab2B
0.5 mv
0.25 s
LFP
10 mv
Spikes
100 HZ
rpr
B
ethyl 3-hydroxy butyrate
C
ab3
ethyl hexanoate
22a
85b
ab3A
ab3B
D
2-heptanone

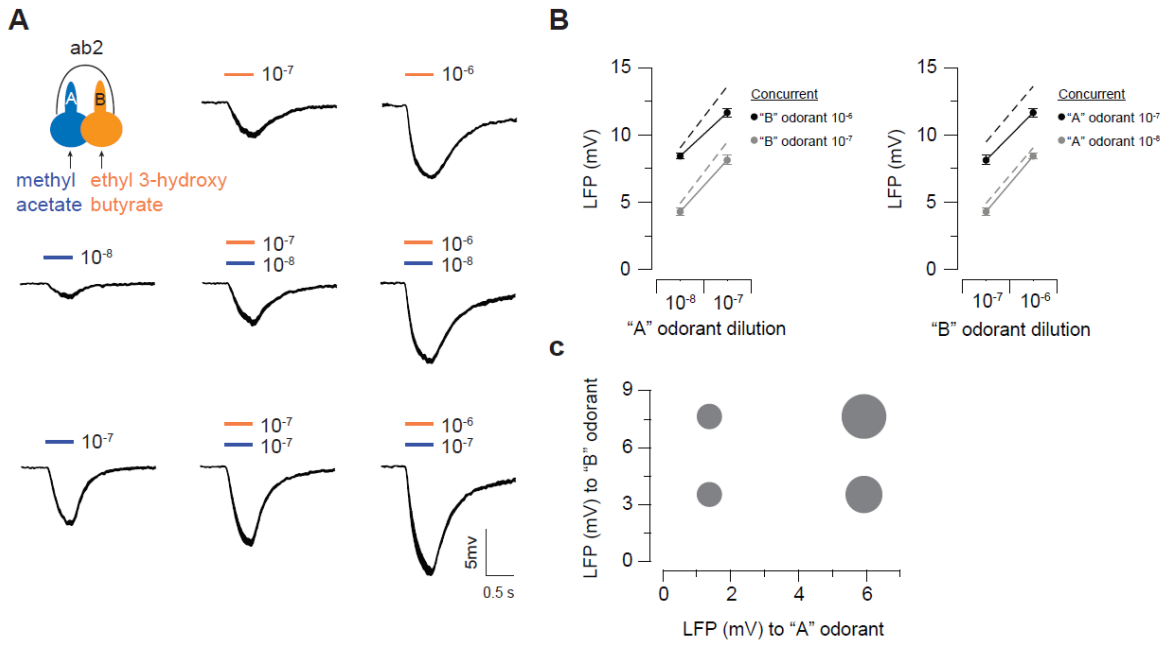


**Figure 2.4. The degree of ephaptic inhibition is influenced by the field responses of grouped ORNs.**

**(A)** LFP responses of the ab2 ORNs to 0.5-sec pulses of their private odorants (ab2A: methyl acetate, blue bar; ab2B: ethyl 3-hydroxy butyrate, orange bar). Odorants were delivered either as individuals or as concurrent binary odor mixtures. *n=8* sensilla, line width indicates s.e.m. **(B)** Peak LFP responses (absolute values) are plotted as a function of odorant dilution for methyl acetate (left panel) or ethyl 3-hydroxy butyrate (right panel). The concentrations of the concurrent odorants that activate the neighboring neurons are indicated. The linear sums of the LFP responses to individual private odorants are connected by dashed lines, predicting the LFP responses to odor mixtures if there is no ephaptic inhibition. The measured LFP responses were smaller than the linear sums, indicating ephaptic inhibition between ORNs, mean ± s.e.m. **(C)** Bubble plot of the magnitude of inhibition in relation to the LFP responses to methyl acetate ("A" odorant, x-axis) or ethyl 3-hydroxy butyrate ("B" odorant, y-axis). Inhibition was determined by subtracting the measured LFP response from the linear sum. The size of the bubble scales with the magnitude of inhibition.

**Figure 2.5. Comparison of the field responses of grouped neurons.**

**(A-F)** Dose-response relationships of grouped ORNs that have distinct extracellular spike amplitudes. **(A)** Left: Spontaneous activity of ab2A (large spike) and ab2B (small spike). Middle: Average local field potential (LFP) responses of ab2A (blue traces) and ab2B (orange traces). Paired ORNs in the same sensilla were recorded in response to their respective private odorants at increasing concentrations. Right: Dose-response relationships of ab2A (blue) and ab2B neurons (orange) to methyl acetate and ethyl 3-hydroxy butyrate (top) or ethyl acetate and E3-hexenol, respectively (bottom). The absolute values of the peak LFP responses are shown. The highest and lowest concentrations of the "A" and "B" odorants are indicated logarithmically on the x-axis and aligned arbitrarily to facilitate comparison. **(B-F)** Additional sensillum types (ab3, ab4, pb1, ac3II and at4) were examined in a similar manner, as shown in **(A)**. **(G-H)** Average LFP responses and dose-response curves of grouped ORNs that exhibit similar extracellular spike amplitudes (**G**: ab5; **H**: ac3I). $n$=9 pairs of ORNs, except for ac3: $n$=6 pairs, mean ± s.e.m. Fit is with the Hill equation.

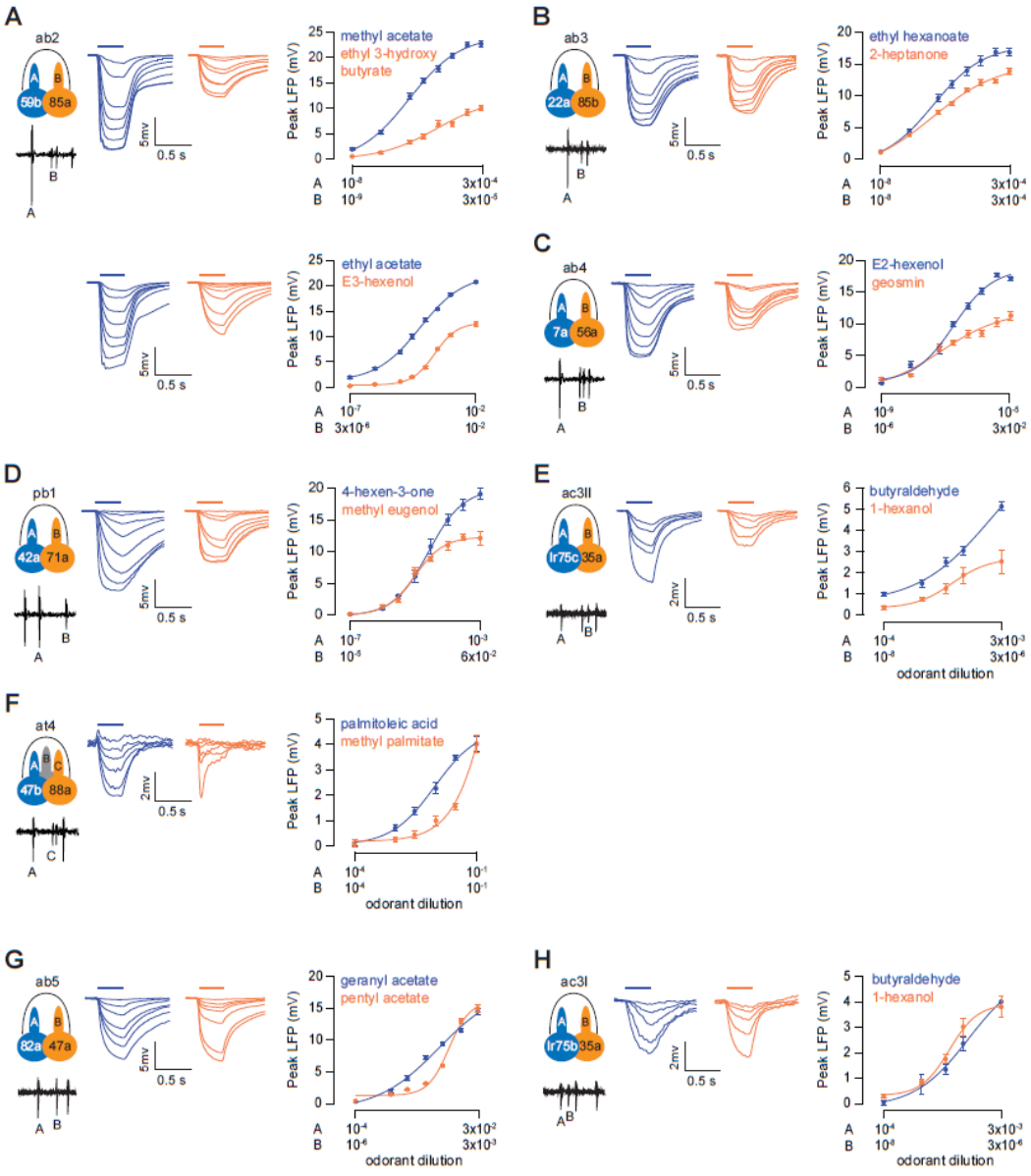
A
ab2
59b
85a
methyl acetate
ethyl 3-hydroxy butyrate
ethyl acetate
E3-hexenol
B
ab3
22a
85b
ethyl hexanoate
2-heptanone
C
ab4
7a
56a
E2-hexenol
geosmin
D
pb1
42a
71a
4-hexen-3-one
methyl eugenol
E
ac3II
Ir75c
35a
butyraldehyde
1-hexanol
F
at4
47b
88a
palmitoleic acid
methyl palmitate
G
ab5
82a
47a
geranyl acetate
pentyl acetate
H
ac3I
Ir75b
35a
butyraldehyde
1-hexanol
Peak LFP (mV)
odorant dilution
5mv
2mv
0.5 s

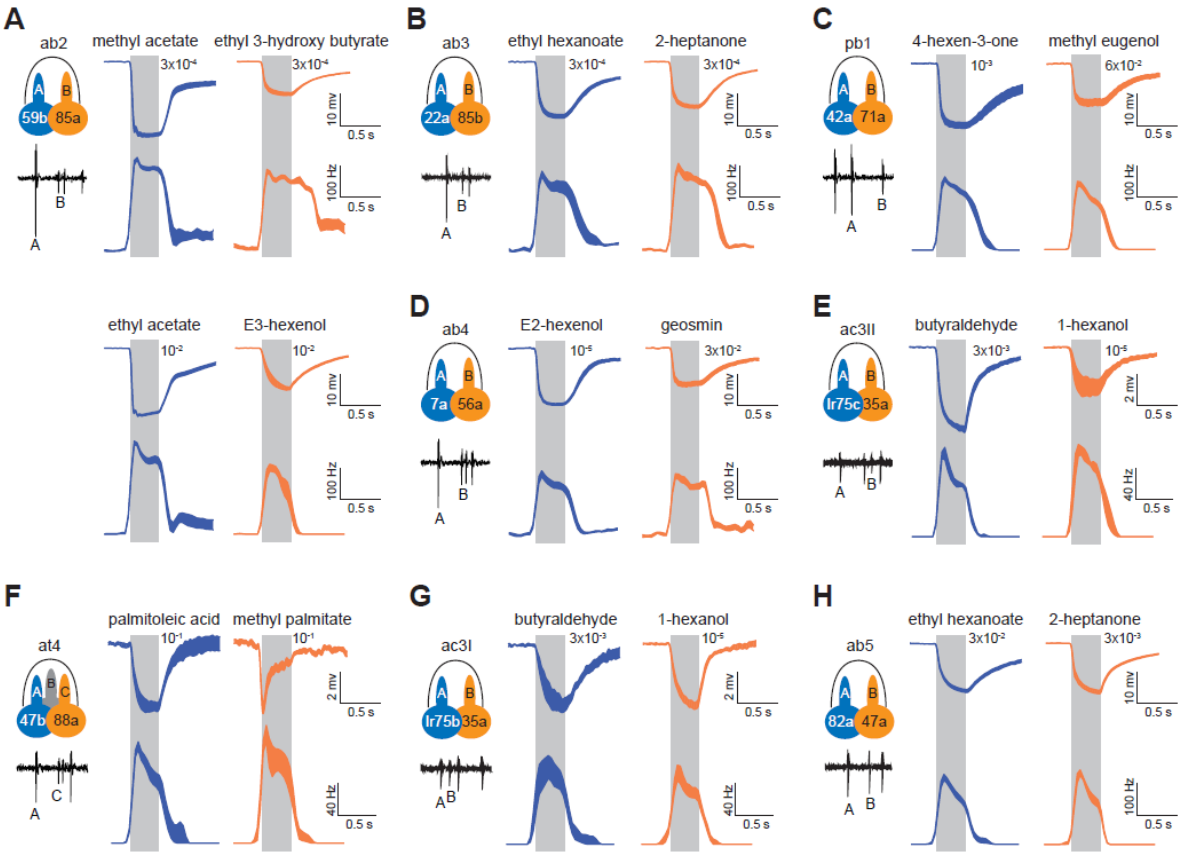


**Figure 2.6. LFP and the corresponding spike responses of grouped ORNs to private odorants.**

ORNs were stimulated with their respective private odorants at the highest possible concentrations (see also **Table 2.1**). Average LFP and the corresponding spike responses are shown for the large-spiking "A" neurons (blue traces) and the small-spiking neighbors (orange traces). Gray rectangles denote periods of odor stimulation (0.5 sec). The concentrations of each odorant are indicated. **(A-H)** Responses were recorded from neighboring neurons housed in the same sensillum. Eight sensillum types were examined (ab2, ab3, ab4, pb1, ac3 type I, ac3 type II, at4). *n=9* pairs of ORNs, except for ac3: *n=6* pairs, line width indicates s.e.m.

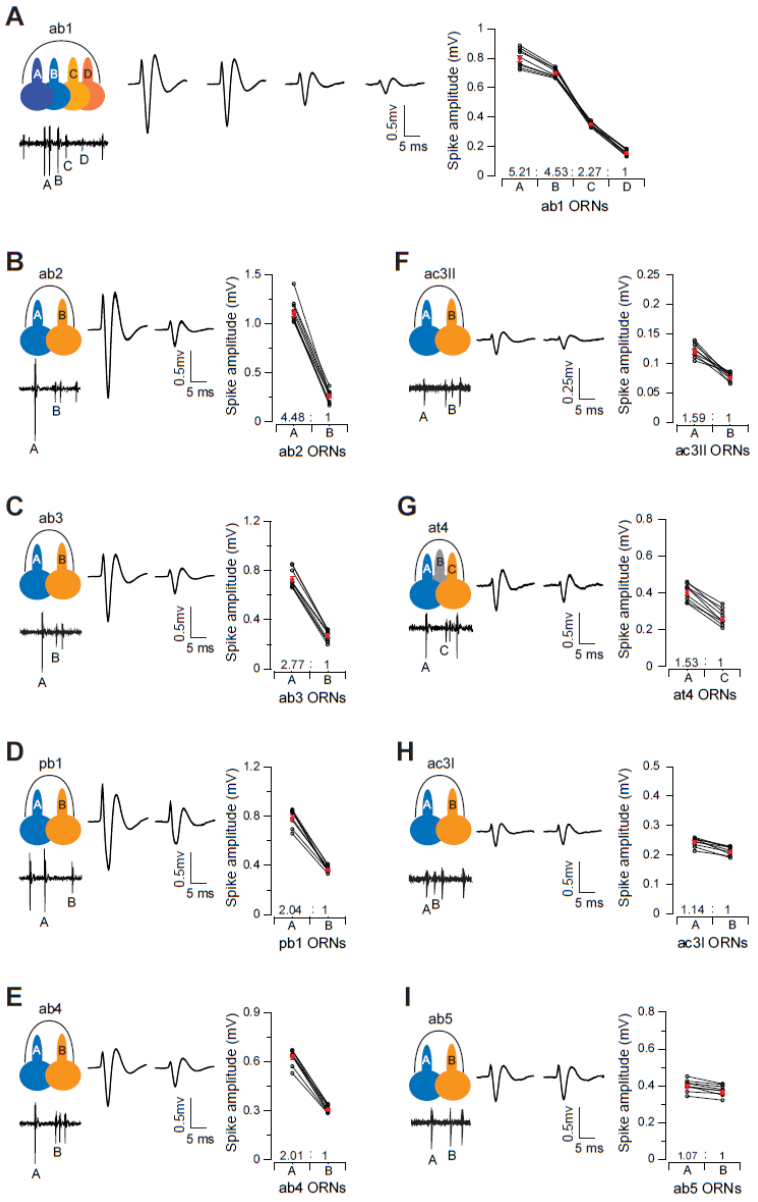


**Figure 2.7. Relative extracellular spike amplitudes of grouped ORNs.**

Spontaneous spike activities from compartmentalized ORNs were recorded to characterize their extracellular spike amplitudes in nine different types of sensilla **(A-I)**. Recordings were bandpass filtered at 100-20k Hz. Left: Average spike waveforms are shown for each of the grouped ORNs. Line width indicates s.e.m. Right: Comparison of the spike amplitudes of compartmentalized ORNs. Each data point represents the average spike amplitude of an ORN based on its spontaneous activity. Lines connect measurements from the same recording. Red dots denote average spike amplitudes. Spike amplitude ratios, relative to the paired ORN with the smallest spike, are indicated for each sensillum types. $n=9$, mean ± s.e.m. Note: for technical issues, the signal-to-noise ratio for ac3 type II is lower than that for other sensillum types and the absolute spike amplitudes may thus be underestimated. See Online **Methods** for the identification of ac3 type I and type II sensilla.

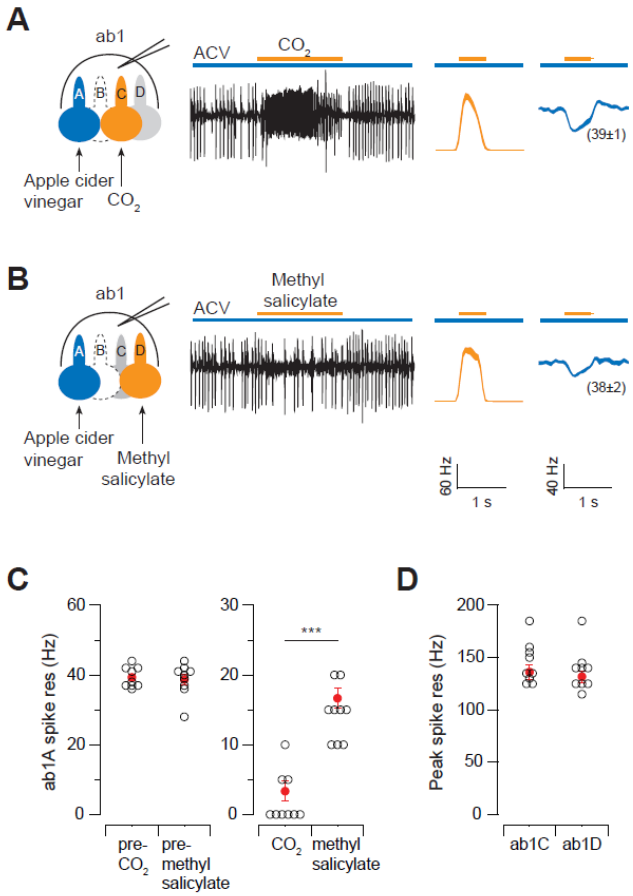


**Figure 2.8. ab1C is more effective than ab1D in inhibiting the chronic response of ab1A.**

**(A)** The sustained response of ab1A was cross-inhibited by the transient activation of ab1C. The ab1B ORNs were ablated by the ectopic expression of a cell death gene, *rpr*. ab1A responded (large spikes in trace) to a sustained stimulus of apple cider vinegar (10-2 dilution, v/v in water, blue bar). A 500-ms pulse of CO2 (5x10-2 dilution, v/v in air, orange bar above trace) activated ab1C (small spikes). In the average spike responses on the right, the orange trace represents the response of ab1C to CO2, and the blue trace represents ab1A response. The sustained spike response of ab1A (blue traces) is indicated in the parentheses (spikes sec-1). Line width indicates s.e.m. **(B)** As in **(A)**, except that ab1D in the same sensillum was activated by methyl salicylate (10-5 dilution, v/v in paraffin oil, orange bar above trace). **(C)** Quantification of the ab1A spike responses before (left) and during CO2 or methyl salicylate stimulation (right). Pre, $P$ = 0.697; During, $P$ = 0.00003 *(n=9)*, paired *t*-test. **(D)** Quantification of the peak spike responses of ab1C and ab1D upon CO2 or methyl salicylate stimulation. Mean ± s.e.m. $P$ = 0.572 *(n=9)*, paired *t*-test.

**Figure 2.9. Comparison of the spiking properties of grouped neurons.**

**(A)** ab3 ORNs were selectively activated by their respective private odorants. Average LFP responses and the corresponding spike responses are shown for ab3A (blue) and ab3B (orange). **(B)** Peak spike responses are plotted as a function of peak LFP responses (left). The absolute values of the peak LFP responses were used for all analyses. Lines indicate linear fits ($y = ax + b$). $n$=9 pairs of ORNs, mean ± s.e.m. The respective "*a"* coefficients (spike/LFP slope) are plotted for comparison (right). Error bars = s.d. **(C-D)** Similar to **(A-B)** except that ab3A and ab3B were activated optogenetically. H134R-Channelrhodopsin2 (ChR2) was expressed in either ab3A or ab3B by the GAL4-UAS system. ORNs were activated by 500-ms pulses of blue light (470 nm, irradiances are indicated above). $n$=9, parallel experiments. **(E)** Optogenetic analyses in five additional sensilla. ORNs expressing H134R-ChR2 were activated by blue light and the peak spike and LFP responses were analyzed as shown in **(D)**. Error bars = s.d. $n$=9, parallel experiments. Statistical analysis was performed with ANCOVA and significant differences ($P < 0.05$) are denoted by different letters.

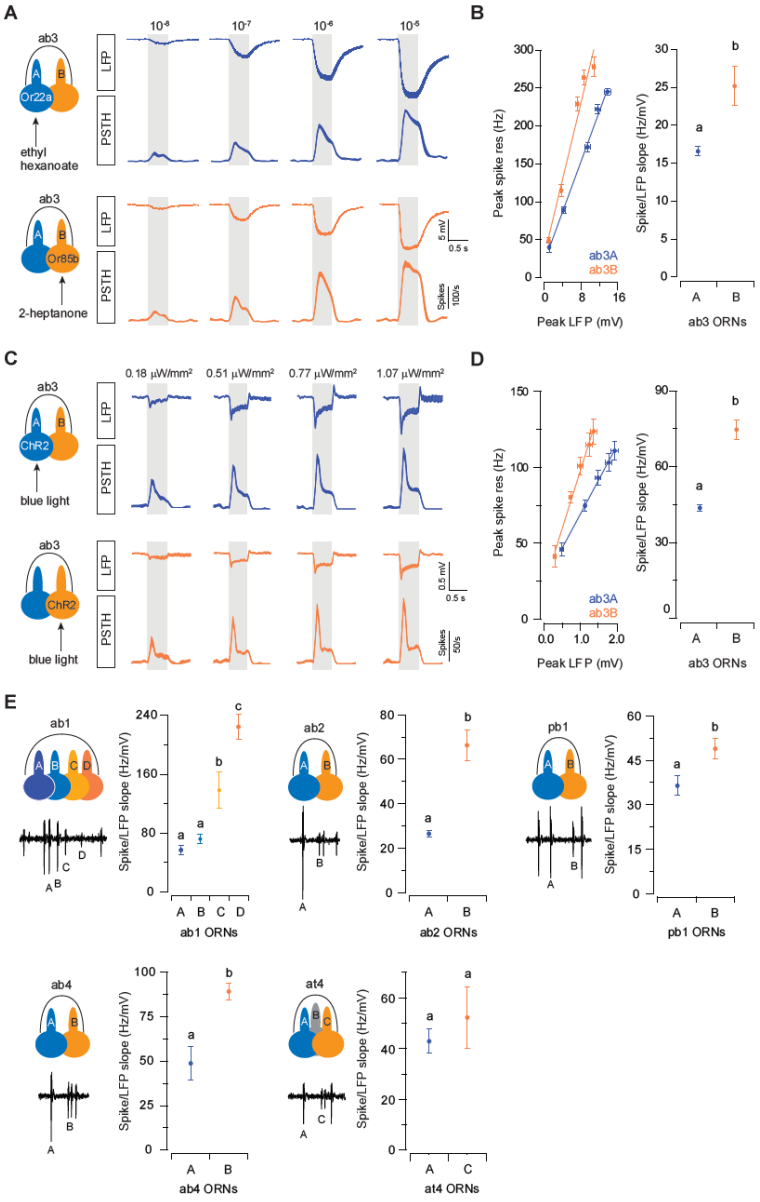
A
ab3
Or22a
ethyl hexanoate
LFP
PSTH
10-8
10-7
10-6
10-5
ab3
Or85b
2-heptanone
5 mV
0.5 s
Spikes 100/s
B
Peak spike res (Hz)
ab3A
ab3B
Peak LFP (mV)
Spike/LFP slope (Hz/mV)
ab3 ORNs
C
0.18 µW/mm²
0.51 µW/mm²
0.77 µW/mm²
1.07 µW/mm²
ChR2
blue light
0.5 mV
Spikes 50/s
D
E
ab1
ab1 ORNs
ab2
ab2 ORNs
pb1
pb1 ORNs
ab4
ab4 ORNs
at4
at4 ORNs

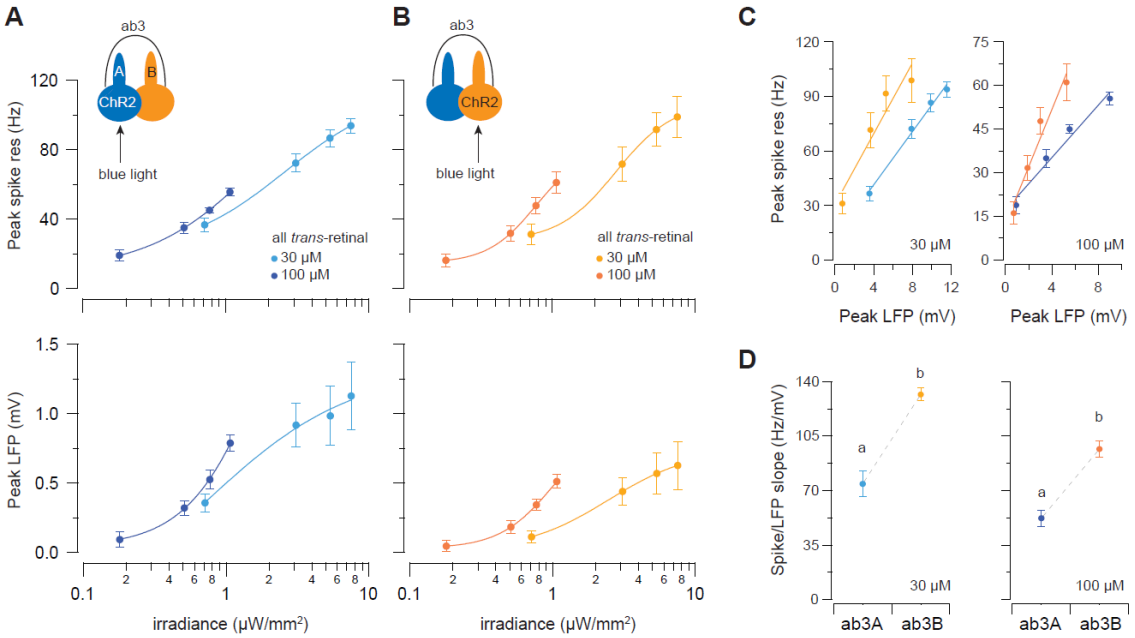


**Figure 2.10. Optogenetic analysis with different retinal concentrations.**

**(A-B)** H134R-Channelrhodopsin2 (ChR2) was expressed in either ab3A **(A)** or ab3B **(B)** by the GAL4-UAS system. Newly emerged female flies were fed with the chromophore, all trans-retinal, at indicated concentrations (30 or 100 µM) for 5 days prior to experiments. ORNs were activated by 500-ms pulses of blue light of graded irradiances. Dose-response curves are shown to demonstrate the peak spike (top panels) and peak LFP responses (bottom panels). Results are from parallel experiments for each retinal concentration. $n$=9, mean ± s.e.m. **(C)** Peak spike responses are plotted as a function of peak LFP responses. Lines indicate linear fits ($y = ax + b$). The spike/LFP relationships are shown based on the retinal concentrations. **(D)** The respective "a" coefficients (spike/LFP slope) for ab3A and ab3B are plotted for comparison. Dotted lines link results from parallel experiments. Statistical analysis was performed with ANCOVA and significant differences ($P < 0.05$) are denoted by different letters. Error bars = s.d.

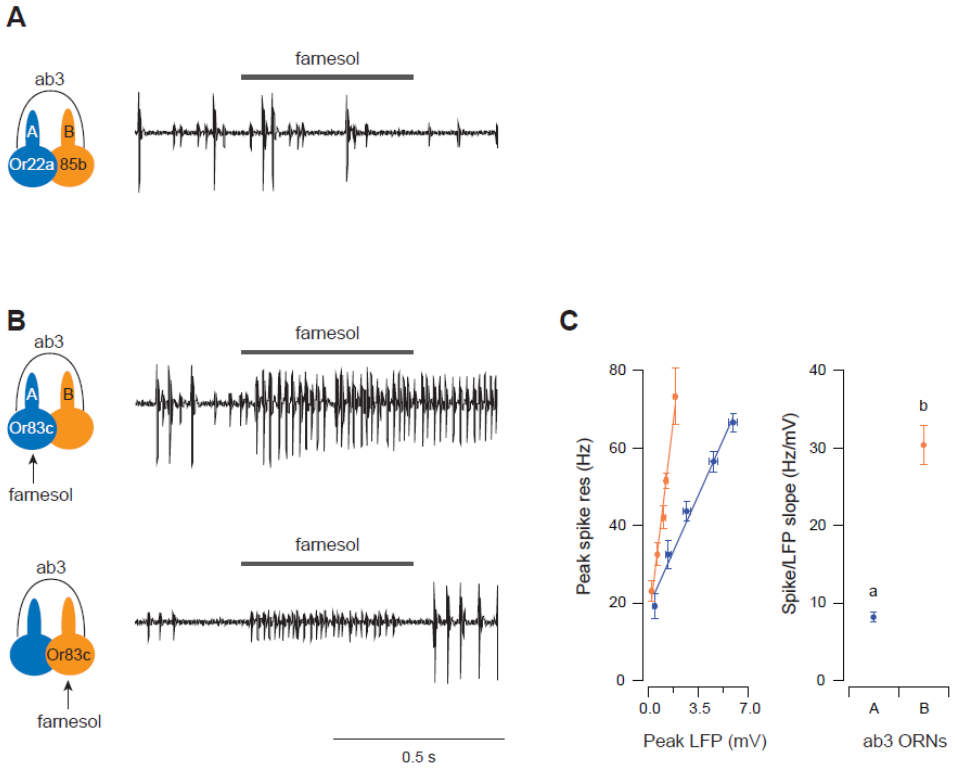


**Figure 2.11. Spike/LFP analysis of ab3 ORNs expressing the Or83c receptor.**

**(A)** Farnesol at 2x10-2 dilution did not activate ab3A or ab3B ORNs in control flies. **(B)** Or83c was ectopically expressed in either ab3A or ab3B using the GAL4-UAS system to confer responses to farnesol in the target ORNs. **(C)** Peak spike responses are plotted as a function of peak LFP responses to different concentrations of farnesol. Left panel: Lines indicate linear fits ($y = ax + b$). $n=9$, mean ± s.e.m. Right panel: The respective "$a$" coefficients (spike/LFP slope) for ab3A and ab3B are plotted for comparison. Error bars = s.d. Statistical analysis was performed with ANCOVA and significant differences ($P < 0.05$) are denoted by different letters.

**Figure 2.12. Spike-LFP analysis in grouped ORNs of similar spike amplitudes.**

**(A-B)** Or83c was ectopically expressed in either ab5A or ab5B using the GAL4-UAS system. ORNs were selectively activated by the odorant, farnesol, at different concentrations. **(A)** Average LFP responses and the corresponding spike responses are shown for ab5A (blue traces) and ab5B ORNs (orange traces). **(B)** Peak spike responses are plotted as a function of peak LFP responses. Left panel: Lines indicate linear fits ($y = ax + b$). $n$=9, mean ± s.e.m. Right panel: The respective "*a"* coefficients (spike/LFP slope) for ab5A and ab5B are plotted for comparison. Error bars = s.d. **(C-F)** Similar to **(A-B)** except that ab5 ORNs **(C-D)** or ac3I ORNs **(E-F)** were selectively activated by their cognate private odorants at different concentrations. $n$=9 pairs of ORNs for **(C-D)** and 6 pairs for **(E-F)**, mean ± s.e.m. Statistical analysis was performed with ANCOVA and significant differences ($P < 0.05$) are denoted by different letters.

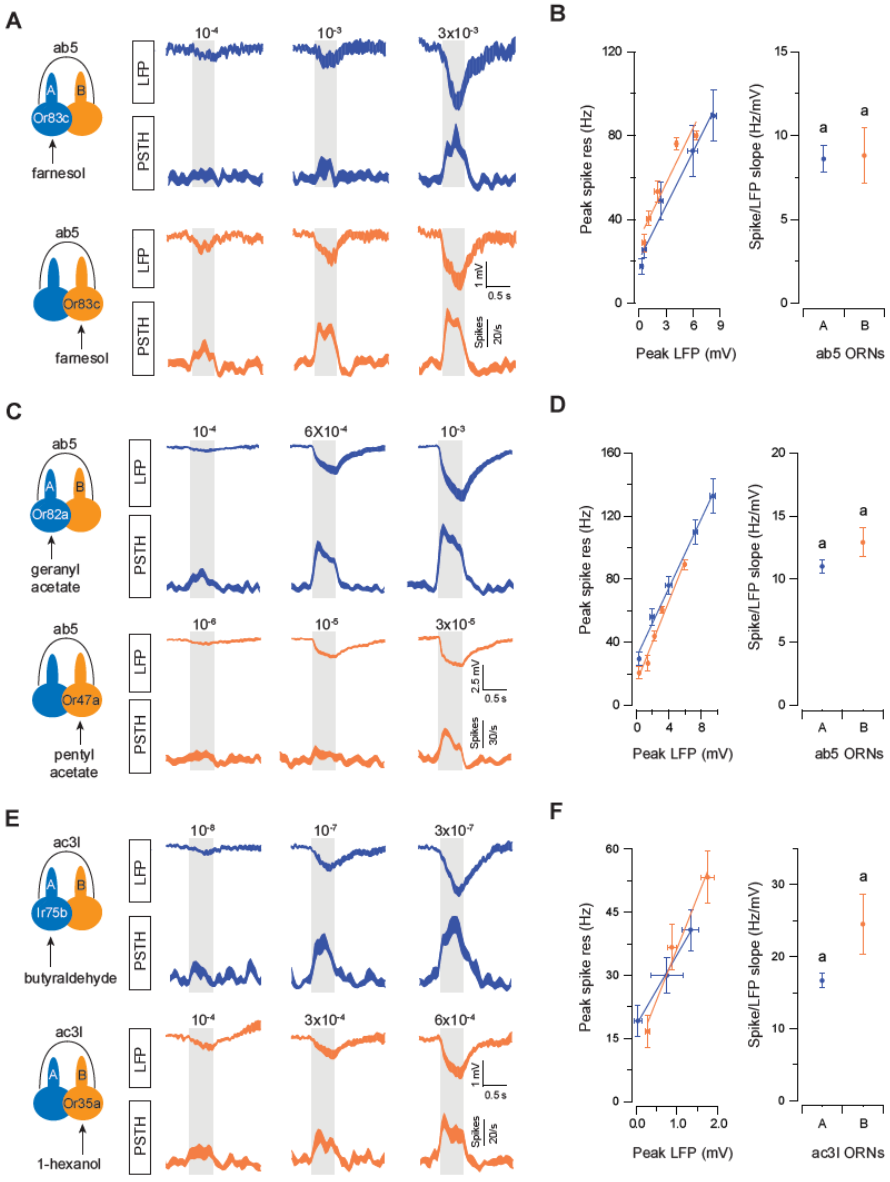
A
ab5
A
B
Or83c
farnesol
LFP
PSTH
10-4
10-3
3x10-3
ab5
Or83c
farnesol
1 mV
0.5 s
Spikes
20/s
B
Peak spike res (Hz)
Peak LFP (mV)
Spike/LFP slope (Hz/mV)
ab5 ORNs
a
C
ab5
Or82a
geranyl acetate
10-4
6X10-4
10-3
ab5
Or47a
pentyl acetate
10-6
10-5
3x10-5
2.5 mV
0.5 s
Spikes
30/s
D
Peak spike res (Hz)
Peak LFP (mV)
Spike/LFP slope (Hz/mV)
ab5 ORNs
E
ac3I
Ir75b
butyraldehyde
10-8
10-7
3x10-7
ac3I
Or35a
1-hexanol
10-4
3x10-4
6x10-4
1 mV
0.5 s
Spikes
20/s
F
Peak spike res (Hz)
Peak LFP (mV)
Spike/LFP slope (Hz/mV)
ac3I ORNs

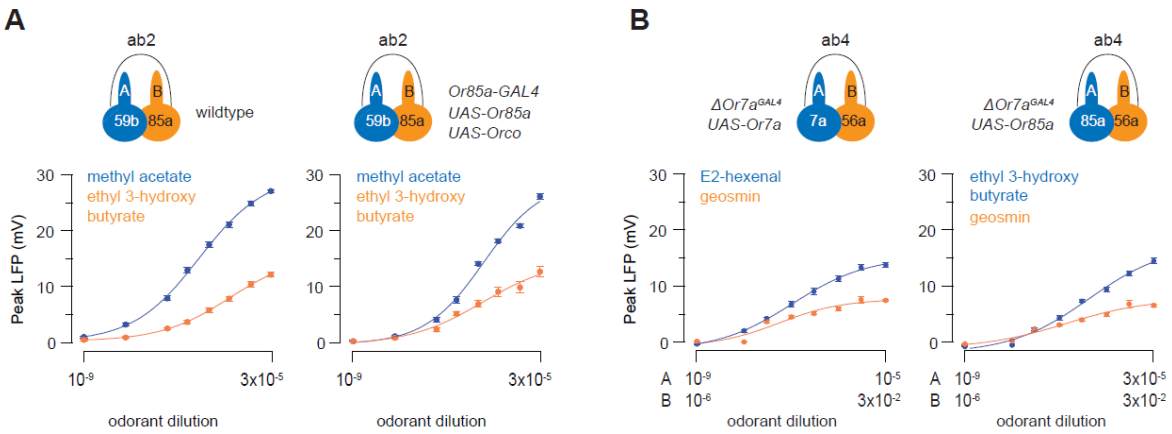


**Figure 2.13. Overexpressing or swapping odorant receptors does not change the maximal LFP responses of an ORN.**

**(A)** Receptor overexpression in the ab2B ORNs. ab2A responded to methyl acetate and ab2B to ethyl 3-hydroxybutyrate. Left panel: in control flies, ab2A had a greater near-saturated LFP response than ab2B (similar results observed in Fig. 2.5A). Right panel: overexpression of the odorant receptor complex, Or85a/Orco, in ab2B did not increase its maximal LFP responses. **(B)** Receptor swap in the ab4A ORNs. Left panel: genetic rescue of Or7a expression in the *ΔOr7a*$^{GAL4}$ mutant flies (Δab4A:Or7a) restored the responses to E2-hexenal. The neighboring neuron, ab4B, responded to geosmin. The rescued ab4A ORNs had a greater near-saturated LFP response than ab4B, as in wildtype flies. The highest and lowest concentrations of the "A" and "B" odorants are indicated logarithmically on the x-axis and aligned arbitrarily to facilitate comparison. Right panel: ectopic expression of Or85a, the cognate receptor of ab2B, in Δab4A resulted in a similar near-saturated LFP response as in Δab4A:Or7a. *n*=9 pairs of ORNs, mean ± s.e.m. All results in **(A)** or **(B)** are from parallel experiments.

**Table 2.1. Private odorants for select ORN pairs in *Drosophila.***

| Sensillum | ORN Pair | | Receptor | Private Odorant | Highest concentration used (v/v dilution in paraffin oil) | Peak spike response (Hz) |
|---|---|---|---|---|---|---|
| Large Basiconic | ab2 | A | Or59b | methyl acetate | 3.00E-04 | 295±4 |
| | | B | Or85a | ethyl 3-hydoxybutyrate | 3.00E-05 | 253±8 |
| | ab2 | A | Or59b | ethyl acetate | 1.00E-02 | 291±6 |
| | | B | Or85a | E3-hexenol | 1.00E-02 | 210±11 |
| | ab3 | A | Or22a | ethyl hexanoate | 3.00E-04 | 252±9 |
| | | B | Or85b | 2-heptanone | 3.00E-04 | 276±10 |
| Small Basiconic | ab4 | A | Or7a | E2-hexenal | 1.00E-05 | 206±10 |
| | | B | Or56a | geosmin | 3.00E-02 | 210±7 |
| | ab5 | A | Or82a | geranyl acetate | 3.00E-02 | 212±9 |
| | | B | Or47a | pentyl acetate | 3.00E-03 | 227±9 |
| | pb1 | A | Or42a | 4-hexen-3-one | 1.00E-03 | 226±6 |
| | | B | Or71a | methyl eugenol | 6.00E-02 | 207±9 |
| Coeloconic | ac3I | A | Ir75b | butyraldehyde | 3.00E-03 | 105±8 |
| | | B | Or35a | 1-hexanol | 1.00E-05 | 109±7 |
| | ac3II | A | Ir75c | butyraldehyde | 3.00E-03 | 98±14 |
| | | B | Or35a | 1-hexanol | 1.00E-05 | 90±10 |
| Trichoid | at4 | A | Or47b | palmitoleic acid | 1.00E-01 | 123±5 |
| | | C | Or88a | methyl palmitate | 1.00E-01 | 138±10 |

**Table 2.2. Responses of paired *Drosophila* ORNs to odorants from natural origins.** Dots indicate spike responses greater than 50 (1/s), based on the functional dataset in Hallem & Carlson (2006) (Hallem and Carlson, 2006).

| Source | Compound | CAS | ab1 | | | ab2 | | ab3 | | ab4 | ab5 | | ab7 | | ab8 | |
|---|---|---|---|---|---|---|---|---|---|---|---|---|---|---|---|---|
| | | | A | B | D | A | B | A | B | A | A | B | A | B | A | B |
| apple (Maarse, 1991) | (E)-2-Hexanal | 6728-26-3 | ● | | | | | | ● | ● | | | | | ● | |
| | Ethyl butanoate | 105-54-4 | | | | | ● | ● | ● | | | ● | ● | ● | ● | ● |
| | (E)-2-Hexenol | 928-95-0 | | | | | ● | ● | ● | ● | | | ● | ● | ● | ● |
| | Hexyl Acetate | 142-92-7 | | | | | | ● | | | | ● | ● | | | |
| | Hexyl butanoate | 2639-63-6 | | | | | | | ● | | | | | | | |
| | hexanal | 66-25-1 | | | | | | ● | ● | ● | | | | | | |
| | 1-Butanol | 71-36-3 | | | | | | ● | | ● | | | | ● | ● | ● |
| | 1-Hexanol | 111-27-3 | ● | | | | ● | ● | ● | ● | ● | ● | ● | ● | ● | ● |
| | (Z)-2-Hexenol | 928-96-1 | | | | | ● | ● | ● | ● | | ● | ● | ● | ● | ● |
| | (E)-2-Hexenyl acetate | 2497-18-9 | | | | | | ● | | ● | | ● | ● | | | |
| | Ethyl Hexanoate | 123-66-0 | | | | | | ● | ● | | | ● | ● | | | |
| orange (Maarse, 1991) | Acetaldehyde | 75-07-0 | | | | ● | | ● | | ● | | | | | | ● |
| | Ethyl acetate | 141-78-6 | ● | ● | | ● | ● | ● | | | | ● | | | ● | |
| | Ethyl propionate | 105-37-3 | | | | ● | | ● | ● | ● | | ● | | | ● | ● |
| | Methyl butanoate | 623-42-7 | | | | ● | | ● | ● | | | ● | ● | ● | ● | ● |
| | ethyl butanoate | 105-54-4 | | | | | ● | ● | ● | | | ● | ● | ● | ● | ● |
| | ethanol | 64-17-5 | | | | | | ● | | | | | | | | |
| | (E)-2-hexen-1-ol | 928-95-0 | | | | | ● | ● | ● | ● | | | ● | ● | ● | ● |
| | (Z)-3-Hexen-1-ol | 928-96-1 | | | | | ● | ● | ● | ● | | ● | ● | ● | ● | ● |
| | linalool | 78-70-6 | | | | | | ● | ● | | | | ● | | | |
| | acetone | 67-64-1 | | | | ● | | | | | | | | | | |
| | 1-propanol | 71-23-8 | | | | | | ● | | | | | | | | ● |
| | butanol | 71-36-3 | | | | | | ● | | ● | | | | ● | ● | ● |
| | 3-methylbutanol | 123-51-3 | | | | | | ● | | ● | ● | | | ● | | ● |
| blackberry and varieties (Maarse, 1991) | 2-heptanone | 110-43-0 | | | | | | ● | ● | | | ● | ● | | ● | ● |
| | hexanol | 111-27-3 | ● | | | | ● | ● | ● | ● | ● | ● | ● | ● | ● | ● |
| | alpha-terpineol | 98-55-5 | | | | | | ● | ● | | | | | | | |
| | octanol | 111-87-5 | | | | | | ● | ● | | | | | | | |
| | (Z)-3-Hexen-1-ol | 928-96-1 | | | | | ● | ● | ● | ● | | ● | ● | ● | ● | ● |
| | (E)-2-Hexen-1-ol | 928-95-0 | | | | | ● | ● | ● | ● | | | ● | ● | ● | ● |
| | linalool | 78-70-6 | | | | | | ● | ● | | | | ● | | | |
| | citronellol | 106-22-9 | | | | | | | | | | | ● | | | |
| | geraniol | 106-24-1 | | | | | | | | | | | ● | | | |
| | (E)-2-Hexenal | 6728-26-3 | ● | | | | | | ● | ● | | | | | ● | |
| | Benzaldehyde | 100-52-7 | | | ● | | | | | ● | | | | | | ● |
| | 2-phenylethanol | 60-12-8 | | | | | | | | | | | | ● | | |
| | eugenol | 97-53-0 | | | ● | | | | | | | | ● | | | |

**Table 2.2. Responses of paired *Drosophila* ORNs to odorants from natural origins (continued).**

| Source | Compound | CAS | ab1 | | | ab2 | | ab3 | | ab4 | ab5 | | ab7 | | ab8 | |
|---|---|---|---|---|---|---|---|---|---|---|---|---|---|---|---|---|
| | | | A | B | D | A | B | A | B | A | A | B | A | B | A | B |
| strawberry (Maarse, 1991) | (E)-2-Hexenal | 6728-26-3 | ● | | | | | | ● | ● | | | | | ● | |
| | (E)-2-Hexenyl acetate | 2497-18-9 | | | | | | ● | | ● | | ● | ● | | | |
| | Methyl butanoate | 623-42-7 | | | | ● | | ● | ● | | | ● | ● | ● | ● | ● |
| | Ethyl butanoate | 105-54-4 | | | | | ● | ● | ● | | | ● | ● | ● | ● | ● |
| | Methyl hexanoate | 106-70-7 | | | | | | ● | ● | | | ● | ● | | ● | ● |
| | Ethyl hexanoate | 123-66-0 | | | | | | ● | ● | | | ● | ● | | | |
| raspberry brandy (Maarse, 1991) | hexanal | 66-25-1 | | | | | | ● | ● | ● | | | | | | |
| | benzaldehyde | 100-52-7 | | | ● | | | | | ● | | | | | | ● |
| | butanol | 71-36-3 | | | | | | ● | | ● | | | | ● | ● | ● |
| | pentanol | 71-41-0 | | | | ● | | ● | ● | ● | ● | ● | ● | ● | ● | ● |
| | hexanol | 111-27-3 | ● | | | | ● | ● | ● | ● | ● | ● | ● | ● | ● | ● |
| | (Z)-3-hexen-1-ol | 928-96-1 | | | | | ● | ● | ● | ● | | ● | ● | ● | ● | ● |
| | octanol | 111-87-5 | | | | | | ● | ● | | | | | | | |
| | ethyl hexanoate | 123-66-0 | | | | | | ● | ● | | | ● | ● | | | |
| | linalool | 78-70-6 | | | | | | ● | ● | | | | ● | | | |
| | geraniol | 106-24-1 | | | | | | | | | | | ● | | | |
| | alpha-terpineol | 98-55-5 | | | | | | ● | ● | | | | | | | |
| | hexyl acetate | 142-92-7 | | | | | | ● | | | | ● | ● | | | |
| | ethyl benzoate | 93-89-0 | | | ● | | | | | | | | ● | | | |
| guava (Chen et al., 2006; Chyau et al., 1992) | ethyl acetate | 141-78-6 | ● | ● | | ● | ● | ● | | | | ● | | | ● | |
| | methyl butanoate | 623-42-7 | | | | ● | | ● | ● | | | ● | ● | ● | ● | ● |
| | ethyl butyrate | 105-54-4 | | | | | ● | ● | ● | | | ● | ● | ● | ● | ● |
| | hexanal | 66-25-1 | | | | | | ● | ● | ● | | | | | | |
| | (E)-2-hexanal | 6728-26-3 | ● | | | | | | ● | ● | | | | | ● | |
| | (Z)-3-hexenol | 928-96-1 | | | | | ● | ● | ● | ● | | ● | ● | ● | ● | ● |
| | hexanol | 111-27-3 | ● | | | | ● | ● | ● | ● | ● | ● | ● | ● | ● | ● |
| | methyl hexanoate | 106-70-7 | | | | | | ● | ● | | | ● | ● | | ● | ● |
| | benzaldehyde | 100-52-7 | | | ● | | | | | ● | | | | | | ● |
| | 6-methyl-5-hepten-2-one | 110-93-0 | | | | | | ● | ● | | ● | | ● | | | ● |
| | ethyl hexanoate | 123-66-0 | | | | | | ● | ● | | | ● | ● | | | |
| | hexyl acetate | 142-92-7 | | | | | | ● | | | | ● | ● | | | |
| | hexanoic acid | 142-62-1 | | | | | | ● | | | | | | | | |
| | linalool | 78-70-6 | | | | | | ● | ● | | | | ● | | | |
| | ethyl benzoate | 93-89-0 | | | ● | | | | | | | | ● | | | |
| | alpha-terpineol | 98-55-5 | | | | | | ● | ● | | | | | | | |
| | ethyl octanoate | 106-32-1 | | | | | | ● | | | | | | | | |
| | ethyl propionate | 105-37-3 | | | | ● | | ● | ● | ● | | ● | | | ● | ● |
| | propyl acetate | 109-60-4 | | | ● | ● | | ● | ● | | | ● | ● | ● | ● | ● |
| | ethyl 2-butenoate | 623-70-1 | | | ● | | ● | ● | ● | | | | ● | | ● | ● |
| | (E)-2-hexeno-1-ol | 928-95-0 | | | | | ● | ● | ● | ● | | | ● | ● | ● | ● |

**Table 2.2. Responses of paired *Drosophila* ORNs to odorants from natural origins (continued).**

| Source | Compound | CAS | ab1 | | | ab2 | | ab3 | | ab4 | ab5 | | ab7 | | ab8 | |
|---|---|---|---|---|---|---|---|---|---|---|---|---|---|---|---|---|
| | | | A | B | D | A | B | A | B | A | A | B | A | B | A | B |
| passion fruit (Macoris et al., 2011; Stensmyr et al., 2001) | propyl acetate | 109-60-4 | | | ● | ● | | ● | ● | | | ● | ● | ● | ● | ● |
| | methyl butanoate | 623-42-7 | | | | ● | | ● | ● | | | ● | ● | ● | ● | ● |
| | ethyl butanoate | 105-54-4 | | | | | ● | ● | ● | | | ● | ● | ● | ● | ● |
| | butyl acetate | 123-86-4 | | | ● | | | ● | ● | | | ● | ● | | ● | ● |
| | hexanal | 66-25-1 | | | | | | ● | ● | ● | | | | | | |
| | 3-methylbutyl acetate | 123-92-2 | | | ● | | | ● | ● | | | ● | ● | | ● | ● |
| | 1-butanol | 71-36-3 | | | | | | ● | | ● | | | | ● | ● | ● |
| | ethyl hexanoate | 123-66-0 | | | | | | ● | ● | | | ● | ● | | | |
| | hexyl acetate | 142-92-7 | | | | | | ● | | | | ● | ● | | | |
| | 1-hexanol | 111-27-3 | ● | | | | ● | ● | ● | ● | ● | ● | ● | ● | ● | ● |
| | cis-3-hexen1-ol | 928-96-1 | | | | | ● | ● | ● | ● | | ● | ● | ● | ● | ● |
| | hexyl butanoate | 2639-63-6 | | | | | | | ● | | | | | | | |
| | geraniol | 106-24-1 | | | | | | | | | | | ● | | | |
| | linalool | 78-70-6 | | | | | | ● | ● | | | | ● | | | |
| cider apple juice (Pello-Palma et al., 2017; Xu et al., 2007) | ethyl acetate | 141-78-6 | ● | ● | | ● | ● | ● | | | | ● | | | ● | |
| | ethyl propanoate | 105-37-3 | | | | ● | | ● | ● | ● | | ● | | | ● | ● |
| | butyl acetate | 123-86-4 | | | ● | | | ● | ● | | | ● | ● | | ● | ● |
| | hexanal | 66-25-1 | | | | | | ● | ● | ● | | | | | | |
| | isopentyl acetate | 123-92-2 | | | ● | | | ● | ● | | | ● | ● | | ● | ● |
| | 1-butanol | 71-36-3 | | | | | | ● | | ● | | | | ● | ● | ● |
| | hexyl acetate | 142-92-7 | | | | | | ● | | | | ● | ● | | | |
| | 6-methyl-5-hepten-2-one | 110-93-0 | | | | | | ● | ● | | ● | | ● | | | ● |
| | hexanol | 111-27-3 | ● | | | | ● | ● | ● | ● | ● | ● | ● | ● | ● | ● |
| | trans-2-hexen-1-ol | 928-95-0 | | | | | ● | ● | ● | ● | | | ● | ● | ● | ● |
| | scetaldehyde | 75-07-0 | | | | ● | | ● | | ● | | | | | | ● |
| | ethyl acetate | 141-78-6 | ● | ● | | ● | ● | ● | | | | ● | | | ● | |
| | 2-methylpropyl acetate | 110-19-0 | | | ● | | | ● | ● | | | ● | ● | ● | ● | ● |
| | ethyl butanoate | 105-54-4 | | | | | ● | ● | ● | | | ● | ● | ● | ● | ● |
| | butyl acetate | 123-86-4 | | | ● | | | ● | ● | | | ● | ● | | ● | ● |
| | pentyl acetate | 628-63-7 | ● | | | ● | | ● | ● | | | ● | ● | | ● | ● |
| | methyl hexanoate | 106-70-7 | | | | | | ● | ● | | | ● | ● | | ● | ● |
| | ethyl hexanoate | 123-66-0 | | | | | | ● | ● | | | ● | ● | | | |
| | methyl octanoate | 111-11-5 | | | | | | ● | ● | | | ● | | | | |
| | ethyl octanoate | 106-32-1 | | | | | | ● | | | | | | | | |
| | 1-octanol | 111-87-5 | | | | | | ● | ● | | | | | | | |
| | 4-terpineol | 98-55-5 | | | | | | ● | ● | | | | | | | |
| | butanoic acid | 107-92-6 | | | | | | ● | | | | | | | | ● |
| | ethyl benzoate | 93-89-0 | | | ● | | | | | | | | ● | | | |
| | hexanoic acid | 142-62-1 | | | | | | ● | | | | | | | | |
| | phenyl alcohol | 60-12-8 | | | | | | | | | | | | ● | | |
| | eugenol | 97-53-0 | | | ● | | | | | | | | ● | | | |

**Table 2.2. Responses of paired *Drosophila* ORNs to odorants from natural origins (continued).**

| Source | Compound | CAS | ab1 | | | ab2 | | ab3 | | ab4 | ab5 | | ab7 | | ab8 | |
|---|---|---|---|---|---|---|---|---|---|---|---|---|---|---|---|---|
| | | | A | B | D | A | B | A | B | A | A | B | A | B | A | B |
| sourdough (Pinu and Villas-boas, 2017) | Ethanol | 64-17-5 | | | | | | ● | | | | | | | | |
| | butyric acid | 107-92-6 | | | | | | ● | | | | | | | | ● |
| | 2,3 butanediol | 513-85-9 | | | | | | ● | | | | | | | ● | ● |
| | phenylethyl alcohol | 60-12-8 | | | | | | | | | | | | ● | | |
| beer (Pinu and Villas-boas, 2017) | Ethanol | 64-17-5 | | | | | | ● | | | | | | | | |
| | butyric acid | 107-92-6 | | | | | | ● | | | | | | | | ● |
| | 2,3 butanediol | 513-85-9 | | | | | | ● | | | | | | | ● | ● |
| | isoamyl alcohol | 123-51-3 | | | | | | ● | | ● | ● | | | ● | | ● |
| | 1-butanol | 71-36-3 | | | | | | ● | | ● | | | | ● | ● | ● |
| | phenylethyl alcohol | 60-12-8 | | | | | | | | | | | | ● | | |
| | Diethyl succinate | 123-25-1 | | | | | | ● | | | | | | | | |
| red wine (Pinu and Villas-boas, 2017; Torrens et al., 2004) | Ethanol | 64-17-5 | | | | | | ● | | | | | | | | |
| | butyric acid | 107-92-6 | | | | | | ● | | | | | | | | ● |
| | 2,3 butanediol | 513-85-9 | | | | | | ● | | | | | | | ● | ● |
| | isoamyl alcohol | 123-51-3 | | | | | | ● | | ● | ● | | | ● | | ● |
| | 1-butanol | 71-36-3 | | | | | | ● | | ● | | | | ● | ● | ● |
| | phenylethyl alcohol | 60-12-8 | | | | | | | | | | | | ● | | |
| | isobutyl acetate | 110-19-0 | | | ● | | | ● | ● | | | ● | ● | ● | ● | ● |
| | ethyl butyrate | 105-54-4 | | | | | ● | ● | ● | | | ● | ● | ● | ● | ● |
| | propanol | 71-23-8 | | | | | | ● | | | | | | | | ● |
| | isoamyl acetate | 123-92-2 | | | ● | | | ● | ● | | | ● | ● | | ● | ● |
| | ethyl hexanoate | 123-66-0 | | | | | | ● | ● | | | ● | ● | | | |
| | hexyl acetate | 142-92-7 | | | | | | ● | | | | ● | ● | | | |
| | ethyl lactate | 97-64-3 | | | | ● | | ● | ● | | | | ● | ● | ● | ● |
| | hexanol | 111-27-3 | ● | | | | ● | ● | ● | ● | ● | ● | ● | ● | ● | ● |
| | cis-3-hexenol | 928-96-1 | | | | | ● | ● | ● | ● | | ● | ● | ● | ● | ● |
| | trans-2-hexenol | 928-95-0 | | | | | ● | ● | ● | ● | | | ● | ● | ● | ● |
| | 1-Octen-3-ol | 3391-86-4 | | | | | | ● | ● | | | ● | ● | | | ● |
| | Furfural | 98-01-1 | | | | ● | | | ● | ● | | | | | | ● |
| | benzaldegyde | 100-52-7 | | | ● | | | | | ● | | | | | | ● |
| | linalool | 78-70-6 | | | | | | ● | ● | | | | ● | | | |
| | gamma-butyrolactone | 96-48-0 | | | | | | | | | | | | | | ● |
| | alpha-terpineol | 98-55-5 | | | | | | ● | ● | | | | | | | |
| | citronellol | 106-22-9 | | | | | | | | | | | ● | | | |
| | geraniol | 106-24-1 | | | | | | | | | | | ● | | | |
| | hexanoic acid | 142-62-1 | | | | | | ● | | | | | | | | |
| | eugenol | 97-53-0 | | | ● | | | | | | | | ● | | | |

**Table 2.2. Responses of paired *Drosophila* ORNs to odorants from natural origins (continued).**

| Source | Compound | CAS | ab1 | | | ab2 | | ab3 | | ab4 | ab5 | | ab7 | | ab8 | |
|---|---|---|---|---|---|---|---|---|---|---|---|---|---|---|---|---|
| | | | A | B | D | A | B | A | B | A | A | B | A | B | A | B |
| white wine (Pinu and Villas-boas, 2017; Torrens et al., 2004) | Ethanol | 64-17-5 | | | | | | ● | | | | | | | | |
| | butyric acid | 107-92-6 | | | | | | ● | | | | | | | | ● |
| | 2,3 butanediol | 513-85-9 | | | | | | ● | | | | | | | ● | ● |
| | cis-3-hexen-1-ol | 928-96-1 | | | | | ● | ● | ● | ● | | ● | ● | ● | ● | ● |
| | isoamyl alcohol | 123-51-3 | | | | | | ● | | ● | ● | | | ● | | ● |
| | phenylethyl alcohol | 60-12-8 | | | | | | | | | | | | ● | | |
| | ethyl caprylate | 106-32-1 | | | | | | ● | | | | | | | | |
| | hexyl acetate | 142-92-7 | | | | | | ● | | | | ● | ● | | | |
| | Diethyl succinate | 123-25-1 | | | | | | ● | | | | | | | | |
| | isobutyl acetate | 110-19-0 | | | ● | | | ● | ● | | | ● | ● | ● | ● | ● |
| | ethyl butyrate | 105-54-4 | | | | | ● | ● | ● | | | ● | ● | ● | ● | ● |
| | propanol | 71-23-8 | | | | | | ● | | | | | | | | ● |
| | isoamyl acetate | 123-92-2 | | | ● | | | ● | ● | | | ● | ● | | ● | ● |
| | ethyl hexanoate | 123-66-0 | | | | | | ● | ● | | | ● | ● | | | |
| | hexanol | 111-27-3 | ● | | | | ● | ● | ● | ● | ● | ● | ● | ● | ● | ● |
| | cis-3-hexenol | 928-96-1 | | | | | ● | ● | ● | ● | | | ● | ● | ● | ● |
| | 1-Octen-3-ol | 3391-86-4 | | | | | | ● | ● | | | ● | ● | | | ● |
| | benzaldegyde | 100-52-7 | | | ● | | | | | ● | | | | | | ● |
| | linalool | 78-70-6 | | | | | | ● | ● | | | | ● | | | |
| | alpha-terpineol | 98-55-5 | | | | | | ● | ● | | | | | | | |
| | citronellol | 106-22-9 | | | | | | | | | | | ● | | | |
| | geraniol | 106-24-1 | | | | | | | | | | | ● | | | |
| | hexanoic acid | 142-62-1 | | | | | | ● | | | | | | | | |
| vinegar (Qian et al., 2013) | furfural | 98-01-1 | | | | ● | | | ● | ● | | | | | | ● |
| | butanoic acid | 107-92-6 | | | | | | ● | | | | | | | | ● |
| | hexanoic acid | 142-62-1 | | | | | | ● | | | | | | | | |
| | 2-phenylethanol | 60-12-8 | | | | | | | | | | | | ● | | |
| papaya (Stensmyr et al., 2001) | meso-2,3-butanediol | 513-85-9 | | | | | | ● | | | | | | | ● | ● |
| | Isoamyl acetate | 123-92-2 | | | ● | | | ● | ● | | | ● | ● | | ● | ● |
| | Isoamyl alcohol | 123-51-3 | | | | | | ● | | ● | ● | | | ● | | ● |
| | linalool | 78-70-6 | | | | | | ● | ● | | | | ● | | | |
| | phenylacetaldehyde | 122-78-1 | | | ● | | | | | | | | | | | |
| lichi (Stensmyr et al., 2001) | meso-2,3-butanediol | 513-85-9 | | | | | | ● | | | | | | | ● | ● |
| | citronellol | 106-22-9 | | | | | | | | | | | ● | | | |
| | geraniol | 106-24-1 | | | | | | | | | | | ● | | | |

**Table 2.2. Responses of paired *Drosophila* ORNs to odorants from natural origins (continued).**

| Source | Compound | CAS | ab1 | | | ab2 | | ab3 | | ab4 | ab5 | | ab7 | | ab8 | |
|---|---|---|---|---|---|---|---|---|---|---|---|---|---|---|---|---|
| | | | A | B | D | A | B | A | B | A | A | B | A | B | A | B |
| banana (Jordan et al., 2001; Stensmyr et al., 2001) | eugenol | 97-53-0 | | | ● | | | | | | | | ● | | | |
| | Hexanoic acid | 142-62-1 | | | | | | ● | | | | | | | | |
| | (E)-2-hexenol | 928-95-0 | | | | | ● | ● | ● | ● | | | ● | ● | ● | ● |
| | Isoamyl acetate | 123-92-2 | | | ● | | | ● | ● | | | ● | ● | | ● | ● |
| | butanol | 71-36-3 | | | | | | ● | | ● | | | | ● | ● | ● |
| | 2-pentanone | 107-87-9 | | | | ● | | ● | ● | | | ● | | ● | ● | ● |
| | 2-pentanol | 6032-29-7 | | | | | | ● | ● | ● | ● | ● | ● | ● | ● | ● |
| | n-propyl acetate | 109-60-4 | | | ● | ● | | ● | ● | | | ● | ● | ● | ● | ● |
| | methyl butyrate | 623-42-7 | | | | ● | | ● | ● | | | ● | ● | ● | ● | ● |
| | 3-methyl-1-butanol | 123-51-3 | | | | | | ● | | ● | ● | | | ● | | ● |
| | Pentanol | 71-41-0 | | | | ● | | ● | ● | ● | ● | ● | ● | ● | ● | ● |
| | Isobutyl acetate | 110-19-0 | | | ● | | | ● | | | | ● | ● | ● | ● | ● |
| | hexanal | 66-25-1 | | | | | | ● | ● | ● | | | | | | |
| | ethyl butyrate | 105-54-4 | | | | | ● | ● | ● | | | ● | ● | ● | ● | ● |
| | butyl acetate | 123-86-4 | | | ● | | | ● | ● | | | ● | ● | | ● | ● |
| | ethyl crotonate | 623-70-1 | | | ● | | ● | ● | ● | | | | ● | | ● | ● |
| | t-2-hexanal | 6728-26-3 | ● | | | | | | ● | ● | | | | | ● | |
| | hexyl acetate | 142-92-7 | | | | | | ● | | | | ● | ● | | | |
| | alpha-terpineol | 98-55-5 | | | | | | ● | ● | | | | | | | |

**Table 2.3. Fly genotypes.**

| | | |
|---|---|---|
| Figure 2.1 | A | Wild-type *Canton-S* |
| | | *Gr63a$^{1}$ (Bloomington #9941, RRID:BDSC_9941) (Jones et al., 2007)* |
| | B | Wild-type *Canton-S* |
| | C | Wild-type *Canton-S* |
| Figure 2.2 | A-E | Wild-type *Canton-S* |
| Figure 2.3 | A | Wild-type *Canton-S* |
| | | *UAS-rpr (Yao et al., 2005); Or59b-GAL4* |
| | B | Wild-type *Canton-S* |
| | | *UAS-rpr; Or85a-GAL4* |
| | C | Wild-type *Canton-S* |
| | | *UAS-rpr; Or22a-GAL4* |
| | D | Wild-type *Canton-S* |
| | | *UAS-rpr; Or85b-GAL4* |
| Figure 2.4 | A-C | Wild-type *Canton-S* |
| Figure 2.5 | A-H | Wild-type *Canton-S* |
| Figure 2.6 | A-H | Wild-type *Canton-S* |
| Figure 2.7 | A-I | Wild-type *Canton-S* |
| Figure 2.8 | A-D | *UAS-rpr; Or92a-GAL4 (Bloomington #23139, RRID:BDSC_23139)* |
| Figure 2.9 | A-B | Wild-type *Canton-S* |
| | C-D | *UAS-H134R-ChR2 (Bloomington #28995, RRID:BDSC_28995); Or22a-GAL4 (Bloomington #9951, RRID:BDSC_9951)* |
| | | *UAS-H134R-ChR2; Or85b-GAL4 (Bloomington #23912, RRID:BDSC_23912)* |
| | E | *UAS-H134R-ChR2; Or42b-GAL4 (Bloomington #9972, RRID:BDSC_9972)* |
| | | *UAS-H134R-ChR2; Or92a-GAL4* |
| | | *UAS-H134R-ChR2; Gr21a-GAL4 (Bloomington #23890, RRID:BDSC_23890)* |
| | | *UAS-H134R-ChR2; Or10a-GAL4 (Bloomington #23885, RRID:BDSC_23885)* |
| | | *UAS-H134R-ChR2; Or59b-GAL4 (Bloomington #23897, RRID:BDSC_23897)* |
| | | *UAS-H134R-ChR2; Or85a-GAL4/Tm3-Sb* |
| | | *UAS-H134R-ChR2; Or47b-GAL4 (Bloomington #9984, RRID:BDSC_9984) (Fishilevich and Vosshall, 2005)* |
| | | *UAS-H134R-ChR2, Or88a-GAL4; + (Bloomington #23294, RRID:BDSC_23294)* |
| | | *ΔOr7a$^{GAL4}$ (Lin et al, 2015); UAS-H134R-ChR2/Cyo; Dr/Tm3-Sb* |
| | | *UAS-H134R-ChR2; Or56a-GAL4 (Bloomington #23896, RRID:BDSC_23896)* |
| | | *UAS-H134R-ChR2; Or42a-GAL4/Tm3-Sb (Bloomington #9969, RRID:BDSC_9969)* |
| | | *UAS-H134R-ChR2; Or71a-GAL4/Tm3-Sb (Bloomington #23122, RRID:BDSC_23122)* |

**Table 2.3. Fly genotypes (continued).**

| | | |
|---|---|---|
| Figure 2.10 | A | *UAS-H134R-ChR2; Or22a-GAL4* |
| | B | *UAS-H134R-ChR2; Or85b-GAL4* |
| Figure 2.11 | A | Wild-type *Canton-S* |
| | B | *Or22a-GAL4/UAS-Or83c; + (Ronderos et al., 2014)* |
| | | *Or85b-GAL4/UAS-Or83c; +* |
| Figure 2.12 | A-B | *Or82a-GAL4/UAS-Or83c; + (Bloomington #23125, RRID:BDSC_23125) (Ronderos et al., 2014)* |
| | | *Or47a-GAL4/UAS-Or83c; +* |
| | C-D | Wild-type *Canton-S* |
| | E-F | Wild-type *Canton-S* |
| Figure 2.13 | A | *+; UAS-Or85a/+ (Bloomington #76051, RRID:BDSC_76051) (Hallem et al., 2004)* |
| | | *10xUAS-myc-Orco/+ (this study); Or85a-GAL4/UAS-Or85a (Bloomington #24461, RRID:BDSC_24461)* |
| | B | *ΔOr7a$^{GAL4}$; Sp/Cyo; UAS-Or7a/Tm3-Sb (Bloomington #68454, RRID:BDSC_68454) (Hallem et al., 2004)* |
| | | *ΔOr7a$^{GAL4}$; Sp/Cyo; UAS-Or85a/Tm3-Sb* |

## 2.6 References


Arvanitaki, A. EFFECTS EVOKED IN AN AXON BY THE ACTIVITY OF A CONTIGUOUS ONE*t.

Benton, R., Vannice, K.S., Gomez-Diaz, C., and Vosshall, L.B. (2009). Variant Ionotropic Glutamate Receptors as Chemosensory Receptors in Drosophila. Cell *136*, 149–162.

Bokil, H., Laaris, N., Blinder, K., Ennis, M., and Keller, A. (2001). Ephaptic Interactions in the Mammalian Olfactory System. J. Neurosci. *21*.

de Bruyne, M., Clyne, P.J., and Carlson, J.R. (1999). Odor coding in a model olfactory organ: the Drosophila maxillary palp. J. Neurosci. *19*, 4520–4532.

de Bruyne, M., Foster, K., and Carlson, J.R. (2001). Odor Coding in the Drosophila Antenna. Neuron *30*, 537–552.

Butterwick, J.A., del Mármol, J., Kim, K.H., Kahlson, M.A., Rogow, J.A., Walz, T., and Ruta, V. (2018). Cryo-EM structure of the insect olfactory receptor Orco. Nature 1.

Buzsáki, G., Anastassiou, C.A., and Koch, C. (2012). The origin of extracellular fields and currents-EEG, ECoG, LFP and spikes. Nat. Rev. Neurosci. *13*, 407–420.

Chen, H.-C., Sheu, M.-J., and Wu, C.-M. (2006). Characterization of volatiles in guava (Psidium guajava L. cv. Chung-Shan Yueh-Pa) fruit from Taiwan. J.Food Drug Anal. *14*, 398–402.

Chyau, C.C., Chen, S.Y., and Wu, C.M. (1992). Differences of Volatile and Nonvolatile Constituents between Mature and Ripe Guava (Psidium Guajava Linn.) Fruits. J. Agric. Food Chem. *40*, 846–849.

Couto, A., Alenius, M., and Dickson, B.J. (2005). Molecular, Anatomical, and Functional Organization of the Drosophila Olfactory System. Curr. Biol. *15*, 1535–1547.

Damasio, A., and Carvalho, G.B. (2013). The nature of feelings: evolutionary and neurobiological origins. Nat. Rev. Neurosci. *14*, 143–152.

Denk, W., and Horstmann, H. (2004). Serial Block-Face Scanning Electron Microscopy to Reconstruct Three-Dimensional Tissue Nanostructure. PLOS Biol. *2*, e329.

Faber, D.S., and Korn, H. (1989). Electrical field effects: their relevance in central neural networks. Physiol. Rev. *69*, 821–863.

Fishilevich, E., and Vosshall, L.B. (2005). Genetic and Functional Subdivision of the Drosophila Antennal Lobe. Curr. Biol. *15*, 1548–1553.

Gnatzy, W., Mohren, W., and Steinbrecht, R.A. (1984). Pheromone receptors in Bombyx mori and Antheraea pernyi - II. Morphometric analysis. Cell Tissue Res. *235*, 35–42.

Van der Goes van Naters, W. (2013). Inhibition among olfactory receptor neurons. Front. Hum. Neurosci. *7*, 690.

Guillet, J.C., and Bernard, J. (1972). Shape and amplitude of the spikes induced by natural or electrical stimulation in insect receptors. J. Insect Physiol. *18*, 2155–2171.

Hallem, E.A., and Carlson, J.R. (2006). Coding of Odors by a Receptor Repertoire. Cell *125*, 143–160.

Hallem, E.A., Ho, M.G., and Carlson, J.R. (2004). The Molecular Basis of Odor Coding in the

Drosophila Antenna. Cell *117*, 965–979.

Han, K.-S., Guo, C., Chen, C.H., Witter, L., Osorno, T., and Regehr, W.G. Ephaptic Coupling Promotes Synchronous Firing of Cerebellar Purkinje Cells. Neuron *0*.

Hansson, B.S., Hallberg, E., Löfstedt, C., and Steinbrecht, R.A. (1994). Correlation between dendrite diameter and action potential amplitude in sex pheromone specific receptor neurons in male Ostrinia nubilalis (Lepidoptera: Pyralidae). Tissue Cell *26*, 503–512.

Hubel, D.H. (1982). CORTICAL NEUROBIOLOGY: A Slanted Historical Perspective.

Jefferys, J.G. (1995). Nonsynaptic modulation of neuronal activity in the brain: electric currents and extracellular ions. Physiol. Rev. *75*, 689–723.

Jeong, Y.T., Shim, J., Oh, S.R., Yoon, H.I., Kim, C.H., Moon, S.J., and Montell, C. (2013). An odorant-binding protein required for suppression of sweet taste by bitter chemicals. Neuron *79*, 725–737.

Jones, W.D., Cayirlioglu, P., Grunwald Kadow, I., and Vosshall, L.B. (2007). Two chemosensory receptors together mediate carbon dioxide detection in Drosophila. Nature *445*, 86–90.

Jordan, M.J., Goodner, K., and Shaw, P.E. (2001). Volatile components in banana (Musa acuminata colla cv. cavendish) and yellow passion fruit (Passiflora edulis Sims. f. flavicarpa Degner) as determined by GC-MS and GC-olfactometry. Florida State Hortic. Soc. *114*, 153–157.

Kaissling, K.E., and Thorson, J. (1980). Insect olfactory sensilla: structure, chemical and electrical aspect of the functional organization. In Receptors for Neurotransmitters, Hormones, and Pheromones in Insects: Proceedings of the Workshop on Neurotransmitter and Hormone Receptors in Insects Held in Cambridge, pp. 261–282.

Kamermans, M., Fahrenfort, I., Schultz, K., Janssen-Bienhold, U., Sjoerdsma, T., and Weiler, R. (2001). Hemichannel-mediated inhibition in the outer retina. Science (80-. ). *292*, 1178–1180.

Katz, B., and Schmitt, O.H. (1940). Electric interaction between two adjacent nerve fibres. J. Physiol. *97*, 471–488.

Keil, T.A. (1984). Reconstruction and morphometry of silkmoth olfactory hairs: A comparative study of sensilla trichodea on the antennae of male Antheraea polyphemus and Antheraea pernyi (Insecta, Lepidoptera). Zoomorphology *104*, 147–156.

Larsson, M.C., Domingos, A.I., Jones, W.D., Chiappe, M.E., Amrein, H., and Vosshall, L.B. (2004). Or83b Encodes a Broadly Expressed Odorant Receptor Essential for Drosophila Olfaction. Neuron *43*, 703–714.

Lin, C.-C., and Potter, C.J. (2015). Re-Classification of Drosophila melanogaster Trichoid and Intermediate Sensilla Using Fluorescence-Guided Single Sensillum Recording. PLoS One *10*, e0139675.

Lin, C.-C., Prokop-Prigge, K.A., Preti, G., and Potter, C.J. (2015). Food odors trigger Drosophila males to deposit a pheromone that guides aggregation and female oviposition decisions. Elife *4*, e08688.

Linz, J., Baschwitz, A., Strutz, A., Dweck, H.K.M., Sachse, S., Hansson, B.S., and Stensmyr, M.C. (2013). Host plant-driven sensory specialization in *Drosophila erecta*. Proc. R. Soc. B Biol. Sci. *280*, 20130626.

Maarse, H. (1991). Volatile Compounds in Foods and Beverages (New York: Marcel Dekker).

Macoris, M.S., Janzantti, N.S., Garruti, D. dos S., and Monteiro, M. (2011). Volatile compounds from organic and conventional passion fruit (Passiflora edulis F. Flavicarpa) pulp. Ciência e Tecnol. Aliment. *31*, 430–435.

Martelli, C., Carlson, J.R., and Emonet, T. (2013). Intensity invariant dynamics and odor-specific latencies in olfactory receptor neuron response. J. Neurosci. *33*, 6285–6297.

Miriyala, A., Kessler, S., Rind, F.C., and Wright, G.A. (2018). Burst Firing in Bee Gustatory Neurons Prevents Adaptation. Curr. Biol. *28*, 1585-1594.e3.

Nagel, K.I., and Wilson, R.I. (2011). Biophysical mechanisms underlying olfactory receptor neuron dynamics. Nat. Neurosci. *14*, 208–216.

Ng, R., Lin, H.H., Wang, J.W., and Su, C.Y. (2017). Electrophysiological Recording from Drosophila Trichoid Sensilla in Response to Odorants of Low Volatility. J. Vis. Exp. e56147.

Ng, R., Salem, S.S., Wu, S.T., Wu, M., Lin, H.H., Shepherd, A.K., Joiner, W.J., Wang, J.W., and Su, C.Y. (2019). Amplification of Drosophila Olfactory Responses by a DEG/ENaC Channel. Neuron *104*, 947-959.e5.

Pello-Palma, J., González-Álvarez, J., Gutiérrez-Álvarez, M.D., Dapena de la Fuente, E., Mangas-Alonso, J.J., Méndez-Sánchez, D., Gotor-Fernández, V., and Arias-Abrodo, P. (2017). Determination of volatile compounds in cider apple juices using a covalently bonded ionic liquid coating as the stationary phase in gas chromatography. Anal. Bioanal. Chem. *409*, 3033–3041.

Pettersen, K.H., and Einevoll, G.T. (2008). Amplitude variability and extracellular low-pass filtering of neuronal spikes. Biophys. J. *94*, 784–802.

Pinu, F., and Villas-boas, S.G. (2017). Rapid Quantification of Major Volatile Metabolites in Fermented Food and Beverages Using Gas Chromatography-Mass Spectrometry. Metabolites *7*, 37.

Prieto-Godino, L.L., Rytz, R., Cruchet, S., Bargeton, B., Abuin, L., Silbering, A.F., Ruta, V., Dal Peraro, M., and Benton, R. (2017). Evolution of Acid-Sensing Olfactory Circuits in Drosophilids. Neuron.

Pulver, S.R., Pashkovski, S.L., Hornstein, N.J., Garrity, P.A., and Griffith, L.C. (2009). Temporal Dynamics of Neuronal Activation by Channelrhodopsin-2 and TRPA1 Determine Behavioral Output in *Drosophila* Larvae. J. Neurophysiol. *101*, 3075–3088.

Qian, K., Zhu, J.J., Sims, S.R., Taylor, D.B., and Zeng, X. (2013). Identification of volatile compounds from a food-grade vinegar attractive to house flies (Diptera: Muscidae). J. Econ. Entomol. *106*, 979–987.

Redkozubov, A. (1995). High electrical resistance of the bombykol cell in an olfactory sensillum of Bombyx mori: Voltage- and current-clamp analysis. J. Insect Physiol. *41*, 451–455.

Ronderos, D.S., Lin, C.-C., Potter, C.J., Smith, D.P., and Snyder, S.H. (2014). Farnesol-Detecting Olfactory Neurons in Drosophila. J. Neurosci *34*, 3959–3968.

Sato, K., Pellegrino, M., Nakagawa, T., Nakagawa, T., Vosshall, L.B., and Touhara, K. (2008). Insect olfactory receptors are heteromeric ligand-gated ion channels. Nature *452*, 1002–1006.

Schnaitmann, C., Haikala, V., Abraham, E., Oberhauser, V., Thestrup, T., Griesbeck, O., and Reiff,

D.F. (2018). Color Processing in the Early Visual System of Drosophila. Cell *172*, 318-330.e18.

Shanbhag, S.., Müller, B., and Steinbrecht, R.. (2000). Atlas of olfactory organs of Drosophila melanogaster: 2. Internal organization and cellular architecture of olfactory sensilla. Arthropod Struct. Dev. *29*, 211–229.

Shimizu, K., and Stopfer, M. (2012). Olfaction: Intimate neuronal whispers. Nature *492*, 44–45.

Stensmyr, M.C., Larsson, M.C., Bice, S., and Hansson, B.S. (2001). Detection of fruit- and flower-emitted volatiles by olfactory receptor neurons in the polyphagous fruit chafer Pachnoda marginata (Coleoptera: Cetoniinae). J. Comp. Physiol. A. *187*, 509–519.

Stensmyr, M.C., Dekker, T., and Hansson, B.S. (2003). Evolution of the olfactory code in the *Drosophila melanogaster* subgroup. Proc. R. Soc. London. Ser. B Biol. Sci. *270*, 2333–2340.

Stensmyr, M.C., Dweck, H.K.M., Farhan, A., Ibba, I., Strutz, A., Mukunda, L., Linz, J., Grabe, V., Steck, K., Lavista-Llanos, S., et al. (2012). A Conserved Dedicated Olfactory Circuit for Detecting Harmful Microbes in Drosophila. Cell *151*, 1345–1357.

Su, C.-Y., Menuz, K., and Carlson, J.R. (2009). Olfactory Perception: Receptors, Cells, and Circuits. Cell *139*, 45–59.

Su, C.-Y., Menuz, K., Reisert, J., and Carlson, J.R. (2012). Non-synaptic inhibition between grouped neurons in an olfactory circuit.

Takemura, S.Y., Xu, C.S., Lu, Z., Rivlin, P.K., Parag, T., Olbris, D.J., Plaza, S., Zhao, T., Katz, W.T., Umayam, L., et al. (2015). Synaptic circuits and their variations within different columns in the visual system of Drosophila. Proc. Natl. Acad. Sci. U. S. A. *112*, 13711–13716.

Torrens, J., Riu-Aumatell, M., López-Tamames, E., and Buxaderas, S. (2004). Volatile compounds of red and white wines by headspace--solid-phase microextraction using different fibers. J. Chromatogr. Sci. *42*, 310–316.

Vermeulen, A., and Rospars, J.-P. (2004). Why are insect olfactory receptor neurons grouped into sensilla? The teachings of a model investigating the effects of the electrical interaction between neurons on the transepithelial potential and the neuronal transmembrane potential. Eur. Biophys. J. *33*, 633–643.

Wicher, D., Schäfer, R., Bauernfeind, R., Stensmyr, M.C., Heller, R., Heinemann, S.H., and Hansson, B.S. (2008). Drosophila odorant receptors are both ligand-gated and cyclic-nucleotide-activated cation channels. Nature *452*, 1007–1011.

Xu, Y., Fan, W., and Qian, M.C. (2007). Characterization of aroma compounds in apple cider using solvent-assisted flavor evaporation and headspace solid-phase microextraction. J. Agric. Food Chem. *55*, 3051–3057.

# Chapter 3: Distinct roles and synergistic function of $Fru^{M}$ isoforms in *Drosophila* olfactory receptor neurons

## 3.1 Abstract

Sexual dimorphism in *Drosophila* courtship circuits requires the male-specific transcription factor $Fru^{M}$, which comprises three splice variants — $Fru^{MA}$, $Fru^{MB}$ and $Fru^{MC}$. Multiple $Fru^{M}$ isoforms are typically expressed in the same neuron; however, the functional significance of their co-expression remains underexplored. By focusing on $fru^{M}$-positive olfactory receptor neurons (ORNs), here I show that $Fru^{MB}$ and $Fru^{MC}$ are both required for males' age-dependent sensitization to aphrodisiac olfactory cues. Interestingly, $Fru^{MB}$ expression, but not $Fru^{MC}$, is upregulated with age, and overexpression of $Fru^{MB}$ can confer elevated responses in courtship-promoting ORNs. Mechanistically, $Fru^{MB}$ is upstream of PPK25, a DEG/ENaC subunit necessary for response amplification, while $Fru^{MC}$ is upstream of PPK23, which is in turn required for PPK25 function. Together, these results illustrate how male-specific olfactory sensitization is synergistically regulated by different $Fru^{M}$ isoforms — through cooperation of their respective downstream effectors, thus providing critical mechanistic insight into how co-expressed $Fru^{M}$ isoforms jointly coordinate dimorphic neurophysiology.

## 3.2 Introduction

In *Drosophila*, sexual dimorphism is determined by genes that regulate the alternative splicing of male- or female-specific transcription factors. In particular, the male products of the *fruitless* gene ($Fru^{M}$) play essential roles in determining dimorphic neural circuits (for reviews, see Billeter et al., 2006a; Dickson, 2008; Pavlou and Goodwin, 2013; Sato et al., 2020; Yamamoto and Koganezawa, 2013). The $fru^{M}$ transcript is further subject to alternative splicing at its 3' end, yielding three functional variants: $Fru^{MA}$, $Fru^{MB}$, $Fru^{MC}$ (Demir and Dickson, 2005; von Philipsborn et al., 2014; Song et al., 2002) — also known as $Fru^{AM}$, $Fru^{EM}$, and $Fru^{BM}$, respectively (Nojima et al., 2014; Sato and Yamamoto, 2020; Usui-Aoki et al., 2000). Each isoform contains a common N-terminal BTB protein dimerization domain and a unique zinc finger DNA-binding domain, and all three are predicted to function as transcription factors (Billeter et al., 2006b; Meissner et al., 2016; Neville et al., 2014;

von Philipsborn et al., 2014; Ryner et al., 1996). While RNAseq, ChIP-seq or genomic occupancy analysis of cells ectopically expressing $Fru^{MA}$, $Fru^{MB}$, or $Fru^{MC}$ reveals unique DNA binding sites for each variant, the three isoforms nevertheless appear to target overlapping sets of genes involved in neural development, synaptic transmission or ion channel signaling (Dalton et al., 2013; Neville et al., 2014; Vernes, 2014).

At the cellular level, $Fru^{MB}$ and $Fru^{MC}$ are largely co-expressed, whereas $Fru^{MA}$ is found in the smallest subset of $fru^{M+}$ neurons (Neville et al., 2014; Nojima et al., 2014; von Philipsborn et al., 2014). Despite their overlapping expression, the isoforms are likely non-redundant in function. Among the three, $Fru^{MC}$ is known to play a central role in male sexual behavior (Billeter et al., 2006b; Neville et al., 2014; von Philipsborn et al., 2014) and is also necessary for development of the male-specific muscle of Lawrence (MOL): in $fru^{M}$ or $fru^{MC}$ mutants, MOL induction can only be rescued by $Fru^{MC}$, but not $Fru^{MA}$ or $Fru^{MB}$, indicating that $Fru^{MC}$ cannot be substituted by the other $Fru^{M}$ isoforms in this context (Billeter et al., 2006b). Furthermore, the mAL/aDT2, aSP4 and vAB3 neural clusters all specifically require $Fru^{MC}$ for male-specific neurite arborizations, despite the co-expression of other $Fru^{M}$ isoforms (von Philipsborn et al., 2014). Mechanistically, $Fru^{MC}$ orchestrates mAL neurons' dimorphic development through interacting with other transcription or chromatin regulators to repress the expression of the axon guidance molecule *robo1* (Chowdhury et al., 2017; Ito et al., 2016; Sato and Yamamoto, 2020). The aforementioned examples suggest that $Fru^{M}$ isoforms play distinct roles in both behavior and neurodevelopment. However, it remains unclear whether the isoforms operate beyond these contexts. It is also unknown whether all isoforms exhibit specific cellular functions, or in which neuronal population these functions are fulfilled. Addressing these questions is essential for understanding why multiple isoforms are typically co-expressed and how isoform-specific functions influence dimorphic circuits.

Co-expressed isoforms may also perform cooperatively. In $fru^{M}$ mutant males, whose serotonergic-abdominal giant neurons (s-Abg) are less numerous and display female-like neurite

morphology (Lee and Hall, 2001), genetic rescue with $Fru^{MB}$ or $Fru^{MC}$ only partially restores the male-specific features, while $Fru^{MA}$ does not alleviate the mutant phenotype (Billeter et al., 2006b). These observations indicate that neither $Fru^{MB}$ nor $Fru^{MC}$ alone is sufficient to confer the full male-specific complement of s-Abg neurons, suggesting that in this context, there is synergistic function between the $Fru^{M}$ isoforms (Neville et al., 2014). But insofar as the mechanism of cooperativity is unidentified, how different $Fru^{M}$ isoforms operate synergistically remains an outstanding question.

Intriguingly, $Fru^{M}$ is expressed well into adulthood (Hueston et al., 2016; Neville et al., 2014; von Philipsborn et al., 2014), suggesting that the isoforms may function beyond regulating neurodevelopment. What roles might they play in adult neurons? Might they underlie dimorphic neurophysiology, i.e. neural response properties? Indeed, a previous study shows that $Fru^{M}$ is required for social context to influence male-specific neurophysiology (Sethi et al., 2019). Of note, sexual dimorphism has been well-characterized in the courtship-promoting Or47b and Ir84a ORNs, which express $Fru^{M}$, and whose responses become more sensitive with age in males but not females (Lin et al., 2016; Ng et al., 2019; Stockinger et al., 2005). This age-dependent sensitization impacts courtship behavior and is regulated by a reproductive hormone — juvenile hormone — through upregulation of Pickpocket 25 (PPK25), an obligate subunit of a DEG/ENaC amplification channel (Lin et al., 2016; Ng et al., 2019). Which $Fru^{M}$ isoform(s) are required for the male-specific regulation of olfactory neurophysiology? Is there a hierarchical relationship between $Fru^{M}$ isoforms, PPK25 and juvenile hormone signaling? If multiple isoforms are involved, do they collaborate directly to modulate common downstream targets; or do different effectors, regulated by their respective isoform, act cooperatively instead?

In this study, I begin by systematically analyzing the functions and expression patterns of all three $Fru^{M}$ isoforms in ORNs. I identify unique roles for co-expressed $Fru^{M}$ isoforms in courtship-promoting ORNs and uncover a molecular mechanism whereby multiple $Fru^{M}$ isoforms cooperate to mediate the neurons' age-dependent sensitization. Specifically, both $Fru^{MB}$ and $Fru^{MC}$ are required for

the elevated Or47b responses of older males. When overexpressed, only $Fru^{MB}$ can mimic the effects of age in sensitizing Or47b ORN responses, consistent with our finding that $Fru^{MB}$ alone shows age-dependent upregulation. Through a series of epistasis experiments, I show that $Fru^{MB}$ operates downstream of juvenile hormone signaling and upstream of PPK25 expression. Interestingly, although $Fru^{MC}$ is not upregulated with age, its downstream target, PPK23, is also required for PPK25 to form an amplification channel. These results illustrate how functional synergy between $Fru^{MB}$ and $Fru^{MC}$ can be achieved: through cooperation of their respective downstream targets. Furthermore, I show that neuronal identity determines the synergy, which is conserved between courtship-promoting Or47b and Ir84a neurons but absent in the courtship-inhibiting Or67d ORNs. By focusing on the Or47b ORN, a representative $Fru^{M}$-positive and dimorphic neuron, this study furthers our understanding of how co-expressed $Fru^{M}$ isoforms can regulate sexually dimorphic neurophysiology in a coordinated manner.

## 3.3 Results

### 3.3.1 $Fru^{M}$ is necessary for age-dependent olfactory sensitization

Among the three types of $fru^{M+}$ ORNs in the male antenna, the courtship-promoting Or47b and Ir84a neurons exhibit age-dependent response increases, while the courtship-inhibiting Or67d neurons do not alter sensitivity with age (Lin et al., 2016; Ng et al., 2019). I first surveyed whether $Fru^{M}$ influences the responses of these ORNs to their ligands: the Or47b receptor responds to palmitoleic acid (Lin et al., 2016), Ir84a to phenylacetaldehyde (Grosjean et al., 2011) and Or67d to *cis*-vaccenyl acetate (van der Goes van Naters and Carlson, 2007; Kurtovic et al., 2007; Tal and Smith, 2006). Using single-sensillum recording, I found that the age-dependent sensitization of Or47b ORNs (Figure 3.1A) was abolished in $fru^{F}$ mutant males, which do not express any functional $Fru^{M}$ proteins (Demir and Dickson, 2005) (Figure 3.1B). On the other hand, the loss of $Fru^{M}$ did not affect the Or47b olfactory responses of 2-day old males (Figure 3.1C), suggesting that $Fru^{M}$ is dispensable for the ORNs' baseline pheromone response.

Similarly in the Ir84a neurons, $Fru^{M}$ was only required for the elevated olfactory responses of 7-day old males (Figures 3.1D–F). Meanwhile, neither age nor $Fru^{M}$ influenced Or67d ORN responses (Figures 3.1G–I). Together, these results indicate that $Fru^{M}$ is selectively required for age-dependent sensitization in the courtship-promoting Or47b and Ir84a ORNs (Figure 3.1J).

### 3.3.2 $Fru^{MB}$ and $Fru^{MC}$ are both required for age-dependent olfactory sensitization

To determine which $Fru^{M}$ isoform is necessary for age-dependent sensitization, I examined isoform-specific $Fru^{M}$ mutant males heterozygous for the $fru^{F}$ allele and the $fru^{\Delta A}$, $fru^{\Delta B}$ or $fru^{\Delta C}$ mutant allele (Billeter et al., 2006b; Neville et al., 2014) (Figure 3.2A). I found that the Or47b ORN responses from 7-day old $fru^{MA}$ mutants remained significantly higher than those from 2-day-olds (Figure 3.2B). Specifically, both response magnitudes and age-dependent sensitization were unaffected in $fru^{MA}$ mutants, which remained indistinguishable from controls (Figure 3.2C). These results indicate that $Fru^{MA}$ does not underlie the elevated Or47b olfactory responses in 7-day old males.

Meanwhile in $fru^{MB}$ or $fru^{MC}$ mutant males, the Or47b ORN responses of 7-day-olds were reduced and resembled those of 2-day-olds (Figures 3.2D–G), indicating that $Fru^{MB}$ and $Fru^{MC}$ are both necessary for age-dependent sensitization. To further determine whether these $Fru^{M}$ proteins operate in a cell-autonomous manner, I employed isoform-specific micro RNAi lines (von Philipsborn et al., 2014) to selectively knock down either $Fru^{MB}$ or $Fru^{MC}$ in the Or47b ORNs, and also observed abolishment of age-dependent sensitization (Figure 3.3). Taken together, these results show that both $Fru^{MB}$ and $Fru^{MC}$, but not $Fru^{MA}$, are required for the elevated Or47b olfactory responses in older males (Figure 3.2H).

### 3.3.3 $Fru^{M}$ isoforms are differentially regulated with age in courtship-promoting ORNs

Given that Or47b ORN sensitization requires $Fru^{MB}$ and $Fru^{MC}$, how are these factors related with age? I postulated that the expression of specific $Fru^{M}$ isoforms is dynamically regulated. To test this hypothesis, I examined published isoform reporter lines in which the C-terminus of an individual

alternative exon (A, B or C) is epitope-tagged (von Philipsborn et al., 2014). With immunohistochemistry, I first determined that all three isoforms are expressed in the Or47b ORNs of male but not female flies (Figure 3.4 and data not shown). Using an established signal threshold for evaluating expression, I then determined whether there is relative up- or down-regulation of each isoform at different ages.

As expected, $Fru^{M}$ expression changed in an age- and isoform-dependent manner (Figure 3.4). In $fru^{A\text{-}myc}$ males, the percentage of Or47b ORNs with positively-scored *myc* staining was 58% in 2-day-olds and 38% in 7-day-olds, indicating downregulated $Fru^{MA}$ expression (Figures 3.4A and 3.4B). In contrast, there was marked increase in the percentage of Or47b ORNs expressing $Fru^{MB}$, rising from 30% to 51% (Figures 3.4C and 3.4D). Finally, I observed a drop in the percentage of $Fru^{MC}$ positive neurons, from 25% in 2-day old males to 6% in 7-day-olds (Figures 3.4E and 3.4F). Together, these results demonstrate that in male Or47b ORNs, $Fru^{MB}$ protein expression is upregulated with age, while $Fru^{MA}$ and $Fru^{MC}$ are downregulated (Figure 3.4G).

Since Ir84a and Or67d ORNs also express $Fru^{M}$, I examined isoform-specific expression in these neurons as well. I observed a similar trend of $Fru^{MB}$ upregulation and $Fru^{MC}$ downregulation in the Ir84a ORNs (Figure 3.5A). Interestingly in the Or67d neurons, although all three isoforms were detected, their expression remained unchanged with age (Figure 3.5B). In summary, our systematic survey shows that $Fru^{M}$ isoforms are differentially regulated with age in the courtship-promoting ORNs, and that a common pattern of isoform-specific modulation — $Fru^{MB}$ upregulation and $Fru^{MC}$ downregulation — may mediate the sensitization of Or47b and Ir84a neurons.

### 3.3.4 Overexpression of $Fru^{MB}$ elevates Or47b ORN responses in males

Given the isoform-specific modulation (Figure 3.4), how might overexpression of an individual isoform affect Or47b ORNs? Can this manipulation mimic age in elevating olfactory responses? To address these questions, I employed the GAL4-UAS system to overexpress a single

$Fru^{M}$ isoform in the Or47b ORNs of 2-day old males. $Fru^{MA}$-overexpression did not alter neuronal responses compared to controls (Figures 3.6A and 3.6B), in agreement with $Fru^{MA}$'s dispensability for Or47b response regulation (Figure 3.2B). On the other hand, $Fru^{MB}$ overexpression markedly increased the responses (Figures 3.6C and 3.6D), supporting the notion that age — through $Fru^{MB}$ upregulation — drives the response increase in Or47b neurons.

Furthermore, I examined whether increased $Fru^{MB}$ expression also underlies Ir84a response sensitization, and found that its overexpression similarly elevated the responses in 2-day old males (Figures 3.7A and 3.7B). In comparison, $Fru^{MB}$ overexpression in Or67d ORNs unexpectedly abolished their olfactory responses (Figures 3.7C and 3.7D), indicating that upregulation of $Fru^{MB}$ does not invariably elevate responses in all $fru^{M+}$ ORN types. It is plausible that additional transcription factors — likely partnering with $Fru^{MB}$ — are involved in selecting the isoform's target genes that either sensitize responses in Or47b and Ir84a neurons or inhibit responses in Or67d ORNs.

Lastly, I examined the impact of $Fru^{MC}$ overexpression on Or47b ORN responses. Consistent with its lack of upregulation (Figure 3.4F), increasing $Fru^{MC}$ expression in Or47b neurons did not elevate responses (Figure 3.6E). Instead, this manipulation reduced olfactory sensitivity (Figure 3.6F), raising the possibility for opposing functions of $Fru^{MB}$ and $Fru^{MC}$ (see Discussion). In all, our overexpression experiments show that upregulation of $Fru^{MB}$, but not $Fru^{MA}$ or $Fru^{MC}$, in the courtship-promoting ORNs can confer elevated olfactory responses (Figure 3.6G).

### 3.3.5 $Fru^{MB}$ is downstream of juvenile hormone signaling and upstream of PPK25 expression in male Or47b neurons

Previous work shows that $Fru^{M}$ expression in the antennae of 7-day old males requires *methoprene-tolerant* (*Met*) (Sethi et al., 2019), a juvenile hormone receptor (Jindra et al., 2013; Wilson and Fabian, 1986). Moreover, juvenile hormone signaling drives the upregulation of PPK25, a DEG/ENaC member which amplifies olfactory inputs in the courtship-promoting ORNs and whose antennal expression level increases with age in males (Ng et al., 2019). Eliminating Met, $Fru^{M}$, or

PPK25 abolishes age-dependent sensitization (Lin et al., 2016; Ng et al., 2019) (Figure 3.1). Conversely, heightened Met signaling or overexpressing $Fru^{MB}$ or PPK25 in the Or47b ORNs increases their pheromone responses (Lin et al., 2016; Ng et al., 2019; Sethi et al., 2019) (Figure 3.6D). These observations suggest that these molecules function in the same pathway to increase Or47b olfactory responses. However, it was unclear how $Fru^{MB}$ operates within this hierarchy.

To establish the relationship between $Fru^{MB}$ and juvenile hormone signaling, I performed epistasis experiments by overexpressing $Fru^{MB}$ in the Or47b ORNs of *Met* mutants. If $Fru^{MB}$ is downstream of Met, I expect this manipulation to elevate Or47b olfactory responses, as in a wildtype background (Figure 3.6D). Indeed, $Fru^{MB}$ overexpression markedly increased Or47b ORN response despite the absence of Met (Figures 3.8A and 3.8B), implying that $Fru^{MB}$ is downstream of juvenile hormone signaling.

I next determined the relationship between $Fru^{MB}$ and PPK25 by overexpressing $Fru^{MB}$ in the Or47b ORNs of *ppk25* mutant males. This manipulation failed to elevate their Or47b olfactory responses (Figures 3.8C and 3.8D), suggesting that $Fru^{MB}$ requires functional PPK25 to sensitize the ORNs and regarding the isoform's hierarchical position, that $Fru^{MB}$ operates upstream of PPK25. Together, these results (Figures 3.8E–G) support a model whereby 1) $Fru^{MB}$ is upregulated with age via juvenile hormone signaling in male Or47b ORNs, and 2) $Fru^{MB}$ further drives the expression of PPK25, which in turn amplifies the olfactory responses of these neurons (Figure 3.8H).

### 3.3.6 $Fru^{MB}$ and $Fru^{MC}$ cooperatively elevate Or47b ORN responses through distinct downstream effectors

Given that $Fru^{MB}$ and $Fru^{MC}$ are both required for age-dependent sensitization (Figure 3.2), we asked how these isoforms cooperate to modulate neurophysiology. I note that overexpression of PPK25 alone in male Or47b ORNs is sufficient to confer increased responses; however, the same manipulation in females fails to elevate olfactory output (Ng et al., 2019). These observations suggest

that PPK25 by itself cannot form a functional DEG/ENaC channel, which is typically composed of three subunits (Hanukoglu and Hanukoglu, 2016; Kellenberger and Schild, 2002; Staruschenko et al., 2005). Therefore, the normal function of PPK25 likely requires at least another DEG/ENaC subunit that is also expressed in male Or47b neurons.

Might a specific isoform regulate the partner subunit(s)? This inquiry is important in the context of a critical question: at which level do co-expressed $Fru^{MB}$ and $Fru^{MC}$ cooperatively mediate Or47b response sensitization? One possible model is that $Fru^{MC}$ collaborate with $Fru^{MB}$ to regulate the expression of both PPK25 and its partner(s) (Figure 3.9A, Model I). Alternatively, $Fru^{MB}$ and $Fru^{MC}$ may operate as independent transcription regulators, each driving the expression of a distinct downstream effector. In this scenario, $Fru^{MB}$ is likely directly upstream of PPK25, given that both molecules are upregulated with age (Ng et al., 2019) (Figure 3.4D); $Fru^{MC}$ might then be required for the expression of PPK25's channel partner(s), independent from the $Fru^{MB}$/PPK25 pathway (Figure 3.9A, Model II). To distinguish between these two possibilities, I targeted female Or47b neurons for genetic manipulations, taking advantage of their lack of $Fru^{M}$ isoform or PPK25 channel partner(s) expression (Ng et al., 2019). Consistent with the functional requirement of $Fru^{MC}$ (Figure 3.2), ectopic expression $Fru^{MB}$ alone in female Or47b ORNs did not elevate their pheromone responses (Figure 3.9B). In contrast, co-expression of $Fru^{MB}$ and $Fru^{MC}$ markedly heightened female responses (Figure 3.9C), indicating that $Fru^{MB}$ and $Fru^{MC}$ together can confer Or47b olfactory sensitization. In comparison, expression of both $Fru^{MB}$ and $Fru^{MA}$ in female Or47b neurons did not affect responses (Figure 3.10).

According to Model I, because both $Fru^{MB}$ and $Fru^{MC}$ are required to regulate PPK25 and its partner(s), overexpressing PPK25 in female neurons together with a single $Fru^{M}$ isoform is not expected to yield response changes. On the other hand, if Model II is correct, expressing PPK25 with $Fru^{MB}$ also will not yield increased responses, because $Fru^{MB}$ and PPK25 operate in the same pathway. However, expressing PPK25 along with $Fru^{MC}$, which regulates a different downstream effector,

should now mimic the effect of $Fru^{MB}$ and $Fru^{MC}$ co-expression (Figure 3.9C), and subsequently elevate the Or47b olfactory responses in females.

In support of Model II, I observed a marked increase in Or47b responses when PPK25 and $Fru^{MC}$ were co-expressed (Figure 3.9D). Moreover, I found that expression of PPK25 together with $Fru^{MB}$ failed to confer sensitization (Figure 3.9E), further supporting Model II in which these two molecules operate in the same pathway. This result also agrees with the previous finding that overexpression of PPK25 alone cannot elevate female Or47b ORN responses (Ng et al., 2019); in both cases, PPK25 lacked its partner(s). Further, based on published bioinformatics studies (Dalton et al., 2013; Neville et al., 2014), I identified putative $Fru^{MB}$ DNA binding domains upstream of *ppk25* (Figure 3.11), suggesting that $Fru^{MB}$ may directly mediate *ppk25* upregulation. In all, these results show that each of the $Fru^{M}$ isoforms has its own unique downstream target(s) in Or47b ORNs (Figure 3.9A, Model II).

I next sought to identify the downstream target of $Fru^{MC}$. I followed a candidate-based approach by focusing on another DEG/ENaC subunit, named PPK23, which is expressed together with PPK25 in a subset of $fru^{M+}$ tarsal gustatory neurons for responses to aphrodisiac contact pheromones (Liu et al., 2018; Pikielny, 2012; Thistle et al., 2012; Toda et al., 2012). I postulated that a similar PPK23-PPK25 partnership also exists in Or47b ORNs. Specifically, I hypothesized that $Fru^{MC}$ is upstream of PPK23, which forms a functional amplification channel with PPK25.

First I verified that age-dependent sensitization was abolished in *ppk23* mutant males (Figure 3.12), indicating PPK23's functional role in Or47b ORNs. In support of our hypothesis, ectopic expression of PPK23 with $Fru^{MC}$ in female Or47b ORNs yielded no response increase (Figure 3.9F), suggesting that these molecules could operate in the same pathway. Consistent with this notion, I also identified putative $Fru^{MC}$ DNA binding domains upstream of *ppk23* (Figure 3.11). On the other hand, expressing PPK23 together with $Fru^{MB}$ markedly increased the pheromone responses (Figure 3.9G), mimicking $Fru^{MC}$/$Fru^{MB}$ co-expression (Figure 3.9C). Together, these results strongly support a model

whereby $Fru^{MB}$ and $Fru^{MC}$ respectively mediate the expression of PPK25 and PPK23, which in turn partner with each other to form an amplification channel that sensitizes Or47b ORN responses. Overall, co-expressed $Fru^{MB}$ and $Fru^{MC}$ coordinate dimorphic neurophysiology at the level of their unique downstream effectors.

### 3.3.7 $Fru^{MA}$ is required for the enlargement of all three sexually-dimorphic glomeruli

Having determined the roles of $Fru^{MB}$ and $Fru^{MC}$ in Or47b neurophysiology (Figure 3.2), I next investigated the function of $Fru^{MA}$. Previous work shows that the male VA1lm glomerulus — innervated by Or47b ORNs — exhibits sexually dimorphic enlargement, and that volumetric difference depends on $Fru^{M}$ expression (Stockinger et al., 2005). Given $Fru^{MA}$'s dispensability for olfactory sensitization (Figure 3.2B), I wondered whether the isoform might instead be required for male-specific glomerular enlargement.

To test this possibility, I quantified the sizes of VA1lm in wildtype and different $fru^{M}$ mutant backgrounds. Consistent with the published phenotype, eliminating the expression of all $Fru^{M}$ proteins markedly reduced the size of male VA1lm, indicated as the volume ratio between sexes (Stockinger et al., 2005) (Figure 3.13A). Interestingly, select disruption of either $Fru^{MA}$ or $Fru^{MC}$ similarly reduced VA1lm volume (Figure 3.13A), indicating functional roles for these isoforms in male-specific glomerular enlargement.

For comparison, I also examined the VL2a and DA1glomeruli, which are innervated by Ir84a and Or67d ORNs, respectively. Elimination of $Fru^{MA}$ similarly downsized these two glomeruli in males (Figures 3.13B–C), while $Fru^{MB}$ did not influence glomerular volumes. Finally, $Fru^{MC}$ plays a distinct role in each glomerulus: mutation of this isoform reduced the size of VA1lm, increased DA1 volume, and left VL2a volume unchanged (Figure 3.13). Collectively, these results point to a role of $Fru^{MA}$ in mediating the sexually-dimorphic enlargement of $fru^{M+}$ glomeruli in males.

### 3.4 Discussion

Here I showed that $Fru^{MA}$, $Fru^{MB}$, and $Fru^{MC}$ are all expressed and differentially regulated with age in the Or47b ORNs (Figure 3) — which are representative $fru^{M+}$ and sexually dimorphic sensory neurons — and that each isoform plays distinct roles in mediating dimorphism. Specifically, I found that $Fru^{MA}$ is required for these neurons' male-specific glomerular enlargement (Figure 3.13), while $Fru^{MB}$ and $Fru^{MC}$ are indispensable for the ORNs' age-dependent sensitization (Figure 3.2).

Notably, our study uncovers a functional role for $Fru^{MA}$, whose importance in sexual dimorphism has not been characterized (Billeter et al., 2006b; Neville et al., 2014; Nojima et al., 2014; von Philipsborn et al., 2014; Wohl et al., 2020). Our finding on $Fru^{MA}$ contrasts with previous studies identifying $Fru^{MC}$ as the dominant isoform in regulating male-specific neural morphology: specifically, the innervation patterns as observed in the s-Abg serotonergic neurons, or the mAL/aDT2, aSP4 and vAB3 neural clusters (Billeter et al., 2006b; von Philipsborn et al., 2014). These observations illustrate that sexually dimorphic neuroanatomy requires different $Fru^{M}$ isoforms in a neuronal type-dependent manner.

$Fru^{M}$ proteins contain a BTB domain, a conserved protein-protein interaction module able to both self-associate and interact with other proteins (Sato and Yamamoto, 2020; Sato et al., 2019; Stogios et al., 2005). $Fru^{MC}$, for example, is able to recruit other transcription or chromatin regulators to modulate dimorphic neurite morphology (Chowdhury et al., 2017; Ito et al., 2012; Sato and Yamamoto, 2020). Intriguingly, $Fru^{MB}$ and $Fru^{MC}$ are commonly co-expressed and can perform synergistically (Billeter et al., 2006b; Neville et al., 2014; von Philipsborn et al., 2014). However, it has been unclear whether functional synergism between isoforms arises from their direct dimerization or through other means. Here I show that in Or47b ORNs, $Fru^{MB}$ and $Fru^{MC}$ independently regulate distinct downstream effectors, PPK25 and PPK23, which then cooperate to elevate Or47b pheromone responses (Figures 3.9). Prior to this study, the individual downstream targets for co-expressed $Fru^{M}$ isoforms within a single cell have never been characterized. Our results now suggest that in neurons

expressing multiple splice variants, each isoform may specifically target unique effector genes, which in turn interact with each other to function cooperatively. Through future research, it will be important to determine whether this logic is conserved in other neurons expressing alternatively spliced isoforms of transcription factors.

Unexpectedly, I found that the expression of individual isoforms is differentially regulated with age in an ORN-dependent manner (Figures 3.4 and 3.5). In the courtship-promoting ORNs, I observed a concomitant $Fru^{MB}$ upregulation and $Fru^{MC}$ downregulation. This isoform-specific regulation is functionally relevant, as overexpression of $Fru^{MB}$ can elevate responses in Or47b and Ir84a ORNs, mimicking the effect of age. On the other hand, the effects of $Fru^{MB}$ overexpression depend on ORN identity as this manipulation instead abolished the olfactory responses of Or67d ORNs (Figures 3.7C–D). These findings indicate that upregulation of $Fru^{MB}$ does not invariably elevate responses in all ORN types, and that $Fru^{MB}$ targets distinct downstream effectors in the courtship-promoting and courtship-inhibiting ORNs. A given $Fru^{M}$ isoform may up- or down-regulate varying target genes in different cells, likely through partnering with distinct transcription factors. Consistent with this idea, Or67d ORNs do not express PPK25 nor exhibit age-dependent sensitization (Lin et al., 2016; Starostina et al., 2012), despite their expression of both $Fru^{MB}$ and $Fru^{MC}$ isoforms (Figure 3.5B). Our results thus highlight the nuanced, non-binary regulation of $Fru^{M}$ isoforms, a sophisticated mechanism which affords the $Fru^{M}$ proteins versatility in their functional output.

What is the biological significance of the opponent modulation with coincident $Fru^{MB}$ upregulation and $Fru^{MC}$ downregulation (Figures 3.4 and 3.5)? Channel stoichiometry may provide the answer. PPK25 and PPK23, the isoforms' respective downstream effectors, are members of the DEG/ENaC family whose cation channels are composed of three subunits (Hanukoglu and Hanukoglu, 2016; Kellenberger and Schild, 2002; Staruschenko et al., 2005). When ectopically expressed, PPK25 alone cannot enhance female Or47b ORN responses (Ng et al., 2019), indicating that PPK25 does not form a functional homotrimeric channel. In contrast, overexpression of PPK25 in the Or47b ORNs of

2-day old males can markedly increase their olfactory responses (Ng et al., 2019), likely due to the presence of PPK23. As such, the opponent modulation of $Fru^{MB}$ and $Fru^{MC}$ is best explained within the scenario in which the functional amplification channel adopts a stoichiometry whereby PPK23/PPK25 ratio is 1:2. In 2-day old males, $Fru^{MC}$ expression is not yet downregulated and $Fru^{MB}$ levels are still low (Figures 3.4 and 3.5), likely resulting in higher PPK23 expression relative to PPK25 in the courtship-promoting ORNs. In this scenario, the trimeric channel may fail to assemble, or adopt a nonfunctional or low-conductance stoichiometry (PPK23/PPK25 ratio 2:1 or 3:0); both cases will prohibit response amplification. When male flies are 7 days old, on the other hand, the ratio of $Fru^{MB}$/$Fru^{MC}$ increases and thus allows PPK25 to be expressed at a higher level than PPK23, favoring the formation of functional amplification channels.

In addition to the aforementioned mechanism, the opponent regulation of $Fru^{MB}$ and $Fru^{MC}$ may further control PPK25/PPK23 ratio via other means. Upstream of the *ppk25* gene, I identified not only $Fru^{MB}$ DNA binding domains, but also a putative $Fru^{MC}$ binding site (Figure 3.11), thus raising the possibility that $Fru^{MC}$ may also play a role in modulating *ppk25* expression. Notably, overexpressing $Fru^{MC}$ in the Or47b ORNs reduced their pheromone responses (Figure 3.6F), which is opposite to the response-enhancing effect of $Fru^{MB}$ (Figure 3.6D). It is therefore possible that apart from promoting *ppk23* expression, $Fru^{MC}$ also reduces *ppk25* expression by operating as a transcription inhibitor (Chowdhury et al., 2017; Ito et al., 2016; Sato and Yamamoto, 2020). Thus, the coordinated up- and down-regulation of $Fru^{MB}$ and $Fru^{MC}$ may further ensure the desired PPK25/PPK23 ratio through the isoforms' antagonist impacts on *ppk25* expression.

In summary, our research has identified a mechanism by which multiple $Fru^{M}$ isoforms cooperatively mediate sexual dimorphism. By focusing on courtship-promoting $fru^{M+}$ ORNs that exhibit male-specific neurophysiology and glomerular enlargement, this study uncovers how the chemosensory and morphological aspects of sexual dimorphism may be coordinated through

differential regulations of the co-expressed splice variants, and through the synergistic cooperation of these isoforms' downstream effectors.

### 3.5 Materials and methods

#### *Drosophila* stocks

All flies (*Drosophila melanogaster*) were raised on standard cornmeal medium at 25°C, ~60% relative humidity in an incubator with a 12-hr light/dark cycle. Flies were collected upon eclosion, separated by sex and raised in groups of 10. Male flies 2 or 7 days post-eclosion were used in all experiments unless noted otherwise. For further information on genotypes, refer to Table S1.

#### Single-sensillum recordings

A fly was wedged into the narrow end of a truncated plastic 200-µl pipette tip to expose the antenna, which was then stabilized between a tapered glass microcapillary and a coverslip covered with double-sided type. Single-unit recordings were performed essentially as described (Ng et al., 2017). Briefly, electrical activity of target ORNs was recorded extracellularly by placing a sharp electrode filled with artificial hemolymph solution (Wang et al., 2003) in the at4 sensillum (Or47b ORN recordings). For at1 (Or67d ORN) or ac4 (Ir84a ORN) sensillum recordings, 0.6X sensillum lymph Ringer solution (Kaissling, K. E., Thorson, 1980) was used instead. The reference electrode filled with the same solution was placed in the eye. No more than three sensilla from the same antenna were recorded per fly.

AC signals (100-20k Hz) were recorded on an NPI EXT-02F amplifier (ALA Scientific Instruments) and digitized at 5 kHz with Digidata 1550 (Molecular Devices). ORN spikes were detected and sorted using threshold search under Event Detection in Clampfit 10.4 (Molecular Devices). Spike timing data were exported and analyzed in Igor Pro 6.3 (Wavemetrics). Peri-stimulus time histograms (PSTHs) were obtained by averaging spike activities in 50-ms bins and smoothed

using a binomial filter (Igor Pro 6.3, Wavemetrics). For dosage curves and statistical analysis, responses were quantified by subtracting the pre-stimulus spike rate (1 s) from the peak spike frequency during odorant stimulation (adjusted peak responses).

**Odor stimuli**

Phenylacetaldehyde was diluted in paraffin oil, applied as 100-µl aliquots on filter discs and delivered to the antenna via a 500-ms air pulse at 200 ml $min^{-1}$ through the main airstream (2000 ml $min^{-1}$). Both *c*VA (10 µl per filer disc) and palmitoleic acid (4.5 µl per filer disc) were diluted in ethanol and delivered via a 500-ms air pulse at 250 ml $min^{-1}$ directly to the antenna from a close range, as previously described (Ng et al., 2017). Ethanol was allowed to evaporate for 1 hour in a vacuum desiccator prior to experiments.

**Immunohistochemistry**

Two-day or seven-day old male files were anesthetized on ice, with their heads aligned in a collar, covered with Cryo-OCT (Tissue-Tek, Fisher Scientific), and frozen on dry ice as described (Saina and Benton, 2013). Cryosectioning was performed with CryoStar NX70 (Thermo Fisher Scientific) and 14-µm antennal sections were collected on Superfrost Plus microscope slides (Fisher Sceintific). Sections were fixed with 4% paraformaldehyde in phosphate-buffered saline (PBS) for 10 minutes, washed in PBST (PBS with 0.3% Triton X-100) for 3 minutes three times, and incubated for 30 minutes in the blocking solution (PBST with 5% normal goat serum). All steps were performed at room temperature unless otherwise noted. Myc-tag epitopes were labeled with rabbit anti-myc antibodies (1: 250 in the blocking solution, 71D10, Cell Signaling Technology) at 4°C overnight. After being washed three times in PBST, sections were incubated with the goat anti-rabbit Alexa 647 secondary antibody (1: 200 in the blocking solution, A21236, Life Technologies) for 2 hours at 4°C temperature, followed by 3x3 minutes washing in PBST. The sections were then mounted in DAPI

Flouromount-G (Fisher Scientific). Confocal microscopy was performed with a Zeiss 880 Airyscan Microscope, and images were processed with ImageJ. As negative controls, parallel experiments were also conducted with 7-day old females, and the samples were imaged with identical acquisition parameters. Compared to male samples, only very faint myc staining signals were observed in females and were therefore considered as background. For the analysis of male samples, the pixel value of myc staining within a neuron has to exceed the background level to be considered as positive signals.

The percentage of the ORNs which express a particular $Fru^M$ isoform was determined by counting the number of $myc^+/GFP^+$ neurons and dividing it by the total number of $GFP^+$ cells. Parallel experiments with identical image acquisition parameters were performed with 2-day and 7-day old males to determine whether the percentage of $myc^+/GFP^+$ neurons changes with age. This analysis — relying on detecting $myc^+$ signals above an arbitrary threshold — aims to assay the relative up- or down-regulation of $Fru^M$ isoforms in each age group, instead of the absolute levels of their expression.

**Whole-mount brain imaging**

Fly brains were dissected in ice cold PBS, fixed first in 4% (w/v) paraformaldehyde and then in 4% (w/v) paraformaldehyde containing 0.25% Triton X-100. Fixation was facilitated by microwaving the samples on ice for 1 min, repeated three times for each fixative. Samples were then placed in PBS and degassed in a vacuum chamber for 10 minutes. This step was repeated three times to remove air in the trachea. Samples were mounted in FocusClear™ (Cedarlane Labs, Canada) before native GFP was imaged for quantification. Samples were processed and imaged on the same day immediately after mounting. Images were acquired with a Zeiss LSM510 confocal microscope and a 40X/1.2 objective using the same laser power and detector gain for samples processed in parallel experiments.

Glomerular volumes were analyzed using ImageJ (NIH). Briefly, the stack range for the glomerulus of interest (i.e., 2-54 out of the 120 acquired images) was first identified. The contours of

the VA1lm and DA1 glomeruli were manually traced in every five serial images until the entire glomerular volume was covered. The VL2a glomerulus, which is smaller than the other two glomeruli, was traced in every image instead. Glomerular sizes were then estimated by summing the area within each glomerular contour. To calculate the sex ratio, the glomerular volume of each male sample was divided by the average volume of the corresponding glomerulus in females.

**$Fru^M$ isoform binding motif alignment**

The DNA sequences of the *ppk25* and *ppk23* genes, as well as the corresponding 5' region (2 kb), were obtained from FlyBase (https://flybase.org/). Published $Fru^M$ isoform binding motifs (Dalton et al., 2013; Neville et al., 2014) were used as queries to identify putative isoform-specific binding sites through sequence alignment using Serial Cloner 2.6 (http://serialbasics.free.fr/Serial_Cloner.html).

**Statistics**

Statistical results (p value and n) are indicated in figure legends corresponding to each experiment. In cases where a dosage curve for odor concentration was performed, two-tailed t tests comparing the experimental and control groups were performed for each concentration and the p-value is indicated on the figure by asterisks (*$p < 0.05$; **$p < 0.01$; ***$p < 0.001$). In cases where quantification of peak spike responses from each neuron was shown, two-way ANOVA followed by Tukey's post hoc test was performed in RStudio (https://www.rstudio.com), and $p < 0.05$ was considered statistically significant. All data are presented as mean ± SEM and plotted in Igor Pro 6.32A (https://www.wavemetrics.com/products/igorpro/igorpro). Dosage response curves were fitted with Hill equation for illustration purposes.

Chapter 3, in part, is currently under submission for publication of the material. Zhang, Ye; Su, Chih-Ying. The dissertation author was the primary investigator and author of this paper.

**Figure 3.1. $Fru^M$ is required for age-dependent olfactory sensitization**

**(A)** Single-sensillum recording. Left panel: representative trace (top), rasters (middle), and peri-stimulus time histogram (PSTH; bottom) are shown for Or47b ORN responses in 7-day wildtype males (palmitoleic acid: $10^{-1}$). Line width, SEM; gray bar, stimulus duration (0.5 s). Right panel: dosage curves of Or47b spike responses from 2-day and 7-day males. Adjusted peak responses (pre-stimulus baseline activity subtracted from peak response). Parallel experiments, mean ± SEM (n=9, from 4 flies). Significant differences are denoted by *$p < 0.05$, **$p < 0.01$, ***$p < 0.001$ as determined by unpaired two-tailed t test. **(B)** As in (A), recordings instead performed in $fru^F$ males. **(C)** Quantification of Or47b ORN responses to palmitoleic acid ($10^{-1}$) in wildtype and $fru^F$ males. Individual dots indicate responses from different neurons, from experiments shown in **(A)** and **(B)**. Significant differences between any two groups ($p < 0.05$) are indicated by different letters; ANOVA followed by Tukey's test. **(D, E and F)** As in **(A)**, **(B)** and **(C)**, Ir84a ORN responses recorded instead from wildtype **(D)** or $fru^F$ **(E)** males. **(G, H and I)** As in **(A)**, **(B)** and **(C)**, Or67d ORN responses recorded instead from wildtype **(G)** or $fru^F$ **(H)** males. **(J)** $Fru^M$ is required for the age-dependent sensitization in the courtship-promoting ORNs.

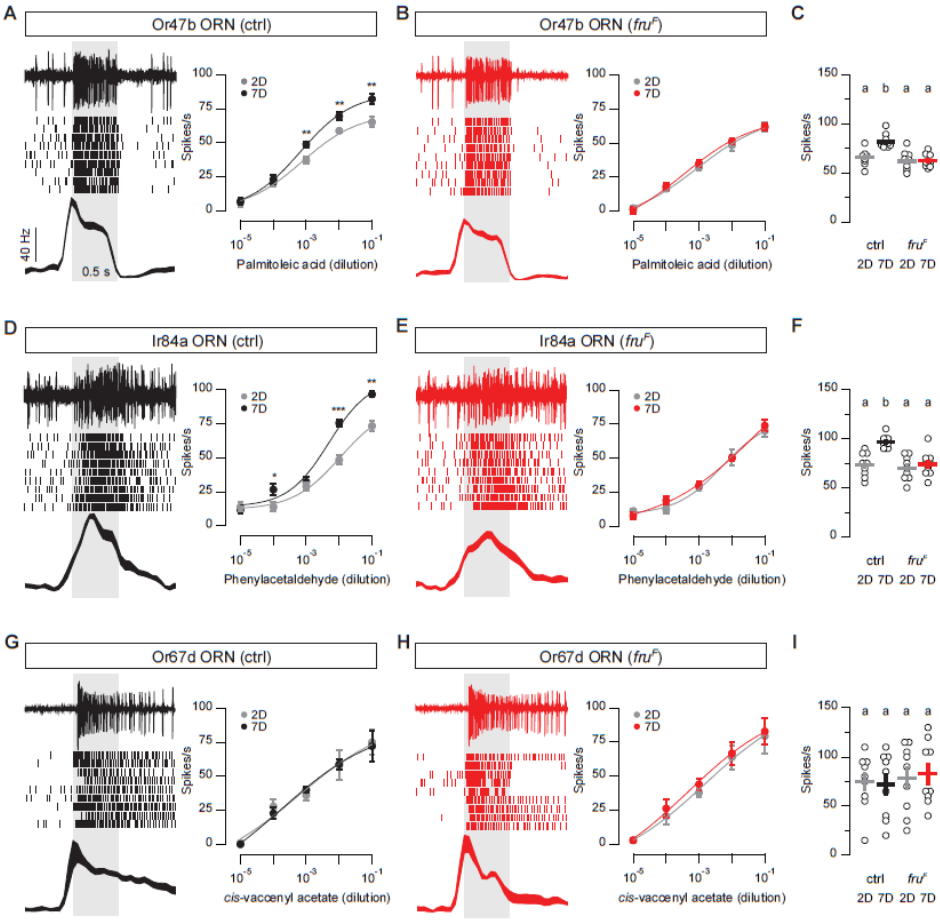


J

| | Or47b | Ir84a | Or67d |
|---|---|---|---|
| Express $Fru^M$ | + | + | + |
| Promote courtship | + | + | – |
| Reduced response in $fru^F$ | + | + | – |

**Figure 3.2. $Fru^{MB}$ and $Fru^{MC}$ are both required for the age-dependent sensitization of male Or47b neurons**

**(A)** Schematics of the *fru* locus, adapted from Billeter et al., 2006 (Billeter et al., 2006b). P1–P4 indicate alternative promoters. The mRNA transcripts generated from the P1 promoter are spliced in a sexually-dimorphic manner, such that only males can produce functional $Fru^{M}$ proteins. The BTB protein-protein interaction domain (black) and the A–C alternative exons encoding zinc-finger DNA binding domains (vertical black lines) are shown. Isoform-specific mutations are illustrated below. **(B)** Single-sensillum recording from $fru^{MA}$ mutant males ($fru^{\Delta A}/fru^{F}$). Sample traces, rasters, PSTHs (palmitoleic acid: $10^{-1}$) and dosage curves are shown. Line width, SEM; gray bar, 0.5-s stimulus duration. Parallel experiments, mean ± SEM (n=9, from 4 flies). ***$p < 0.001$; t test. **(C)** Quantification of Or47b ORN responses to palmitoleic acid ($10^{-1}$) from the indicated genotypes. Recordings were performed in parallel, mean ± SEM (n=9, from 4 flies). Significant differences between any two groups ($p < 0.05$) are indicated by different letters; ANOVA followed by Tukey's test. **(D–G)** As in (B) and **(C)**, recordings were instead performed in $fru^{MB}$ mutants **(D and E)** or $fru^{MC}$ mutants **(F and G)**. **(H)** $Fru^{MB}$ and $Fru^{MC}$ are both required for the age-dependent sensitization of Or47b ORNs.

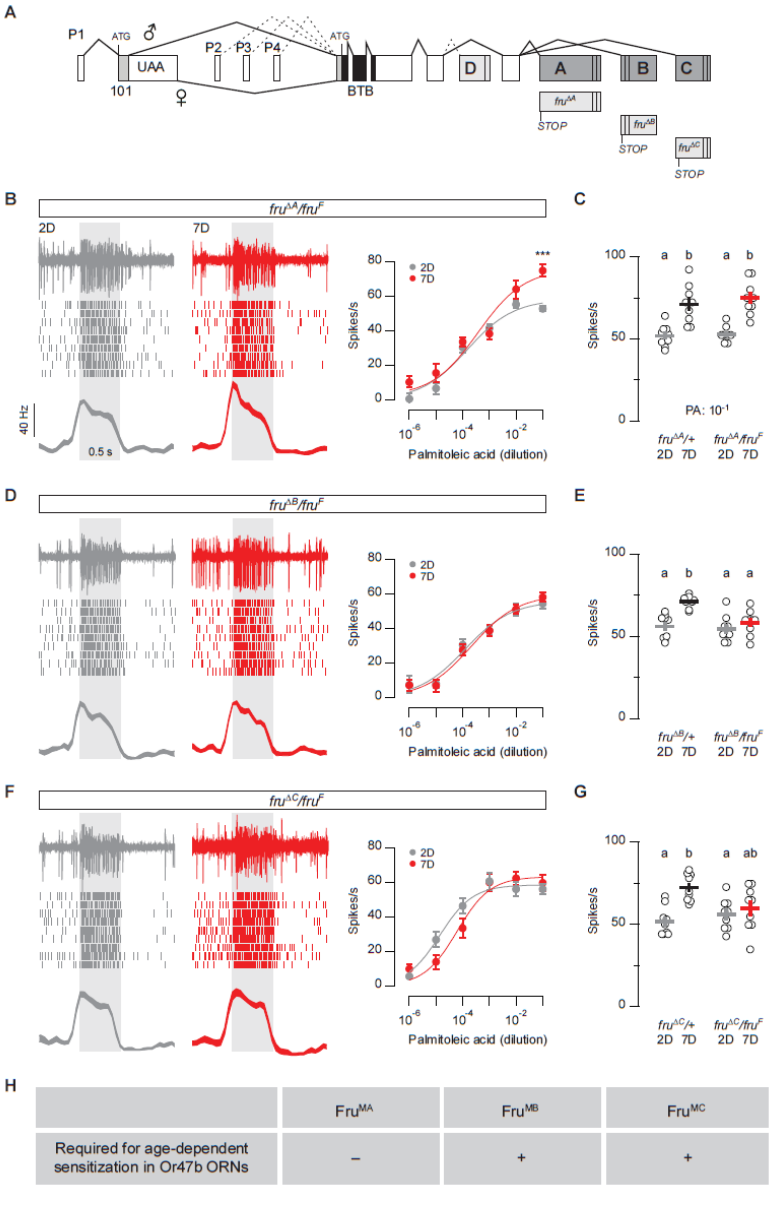


H

| | $Fru^{MA}$ | $Fru^{MB}$ | $Fru^{MC}$ |
|---|---|---|---|
| Required for age-dependent sensitization in Or47b ORNs | – | + | + |

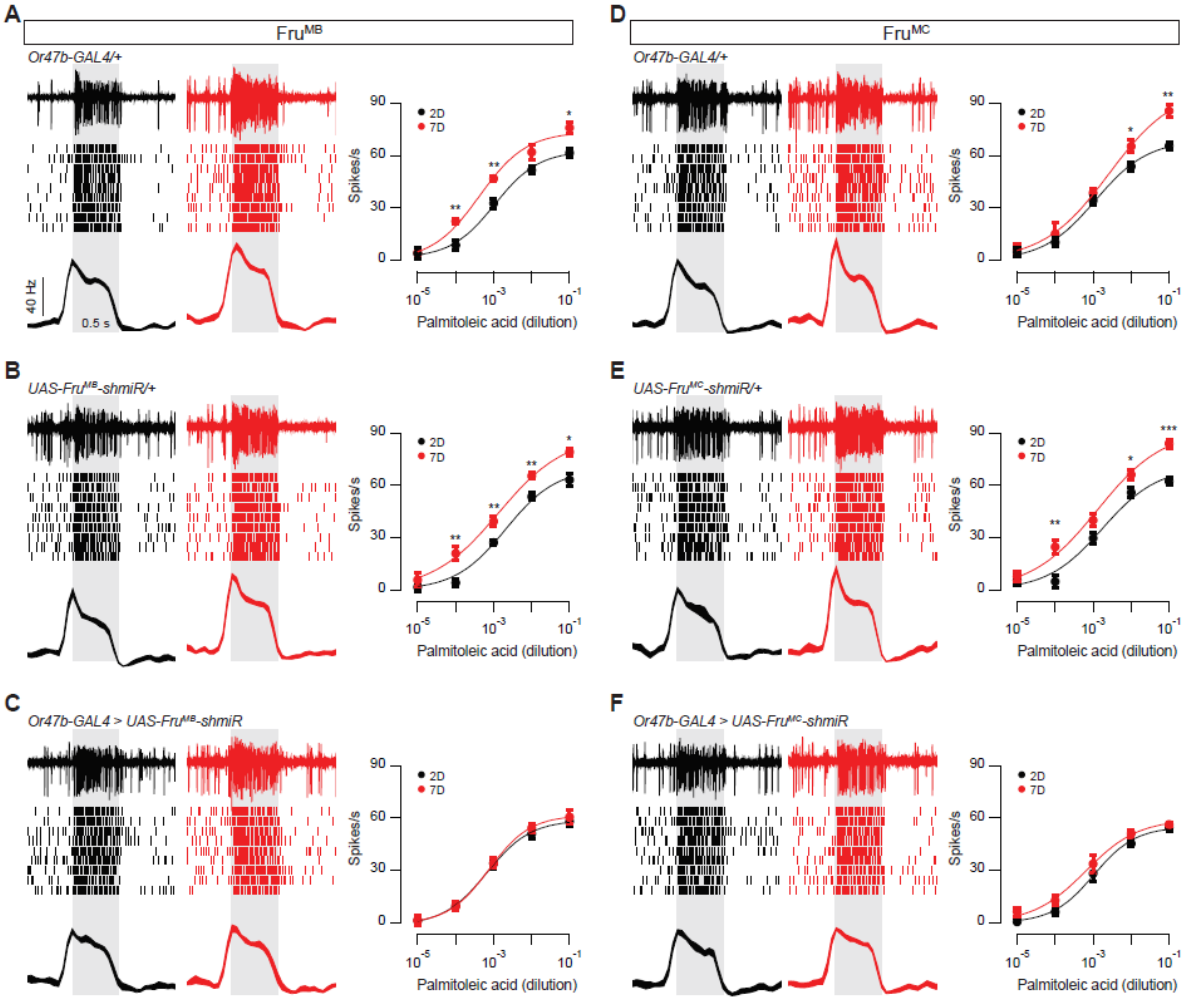


**Figure 3.3. Fru$^{MB}$ and Fru$^{MC}$ are both required for the age-dependent sensitization of male Or47b neurons**

Single-sensillum recordings from males in which Fru$^{MB}$ **(A, B and C)** or Fru$^{MC}$ **(D, E and F)** was selectively knocked down in Or47b ORNs. Left two panels: representative traces (top), rasters (middle), and PSTHs (bottom) are shown for Or47b ORN responses in the controls **(A and B)**, and Fru$^{MB}$ knockdown males **(C)** (palmitoleic acid: $10^{-1}$). Line width, SEM; gray bar, 0.5-s stimulus duration. Right panels: dosage curves of Or47b spike responses from 2-day and 7-day old males (adjusted peak responses). Parallel experiments, mean ± SEM (n=9, from 4 flies). *p < 0.05, **p < 0.01; t test. **(D, E and F)** As in **(A)**, **(B)** and **(C)** except that recordings were conducted in the controls **(D)** and **(E)**, and Fru$^{MC}$ knockdown males.

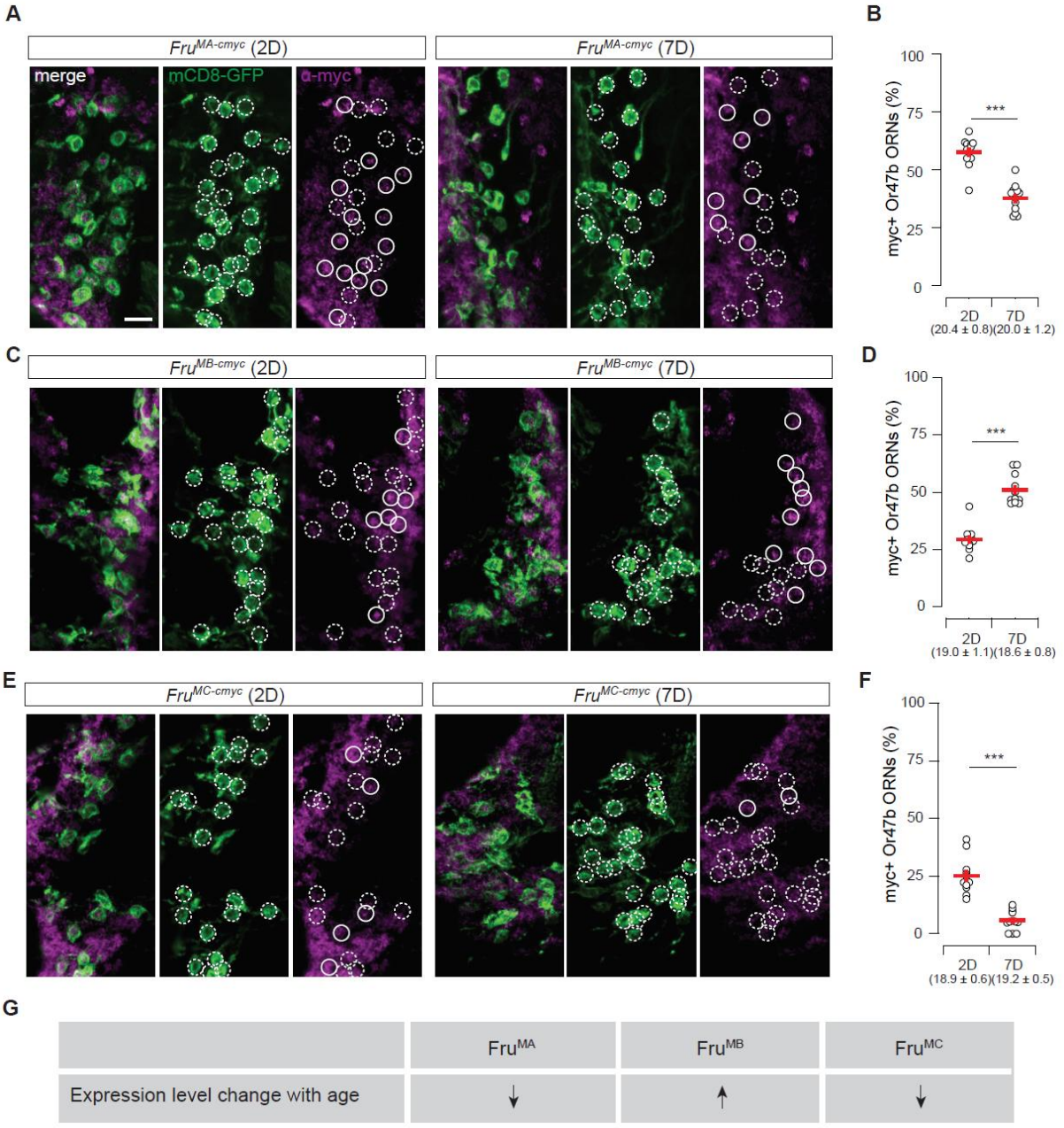


**Figure 3.4. Fru$^{M}$ isoforms are differentially regulated by age in Or47b neurons**

**(A)** Confocal images of antennal sections. GFP-labeled Or47b ORNs were outlined in dotted circles (middle and right panels). Fru$^{A\text{-}myc}$ was immunolabeled with anti-*myc* antibodies (α-myc, in magenta). Solid circles indicate myc$^{+}$/GFP$^{+}$ neurons (right panels). Images were acquired with identical parameters in parallel experiments. Scale bar, 5 μm. **(B)** Quantification of the percentage of Or47b neurons which stained positive for α-myc signals. The average number of GFP-labeled Or47b neurons per antennal section is indicated in parentheses. Individual dots indicate data points from different flies, red lines represent mean ± SEM (n=11 sections, one section per fly). ***p < 0.001; t test. **(C–F)** Similar to **(A)** and **(B)** except that Fru$^{B\text{-}myc}$ **(C and D)** or Fru$^{C\text{-}myc}$ **(E and F)** was immunolabeled and scored. **(G)** In male Or47b ORNs, Fru$^{MB}$ expression is upregulated with age, while Fru$^{MA}$ and Fru$^{MC}$ are downregulated.

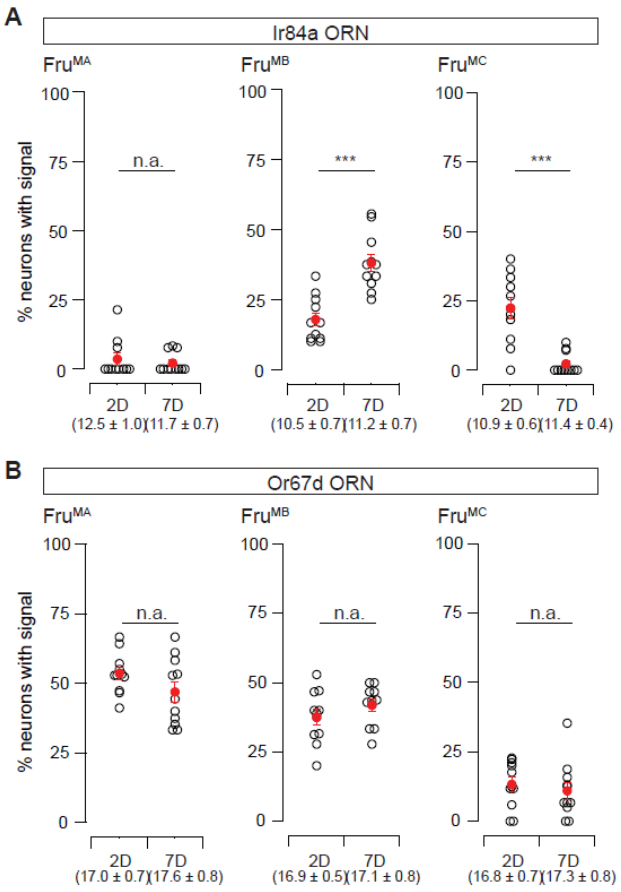


**Figure 3.5. Analysis of Fru$^{M}$ isoform expression in Ir84a and Or67d ORNs**

**(A)** Quantification of the percentage of Ir84a neurons which stained positive for α-myc signals from confocal images of antennal sections. Fru$^{MA\text{-}myc}$ (left), Fru$^{MB\text{-}myc}$ (middle) or Fru$^{MC\text{-}myc}$ (right) was immunolabeled with anti-*myc* antibodies. The number of GFP-labeled Ir84a neurons per antennal section is indicated in parentheses. Individual dots indicate data points from different flies, mean ± SEM in red (n=11 sections, one section per fly). ***$p < 0.001$; t test. **(B)** Similar to **(A)** except that Or67d neurons were labeled and scored.

**Figure 3.6. Overexpression of $Fru^{MB}$ elevates male Or47b ORN responses**

**(A)** Single-sensillum recording. Representative traces (top), rasters (middle), and PSTHs (bottom) are shown for Or47b ORN responses in 2-day males (palmitoleic acid: $10^{-1}$). Line width, SEM; gray bar, 0.5-s stimulus duration. **(B)** Dosage curves of Or47b spike responses from controls and $Fru^{MA}$ overexpression group (adjusted peak responses). Parallel experiments, mean ± SEM (n=9, from 4 flies for each genotype). **(C–F)** Similar to (A) and (B) except that $Fru^{MB}$ **(C and D)** or $Fru^{MC}$ **(E and F)** was overexpressed. **(G)** Upregulation of $Fru^{MB}$, but not $Fru^{MA}$ or $Fru^{MC}$, increases Or47b olfactory responses in 2-day males.

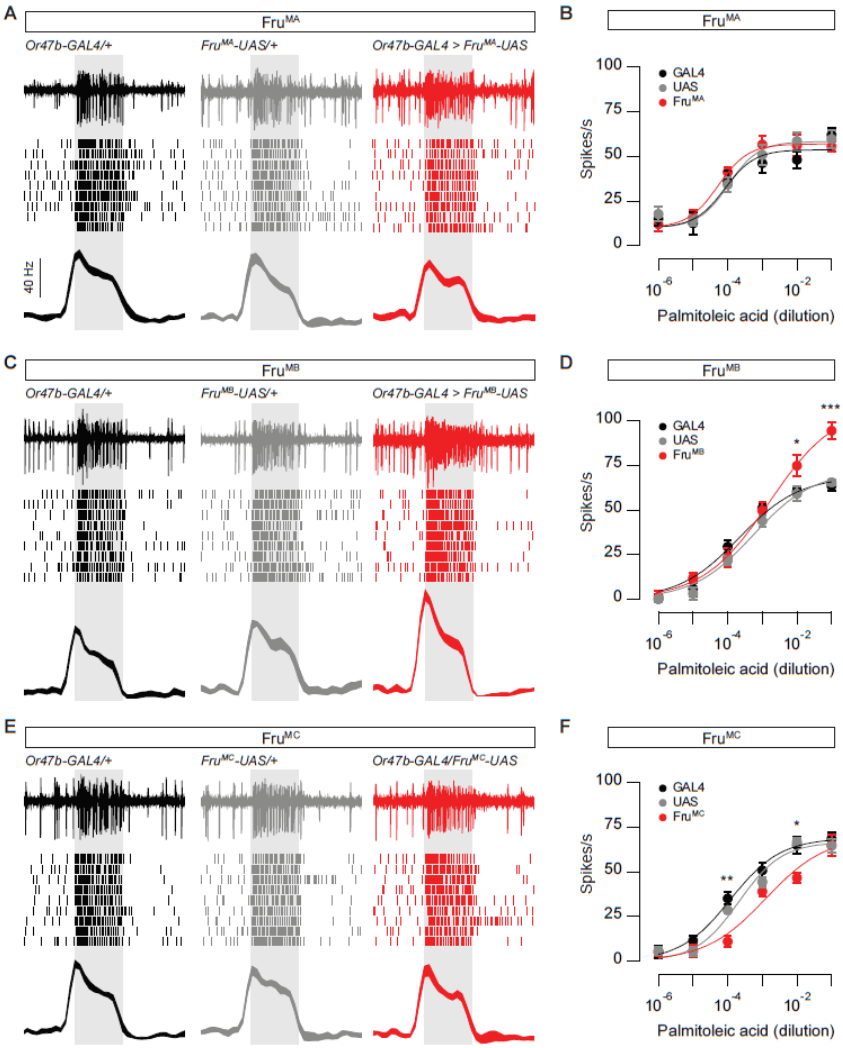


G

| | Fru^MA | Fru^MB | Fru^MC |
|---|---|---|---|
| Overexpression changes Or47b responses | NA | increase | decrease |

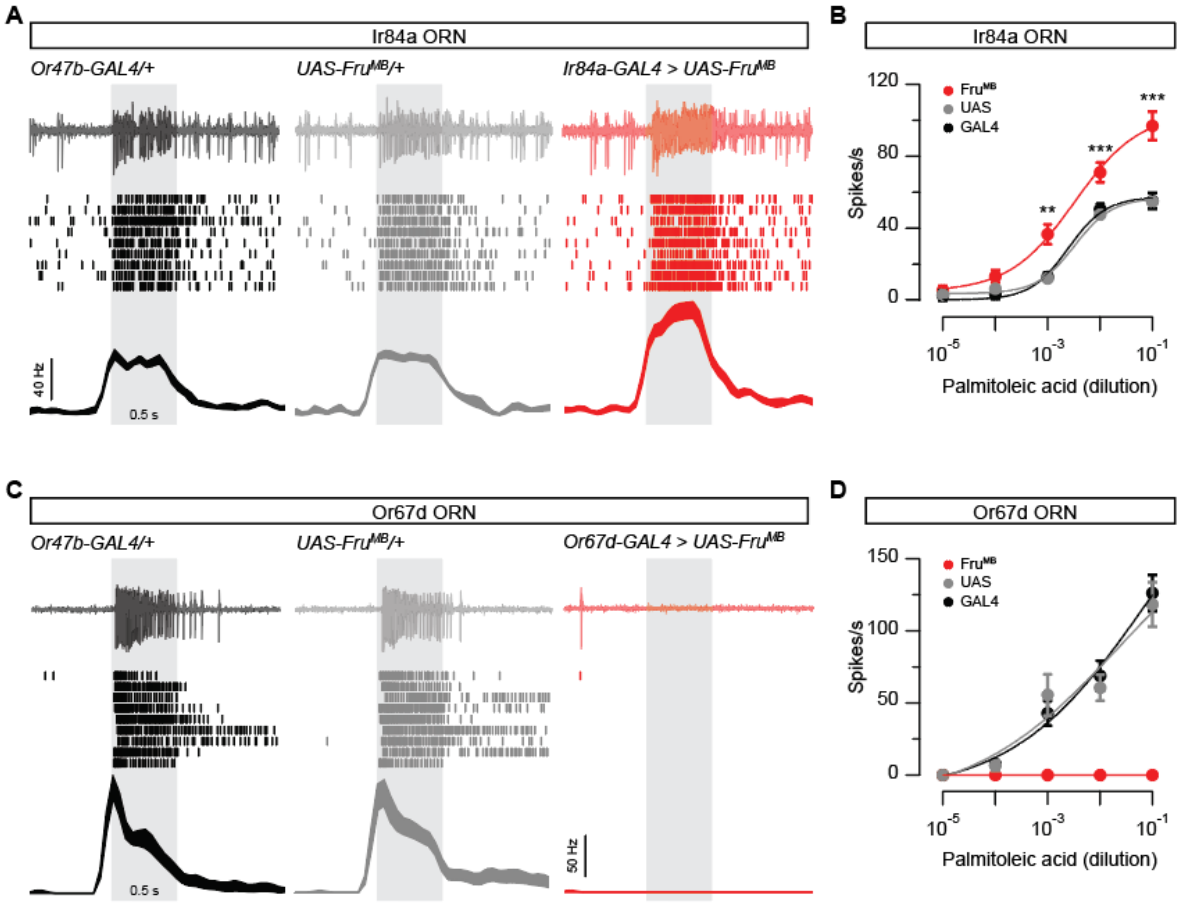


**Figure 3.7. Overexpression of Fru$^{MB}$ increases Ir84a but not Or67d ORN responses in males**

**(A)** Single-sensillum recording. Representative traces (top), raster plots (middle), and peri-stimulus time histograms (PSTHs; bottom) are shown for Ir84a ORN responses in 2-day males (palmitoleic acid: $10^{-1}$). Line width, SEM; gray bar, 0.5-s stimulus duration. **(B)** Dosage curves of Ir84a spike responses from controls and Fru$^{MB}$ overexpression group (adjusted peak responses). Parallel experiments, mean ± SEM (n=9, from 4 flies for each genotype). **(C and D)** Similar to **(A)** and **(B)** except that Fru$^{MB}$ was overexpressed in Or67d ORNs.

**Figure 3.8. Epitasis analysis of juvenile hormone signaling, $Fru^{MB}$ upregulation and PPK25 expression in male Or47b ORNs**

**(A)** Single-sensillum recording with 2-day old males in the *Met* mutant background ($Met^{[1]}$). Representative traces (top), raster plots (middle), and peri-stimulus time histograms (PSTHs; bottom) are shown for Or47b ORN responses in controls and $Fru^{MB}$ overexpression males (palmitoleic acid: $10^{-1}$). Line width, SEM; gray bar, 0.5-s stimulus duration. **(B)** Dosage curves of Or47b ORN responses from controls and $Fru^{MB}$ overexpression group (adjusted peak responses). Parallel experiments, mean ± SEM (n=9, from 4 flies for each genotype). **(C and D)** Similar to (A) and (B) except that recordings were performed with 2-day old males in the *ppk25* mutant background (Δ*ppk25*). **(E)** Quantification of Or47b ORN responses to palmitoleic acid ($10^{-1}$) in 2-day old males. The data points are the same as shown in Figure 3.6C, all flies were in wildtype background. Significant differences between any two groups ($p < 0.05$) are indicated by different letters; ANOVA followed by Tukey's test. **(F)** Similar to **(E)** except that recordings were performed with males in the *ppk25* mutant background. **(G)** Similar to **(E)** except that recordings were performed with males in the *Met* mutant background. **(H)** Model based on the epistasis analysis. In male Or47b neurons, juvenile hormone (JH) binds to its receptor, Methoprene-tolerant (Met), which increases $Fru^{MB}$ expression in older males. $Fru^{MB}$ in turn mediates PPK25 upregulation, thereby increasing Or47b neuronal response.

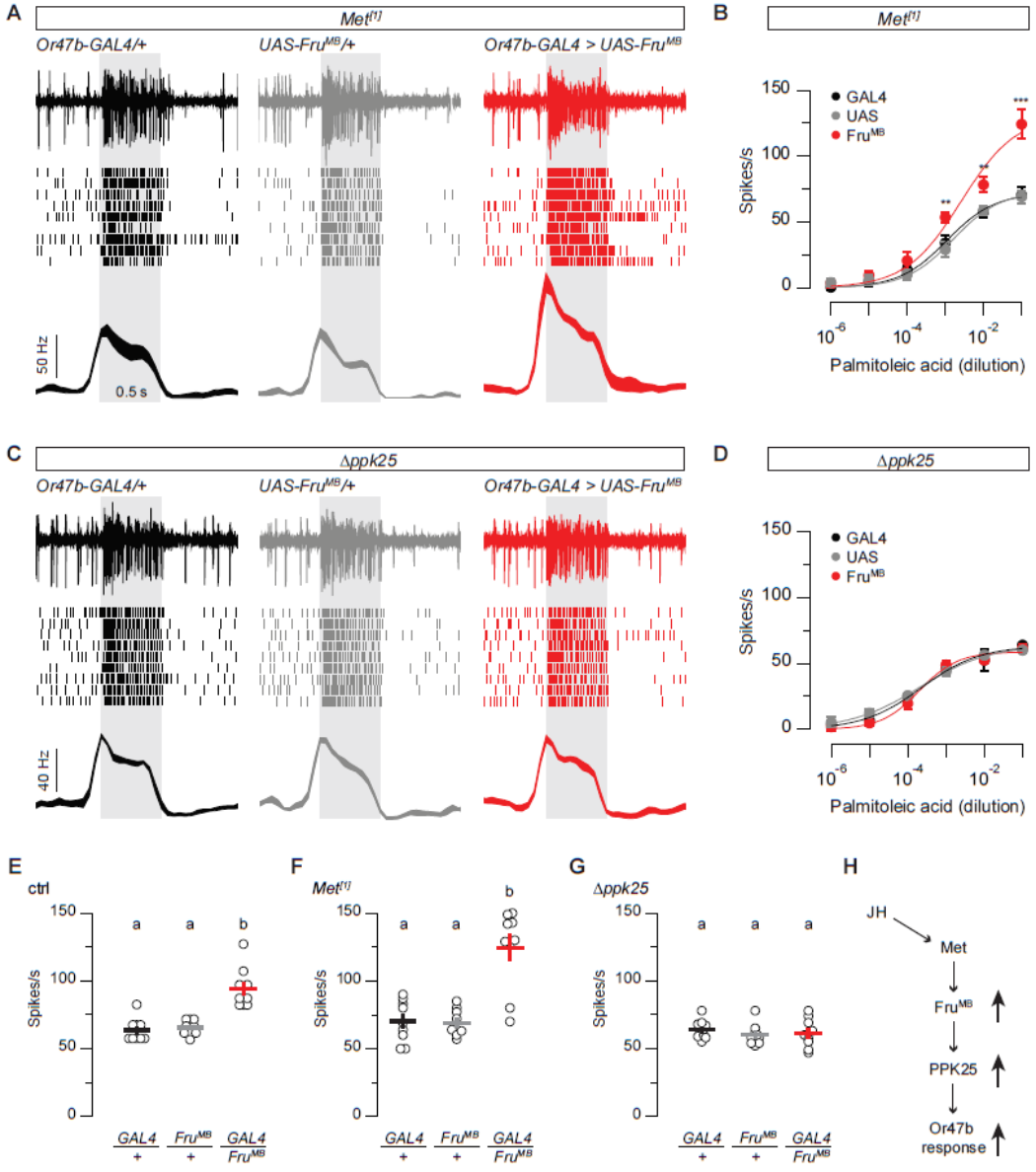
A
Met[1]
Or47b-GAL4/+
UAS-FruMB/+
Or47b-GAL4 > UAS-FruMB
50 Hz
0.5 s
B
Met[1]
GAL4
UAS
FruMB
Spikes/s
Palmitoleic acid (dilution)
C
Δppk25
Or47b-GAL4/+
UAS-FruMB/+
Or47b-GAL4 > UAS-FruMB
40 Hz
D
Δppk25
GAL4
UAS
FruMB
Spikes/s
Palmitoleic acid (dilution)
E
ctrl
F
Met[1]
G
Δppk25
Spikes/s
GAL4 +
FruMB +
GAL4 FruMB
H
JH
Met
FruMB
PPK25
Or47b response

**Figure 3.9. $Fru^{MB}$ and $Fru^{MC}$ cooperatively elevate Or47b ORN responses through distinct downstream effectors**

**(A)** Working models. In Model I, $Fru^{MB}$ and $Fru^{MC}$ requires each other in order to mediate the expression of PPK25 and its partner. In Model II, $Fru^{MB}$ and $Fru^{MC}$ are upstream of distinct targets that are required for the elevated Or47b pheromone responses. **(B)** Single-sensillum recording for Or47b ORN responses in 2-day old females. Quantification of the responses to palmitoleic acid ($10^{-1}$). Flies are *Or47b-GAL4/+*, *UAS-$Fru^{MB}$/+* or *Or47b-GAL4/UAS-$Fru^{MB}$*. Individual dots indicate data points from different flies, red lines represent mean ± SEM (n=9, from 4 flies, parallel experiments). ANOVA followed by Tukey's test. **(C)** Single-sensillum recordings in 2-day old virgin female flies whose Or47b ORNs expressed $Fru^{MB}$, $Fru^{MC}$ or both of the isoforms. Dosage curves (left) and quantifications of the responses to palmitoleic acid ($10^{-1}$) (right) are shown. Parallel experiments, mean ± SEM (n=9, from 4 flies per genotype). Significant differences are indicated by asterisks (**$p < 0.01$; t test, left panel) or different letters ($p < 0.05$; ANOVA followed by Tukey's test; right panel). **(D)** As in (C) except that female flies expressed PPK25, $Fru^{MC}$ or both of the transgenes in their Or47b ORNs. **(E)** As in **(C)** except that female flies expressed PPK25, $Fru^{MB}$ or both of the transgenes in their Or47b ORNs. **(F)** As in **(C)** except that female flies expressed PPK23, $Fru^{MC}$ or both of the transgenes in their Or47b ORNs. **(G)** As in **(C)** except that female flies expressed PPK23, $Fru^{MB}$ or both of the transgenes in their Or47b ORNs.

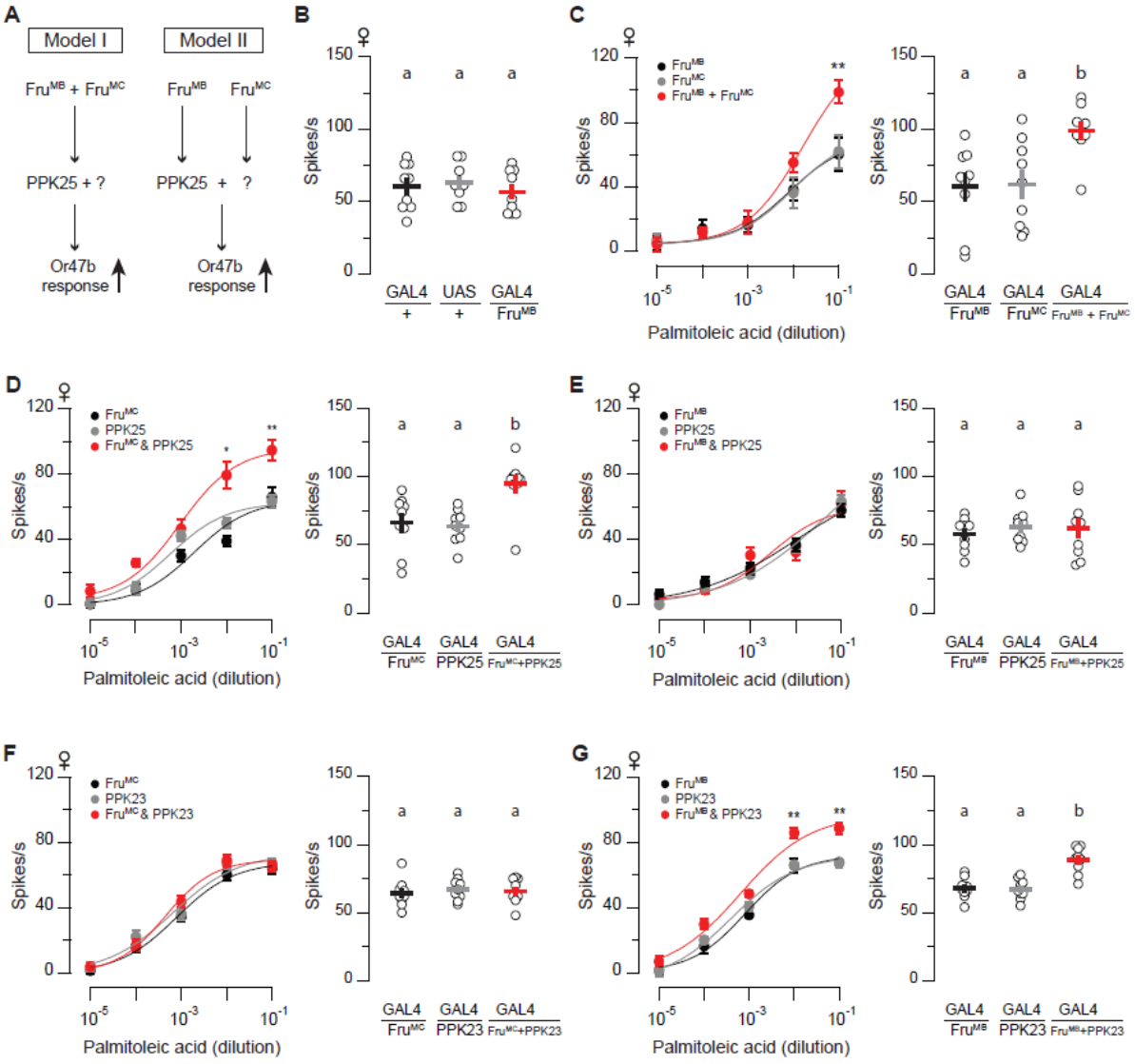
A
Model I
Model II
Fru^MB + Fru^MC
PPK25 + ?
Or47b response
Fru^MB
Fru^MC
PPK25 + ?
Or47b response
B
♀
Spikes/s
GAL4 / +
UAS / +
GAL4 / Fru^MB
C
Fru^MB
Fru^MC
Fru^MB + Fru^MC
**
Palmitoleic acid (dilution)
GAL4 / Fru^MB
GAL4 / Fru^MC
GAL4 / Fru^MB + Fru^MC
D
Fru^MC
PPK25
Fru^MC & PPK25
*
**
Palmitoleic acid (dilution)
GAL4 / Fru^MC
GAL4 / PPK25
GAL4 / Fru^MC+PPK25
E
Fru^MB
PPK25
Fru^MB & PPK25
Palmitoleic acid (dilution)
GAL4 / Fru^MB
GAL4 / PPK25
GAL4 / Fru^MB+PPK25
F
Fru^MC
PPK23
Fru^MC & PPK23
Palmitoleic acid (dilution)
GAL4 / Fru^MC
GAL4 / PPK23
GAL4 / Fru^MC+PPK23
G
Fru^MB
PPK23
Fru^MB & PPK23
**
**
Palmitoleic acid (dilution)
GAL4 / Fru^MB
GAL4 / PPK23
GAL4 / Fru^MB+PPK23

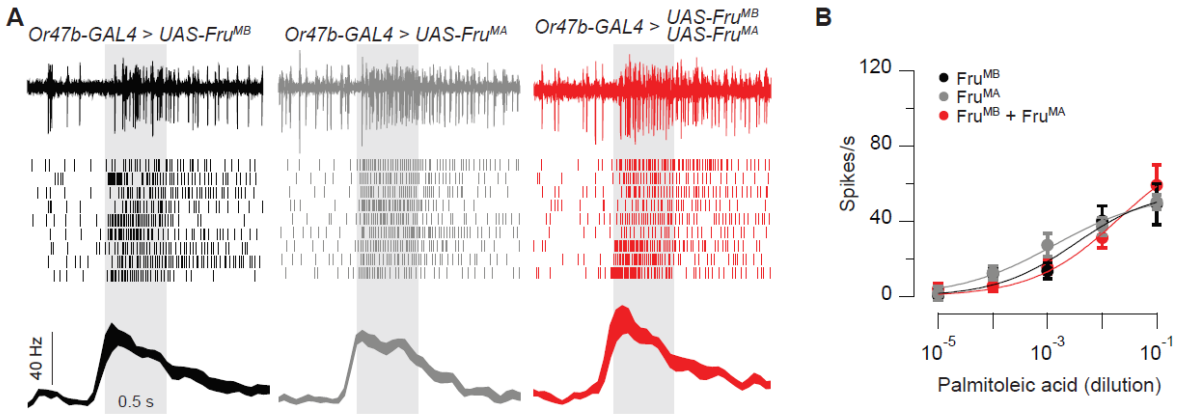


**Figure 3.10. Expression of Fru$^{MB}$ or Fru$^{MA}$ alone is not sufficient to increase Or47b response in females**

**(A)** Single-sensillum recording in 2-day females. Representative traces (top), raster plots (middle), and peri-stimulus time histograms (PSTHs; bottom) are shown for Or47b ORN responses in Fru$^{MB}$ ectopic expression (left), Fru$^{MA}$ ectopic expression (middle), and Fru$^{MB}$ & Fru$^{MA}$ co-expressed females (palmitoleic acid: $10^{-1}$). Line width, SEM; gray bar, stimulus duration. **(B)** Dosage curves of Or47b ORN responses to palmitoleic acid ($10^{-1}$) in 2-day females (adjusted peak responses). Parallel experiments, mean ± SEM (n=9, from 4 flies).

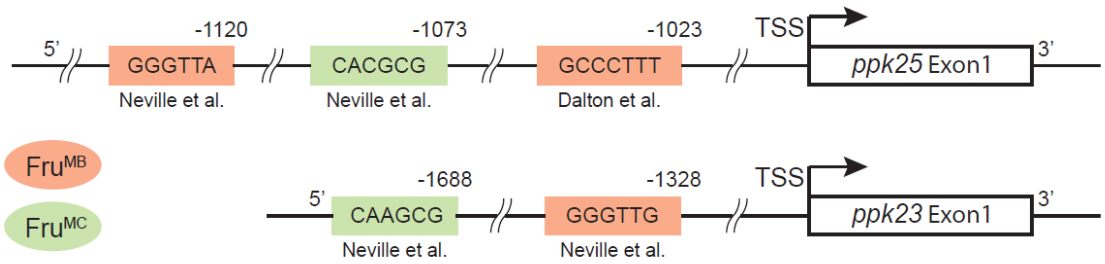


**Figure 3.11. Putative Fru$^{MB}$ or Fru$^{MC}$ DNA binding motifs upstream of *ppk25* and *ppk23***

The 5' untranslated regions of *ppk23* and *ppk25* are shown to indicate the positions of putative Fru$^{MB}$ and Fru$^{MC}$ DNA binding sites, based on Neville et al. (Neville et al., 2014) and Dalton et al. (Dalton et al., 2013). The transcription start site (TSS) and the first exon (Exon 1) are labeled.

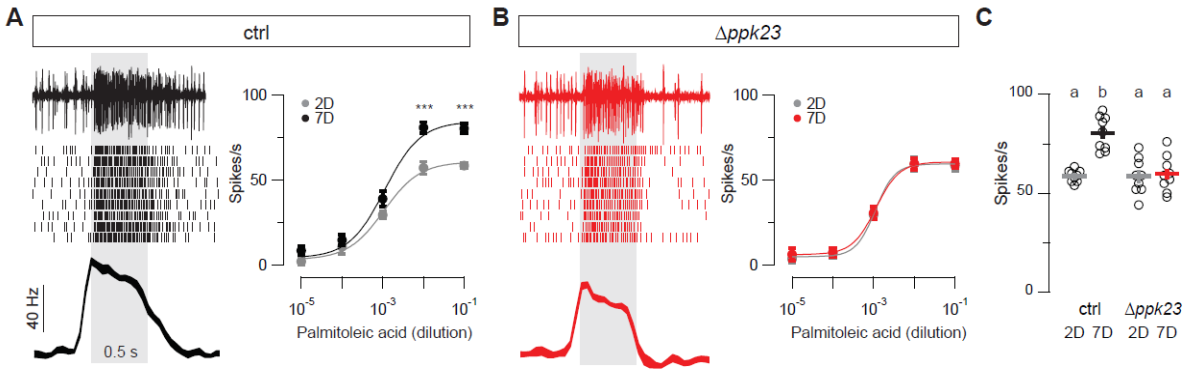


**Figure 3.12. *ppk23* is required for Or47b neuronal sensitization**

**(A)** Single-sensillum recording. Left panel: representative trace (top), raster plot (middle), and PSTH (bottom) are shown for Or47b ORN responses in 7-day wildtype males (palmitoleic acid: $10^{-1}$). Line width, SEM; gray bar, 0.5-s stimulus duration. Right panel: dosage curves of Or47b spike responses from 2-day and 7-day males (adjusted peak responses). Parallel experiments, mean ± SEM (n=9, from 4 flies). ***p < 0.001; t test. **(B)** As in **(A)**, recordings instead performed from *ppk23* mutant males (Δ*ppk23*). **(C)** Quantification of Or47b ORN responses to palmitoleic acid ($10^{-1}$) in wildtype or *ppk23* mutant males. Significant differences between any two groups ($p < 0.05$) are indicated by different letters; ANOVA followed by Tukey's test.

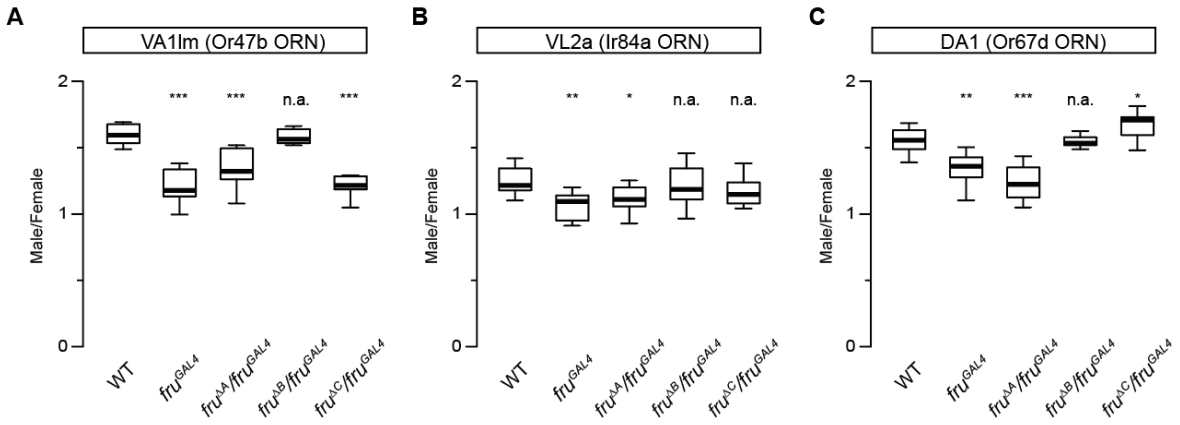


**Figure 3.13. The roles of Fru$^{M}$ isoforms in male-specific glomerular enlargement**

Box plots indicating the sex ratio in the volumes of specific glomeruli innervated by *fru*$^{M+}$ ORNs expressing the Or47b **(A)**, Ir84a **(B)** or Or67d receptor **(C)** (n=10 antennal lobes from 10 flies per genotype). Glomeruli were labeled by mCD8-GFP driven by *fru*$^{GAL4.P1}$ in the wildtype or different *fru*$^{M}$ mutant backgrounds. Significant differences are indicated by asterisks (*p < 0.05; **p < 0.01; ***p < 0.001; t test)

**Table 3.1. Fly genotypes.**

| | | |
|---|---|---|
| Figure 3.1 | A | Wild-type $w^{1118}$ |
| | B | $fru^{F}$ *(Bloomington #66873, RRID:BDSC_66873) (Demir & Dickson, 2005, Cell)* |
| | D | Same as A |
| | E | Same as B |
| | G | Same as A |
| | H | Same as B |
| Figure 3.2 | B | $w^{1118}$*, +;* $fru^{\Delta A}/fru^{F}$ *(Neville et al., 2014)* |
| | D | $w^{1118}$*, +;* $fru^{\Delta B}/fru^{F}$ *(Neville et al., 2014)* |
| | F | $w^{1118}$*, +;* $fru^{\Delta C}/fru^{F}$ *(Billeter et al., 2006)* |
| Figure 3.3 | A | *+; Or47b-GAL4/+* |
| | B | *UAS-*$Fru^{MB}$*-shmiR/+; + (von Philipsborn Lab, Aarhus University)* |
| | C | *UAS-*$Fru^{MB}$*-shmiR/+; Or47b-GAL4/+* |
| | D | *+; Or47b-GAL4/+* |
| | E | *UAS-*$Fru^{MC}$*-shmiR/+; + (von Philipsborn et al., 2014, curr. biol)* |
| | F | *UAS-*$Fru^{MC}$*-shmiR/+; Or47b-GAL4/+* |
| Figure 3.4 | A-B | *Or47b-GAL4/UAS-mCD8-GFP;* $Fru^{A\text{-}myc}$*/UAS-mCD8-GFP (Bloomington #9983, RRID:BDSC_9983)(von Philipsborn et al., 2014, curr. biol)* |
| | C-D | *Or47b-GAL4/UAS-mCD8-GFP;* $Fru^{B\text{-}myc}$*/UAS-mCD8-GFP (von Philipsborn et al., 2014, curr. biol)* |
| | E-F | *Or47b-GAL4/UAS-mCD8-GFP;* $Fru^{C\text{-}myc}$*/UAS-mCD8-GFP (von Philipsborn et al., 2014, curr. biol)* |
| Figure 3.5 | A | *Ir84a-GAL4/UAS-mCD8-GFP;* $Fru^{MA\text{-}myc}$*/UAS-mCD8-GFP (Bloomington #41734, RRID:BDSC_41734)*<br>*Ir84a-GAL4/UAS-mCD8-GFP;* $Fru^{MB\text{-}myc}$*/UAS-mCD8-GFP*<br>*Ir84a-GAL4/UAS-mCD8-GFP;* $Fru^{MC\text{-}myc}$*/UAS-mCD8-GFP* |
| | B | *Or67d-GAL4/UAS-mCD8-GFP;* $Fru^{MA\text{-}myc}$*/UAS-mCD8-GFP (Bloomington #9998, RRID:BDSC_9998)*<br>*Or67d-GAL4/UAS-mCD8-GFP;* $Fru^{MB\text{-}myc}$*/UAS-mCD8-GFP*<br>*Or67d-GAL4/UAS-mCD8-GFP;* $Fru^{MC\text{-}myc}$*/UAS-mCD8-GFP* |
| Figure 3.6 | A-B | *Or47b-GAL4/+; +*<br>*+;* $UAS\text{-}Fru^{MA}$*/+ (Goodwin Lab, University of Glasgow)*<br>*Or47b-GAL4/+;* $UAS\text{-}Fru^{MA}$*/+* |
| | C-D | *Or47b-GAL4/+; +*<br>*+;* $UAS\text{-}Fru^{MB}$*/+ (Goodwin Lab, University of Glasgow)*<br>*Or47b-GAL4/+;* $UAS\text{-}Fru^{MB}$*/+* |
| | E-F | *Or47b-GAL4/+; +*<br>*+;* $UAS\text{-}Fru^{MC}$*/+ (Goodwin Lab, University of Glasgow)*<br>*Or47b-GAL4/+;* $UAS\text{-}Fru^{MC}$*/+* |

**Table 3.1. Fly genotypes (continued).**

| | | |
|---|---|---|
| Figure 3.7 | A-B | *Ir84a-GAL4/+; +* |
| | | *+; UAS-Fru$^{MB}$/+* |
| | | *Ir84a/+; UAS-Fru$^{MB}$/+* |
| | C-D | *Or67d-GAL4/+; +* |
| | | *+; UAS-Fru$^{MB}$/+* |
| | | *Or67d/+; UAS-FruMB/+* |
| Figure 3.8 | A-B | *Met$^{[1]}$, Or47b-GAL4/+; + (Bloomington #3473, RRID:BDSC_3472) (Wilson & Fabian, 1986)* |
| | | *Met$^{[1]}$, +; UAS-Fru$^{MB}$/+* |
| | | *Met$^{[1]}$, Or47b-GAL4/+; UAS-Fru$^{MB}$/+* |
| | C-D | *ppk25$^{\Delta 5\text{-}22}$, Or47b-GAL4/+; + (Lin et al., 2005)* |
| | | *ppk25$^{\Delta 5\text{-}22}$, +; UAS-Fru$^{MB}$/+* |
| | | *ppk25$^{\Delta 5\text{-}22}$, Or47b-GAL4/+; UAS-Fru$^{MB}$/+* |
| | E | *Or47b-GAL4/+; +* |
| | | *+; UAS-Fru$^{MB}$/+* |
| | | *Or47b-GAL4/+; UAS-Fru$^{MB}$/+* |
| | F | Same as A-B |
| | G | Same as A-B |
| Figure 3.9 | B | *Or47b-GAL4/+; +* |
| | | *+; UAS-Fru$^{MB}$/+* |
| | | *Or47b-GAL4/+; UAS-Fru$^{MB}$/+* |
| | C | *Or47b-GAL4/+; UAS-Fru$^{MB}$/+* |
| | | *Or47b-GAL4/+; UAS-Fru$^{MC}$/+* |
| | | *Or47b-GAL4/+; UAS-Fru$^{MB}$/UAS-Fru$^{MC}$* |
| | D | *Or47b-GAL4/+; UAS-Fru$^{MB}$/+* |
| | | *Or47b-GAL4/+; UAS-PPK25/+ (Vijayan et al., 2014)* |
| | | *Or47b-GAL4/+; UAS-Fru$^{MB}$/UAS-PPK25* |
| | E | *Or47b-GAL4/+; UAS-Fru$^{MC}$/+* |
| | | *Or47b-GAL4/+; UAS-PPK25/+* |
| | | *Or47b-GAL4/+; UAS-Fru$^{MC}$/UAS-PPK25* |
| | F | *Or47b-GAL4/+; UAS-Fru$^{MB}$/+* |
| | | *UAS-PPK23/+; Or47b-GAL4/+ (Thistle et al., 2012, Cell) (Bloomington #9984, RRID:BDSC_9984)* |
| | | *Or47b-GAL4/UAS-PPK23; UAS-Fru$^{MB}$/+* |
| | G | *Or47b-GAL4/+; UAS-Fru$^{MC}$/+* |
| | | *UAS-PPK23/+; Or47b-GAL4/+* |
| | | *Or47b-GAL4/UAS-PPK23; UAS-Fru$^{MC}$/+* |

**Table 3.1. Fly genotypes (continued).**

| | | |
|---|---|---|
| Figure 3.10 | A-B | *Or47b-GAL4/+; UAS-Fru$^{MB}$/+* |
| | | *Or47b-GAL4/+; UAS-Fru$^{MA}$/+* |
| | | *Or47b-GAL4/+; UAS-Fru$^{MB}$/UAS-Fru$^{MA}$* |
| Figure 3.12 | A | Wild-type *w$^{1118}$* |
| | B | *∆ppk23 (Thistle et al., 2012, Cell)* |
| Figure 3.13 | A-C | *fru$^{GAL4}$/UAS-mCD8-GFP > UAS-mCD8-GFP* |
| | | *fru$^{GAL4}$ > UAS-mCD8-GFP/+* |
| | | *fru$^{GAL4}$/fru$^{\Delta A}$ > UAS-mCD8-GFP/+* |
| | | *fru$^{GAL4}$/fru$^{\Delta B}$ > UAS-mCD8-GFP/+* |
| | | *fru$^{GAL4}$/fru$^{\Delta C}$ > UAS-mCD8-GFP/+* |

### 3.6 References


Billeter, J.C., Rideout, E.J., Dornan, A.J., and Goodwin, S.F. (2006a). Control of Male Sexual Behavior in Drosophila by the Sex Determination Pathway. Curr. Biol. *16*, 766–776.

Billeter, J.C., Villella, A., Allendorfer, J.B., Dornan, A.J., Richardson, M., Gailey, D.A., and Goodwin, S.F. (2006b). Isoform-Specific Control of Male Neuronal Differentiation and Behavior in Drosophila by the fruitless Gene. Curr. Biol. *16*, 1063–1076.

Chowdhury, Z.S., Sato, K., and Yamamoto, D. (2017). The core-promoter factor TRF2 mediates a Fruitless action to masculinize neurobehavioral traits in Drosophila. Nat. Commun. *8*.

Dalton, J.E., Fear, J.M., Knott, S., Baker, B.S., McIntyre, L.M., and Arbeitman, M.N. (2013). Male-specific Fruitless isoforms have different regulatory roles conferred by distinct zinc finger DNA binding domains. BMC Genomics *14*, 659.

Demir, E., and Dickson, B.J. (2005). fruitless splicing specifies male courtship behavior in Drosophila. Cell *121*, 785–794.

Dickson, B.J. (2008). Wired for sex: the neurobiology of Drosophila mating decisions. Science (80-. ). *322*, 904–909.

van der Goes van Naters, W., and Carlson, J.R. (2007). Receptors and Neurons for Fly Odors in Drosophila. Curr. Biol. *17*, 606–612.

Grosjean, Y., Rytz, R., Farine, J.-P., Abuin, L., Cortot, J., Jefferis, G.S.X.E., and Benton, R. (2011). An olfactory receptor for food-derived odours promotes male courtship in Drosophila. Nature *478*, 236–240.

Hanukoglu, I., and Hanukoglu, A. (2016). Epithelial sodium channel (ENaC) family: Phylogeny, structure-function, tissue distribution, and associated inherited diseases. Gene *579*, 95–132.

Hueston, C.E., Olsen, D., Li, Q., Okuwa, S., Peng, B., Wu, J., and Volkan, P.C. (2016). Chromatin Modulatory Proteins and Olfactory Receptor Signaling in the Refinement and Maintenance of Fruitless Expression in Olfactory Receptor Neurons. PLOS Biol. *14*, e1002443.

Ito, H., Sato, K., Koganezawa, M., Ote, M., Matsumoto, K., Hama, C., and Yamamoto, D. (2012). Fruitless recruits two antagonistic chromatin factors to establish single-neuron sexual dimorphism. Cell *149*, 1327–1338.

Ito, H., Sato, K., Kondo, S., Ueda, R., and Yamamoto, D. (2016). Fruitless Represses robo1 Transcription to Shape Male-Speci fi c Neural Morphology and Behavior in Drosophila. Curr. Biol. *26*, 1532–1542.

Jindra, M., Palli, S.R., and Riddiford, L.M. (2013). The Juvenile Hormone Signaling Pathway in Insect Development. Annu. Rev. Entomol. *58*, 181–204.

Kaissling, K. E., Thorson, J. (1980). Insect olfactory sensilla: Structure, chemical and electrical aspect of the functional organization.

Kellenberger, S., and Schild, L. (2002). Epithelial sodium channel/Degenerin family of ion channels: A variety of functions for a shared structure. Physiol. Rev. *82*, 735–767.

Kurtovic, A., Widmer, A., and Dickson, B.J. (2007). A single class of olfactory neurons mediates behavioural responses to a Drosophila sex pheromone. Nature *446*, 542–546.

Lee, G., and Hall, J.C. (2001). Abnormalities of male-specific FRU protein and serotonin expression in the CNS of fruitless mutants in Drosophila. J. Neurosci. *21*, 513–526.

Lin, H.-H., Cao, D.-S., Sethi, S., Zeng, Z., Chin, J.S.R., Chakraborty, T.S., Shepherd, A.K., Nguyen, C.A., Yew, J.Y., Su, C.-Y., et al. (2016). Hormonal modulation of pheromone detection enhances male courtship success. Neuron *90*, 1272–1285.

Liu, T., Wang, Y., Tian, Y., Zhang, J., Zhao, J., and Guo, A. (2018). The receptor channel formed by ppk25, ppk29 and ppk23 can sense the Drosophila female pheromone 7,11-heptacosadiene. Genes, Brain Behav. 1–10.

Meissner, G.W., Luo, S.D., Dias, B.G., Texada, M.J., and Baker, B.S. (2016). Sex-specific regulation of *Lgr3* in *Drosophila* neurons. Proc. Natl. Acad. Sci. *113*, E1256–E1265.

Neville, M.C., Nojima, T., Ashley, E., Parker, D.J., Walker, J., Southall, T., Van de Sande, B., Marques, A.C., Fischer, B., Brand, A.H., et al. (2014). Male-Specific Fruitless Isoforms Target Neurodevelopmental Genes to Specify a Sexually Dimorphic Nervous System. Curr. Biol. *24*, 229–241.

Ng, R., Lin, H.-H., Wang, J.W., and Su, C.-Y. (2017). Electrophysiological recording from Drosophila trichoid sensilla in response to odorants of low volatility. J. Vis. Exp. e56147.

Ng, R., Salem, S.S., Wu, S.-T., Wu, M., Lin, H., Shepherd, A.K., Joiner, W.J., Wang, J.W., and Su, C. (2019). Amplification of Drosophila Olfactory Responses by a DEG/ENaC Channel. Neuron *104*, 947–959.e5.

Nojima, T., Neville, M.C., and Goodwin, S.F. (2014). Fruitless isoforms and target genes specify the sexually dimorphic nervous system underlying Drosophila reproductive behavior. Fly (Austin). *8*, 95–100.

Pavlou, H.J., and Goodwin, S.F. (2013). Courtship behavior in Drosophila melanogaster: Towards a "courtship connectome." Curr. Opin. Neurobiol. *23*, 76–83.

von Philipsborn, A.C., Jörchel, S., Tirian, L., Demir, E., Morita, T., Stern, D.L., and Dickson, B.J. (2014). Cellular and behavioral functions of fruitless isoforms in Drosophila courtship. Curr. Biol. *24*, 242–251.

Pikielny, C.W. (2012). Sexy DEG/ENaC channels involved in gustatory detection of fruit fly pheromones. Sci. Signal. *5*, pe48.

Ryner, L.C., Goodwin, S.F., Castrillon, D.H., Anand, A., Villella, A., Baker, B.S., Hall, J.C., Taylor, B.J., and Wasserman, S.A. (1996). Control of male sexual behavior and sexual orientation in Drosophila by the fruitless gene. Cell *87*, 1079–1089.

Saina, M., and Benton, R. (2013). Visualizing olfactory receptor expression and localization in Drosophila. In Olfactory Receptors: Methods and Protocols, pp. 211–228.

Sato, K., and Yamamoto, D. (2020). The mode of action of Fruitless: Is it an easy matter to switch the sex? Genes, Brain Behav. *19*, gbb.12606.

Sato, K., Ito, H., Yokoyama, A., Toba, G., and Yamamoto, D. (2019). Partial proteasomal degradation of Lola triggers the male-to-female switch of a dimorphic courtship circuit. Nat. Commun. *10*.

Sato, K., Tanaka, R., Ishikawa, Y., and Yamamoto, D. (2020). Behavioral Evolution of Drosophila: Unraveling the Circuit Basis. Genes (Basel). *11*, 157.

Sethi, S., Lin, H., Shepherd, A.K., Volkan, P.C., Su, C., Wang, J.W., Sethi, S., Lin, H., Shepherd, A.K., Volkan, P.C., et al. (2019). Social Context Enhances Hormonal Modulation of Pheromone Detection in Drosophila Social Context Enhances Hormonal Modulation of Pheromone Detection in Drosophila. Curr. Biol. 1–12.

Song, H.J., Billeter, J.C., Reynaud, E., Carlo, T., Spana, E.P., Perrimon, N., Goodwin, S.F., Baker, B.S., and Taylor, B.J. (2002). The fruitless gene is required for the proper formation of axonal tracts in the embryonic central nervous system of Drosophila. Genetics *162*, 1703–1724.

Starostina, E., Liu, T., Vijayan, V., Zheng, Z., Siwicki, K.K., and Pikielny, C.W. (2012). A Drosophila DEG/ENaC subunit functions specifically in gustatory neurons required for male courtship behavior. J. Neurosci. *32*, 4665–4674.

Staruschenko, A., Adams, E., Booth, R.E., and Stockand, J.D. (2005). Epithelial Na+ channel subunit stoichiometry. Biophys. J. *88*, 3966–3975.

Stockinger, P., Kvitsiani, D., Rotkopf, S., Tirián, L., and Dickson, B.J. (2005). Neural circuitry that governs Drosophila male courtship behavior. Cell *121*, 795–807.

Stogios, P.J., Downs, G.S., Jauhal, J.J.S., Nandra, S.K., and Privé, G.G. (2005). Sequence and structural analysis of BTB domain proteins. Genome Biol. *6*, 1–18.

Tal, S.H., and Smith, D.P. (2006). A pheromone receptor mediates 11-cis-vaccenyl acetate-induced responses in Drosophila. J. Neurosci. *26*, 8727–8733.

Thistle, R., Cameron, P., Ghorayshi, A., Dennison, L., and Scott, K. (2012). Contact chemoreceptors mediate male-male repulsion and male-female attraction during Drosophila courtship. Cell *149*, 1140–1151.

Toda, H., Zhao, X., and Dickson, B.J. (2012). The Drosophila female aphrodisiac pheromone activates ppk23+ sensory neurons to elicit male courtship behavior. Cell Rep. *1*, 599–607.

Usui-Aoki, K., Ito, H., Ui-Tei, K., Takahashi, K., Lukacsovich, T., Awano, W., Nakata, H., Piao, Z.F., Nilsson, E.E., Tomida, J., et al. (2000). Formation of the male-specific muscle in female Drosophila by ectopic fruitless expression. Nat. Cell Biol. *2*, 500–506.

Vernes, S.C. (2014). Genome wide identification of Fruitless targets suggests a role in upregulating genes important for neural circuit formation. Sci. Rep. *4*, 1–11.

Wang, J.W., Wong, A.M., Flores, J., Vosshall, L.B., and Axel, R. (2003). Two-photon calcium imaging reveals an odor-evoked map of activity in the fly brain. Cell *112*, 271–282.

Wilson, T.G., and Fabian, J. (1986). A Drosophila melanogaster mutant resistant to a chemical analog of juvenile hormone. Dev. Biol. *118*, 190–201.

Wohl, M., Ishii, K., and Asahina, K. (2020). Layered roles of fruitless isoforms in specification and function of male aggression-promoting neurons in Drosophila. Elife *9*, 1–31.

Yamamoto, D., and Koganezawa, M. (2013). Genes and circuits of courtship behaviour in Drosophila males. Nat. Rev. Neurosci. *14*, 681–692.

# Chapter 4: Hormonal modulation of pheromone detection increases selectivity for remating in *Drosophila* females

## 4.1 Abstract

*Drosophila* females are polyandrous, having multiple mates in their lifetime. Curiously, while virgins are receptive to most courting males, mated females become discriminant and prefer males with high levels of cuticular pheromones — a likely indication of fitness. However, the neural mechanism underlying the postcopulatory switch of mate selectivity remains unclear. Here, we find that inputs from the pheromone-sensing Or47b olfactory receptor neurons (ORNs) are critical to females' remating decision. Single-sensillum recordings show that copulation markedly reduces female Or47b pheromone sensitivity. Mechanistically, this olfactory desensitization is mediated by juvenile hormone, a reproductive hormone whose levels rise in mated females. Genetic knockdown of the hormone receptor Methoprene-tolerant in Or47b ORNs abolishes desensitization and renders females indiscriminant in mate selection. Together, our findings uncover a neuromodulatory mechanism, which allows mated females to be aroused preferentially by males with high pheromones, thereby providing a means to maximize reproductive fitness through polyandrous activities.

## 4.2 Introduction

After copulation, female flies undergo a variety of behavioral and physiological changes, including unreceptivity to subsequent copulatory attempts, increased oviposition (Kubli, 2003), changes in sleep and activity patterns (Isaac et al., 2010), and also switches in dietary preferences (Kubli, 2010). These post-mating responses are triggered primarily by a sperm-bound peptide, named sex peptide (SP), which is synthesized in the male accessory glands and transferred to the female during insemination (Kubli, 2003).

In the nervous system, SP acts via the SP receptor (SPR), a G protein-coupled receptor (Yapici et al., 2008). One important type of SPR-expressing cells is the SP-sensing neuron (SPSN) population which innervates the female uterus and oviduct (Häsemeyer et al., 2009; Yang et al., 2009). SPSNs synapse onto the sex peptide abdominal ganglion (SAG) neurons, which further ascends and transmit

mating-related information to higher brain centers (Feng et al., 2014). Upon copulation, SPs transfer leads to SPR activation, triggering an inhibitory signaling cascade that silences the SPSNs and their inputs onto SAG neurons (Feng et al., 2014). Interestingly, SPRs are broadly expressed in the nervous system of not only females, but also in males which are likely not exposed to SPs (Yapici et al., 2008). This observation suggests that SPR may respond to other neuropeptides. Indeed, myoinhibitory peptides (MIPs) are another family of SPR ligands (Kim et al., 2010), but in contrast to SP, MIPs are broadly expressed in the nervous system of both males and females and function as endogenous SPR ligands (Kim et al., 2010; Poels et al., 2010). While the sex-specific function of MIP-expressing neurons in males is unclear, in females these neurons play central roles in neural circuits that mediate post-mating behavioral change such as reduced receptivity (Jang et al., 2017; Shao et al., 2019). For example, the MIP-positive *v*AL and *v*AM interneurons located in the abdominal ganglion function downstream of SPSNs and relay the SP signal to SAG neurons, and silencing these neurons decrease female receptivity (Jang et al., 2017). Expression of MIPs and neural activity of MIP neurons are also required for the post-mating female receptivity reduction (Shao et al., 2019).

Neurophysiologically, chemosensory neurons also undergo post-mating modulations to promote nutritionally beneficial behaviors for egg-production and oviposition in females (Hussain et al., 2016a). Compared to virgins, mated females show greater preference for foods with high level of polyamines to use as egg-laying sites. This preference is mediated by specific polyamine-detecting neurons in the olfactory and gustatory systems (Hussain et al., 2016b, 2016a). Mechanistically, the expression of both MIP and SPR are required for the post-mating neuromodulation of these polyamine-detecting chemosensory neurons (Hussain et al., 2016a). These findings suggest that through regulating the SPR expression in the periphery, the neurophysiology of certain chemosensory neurons can be modulated in a cell-autonomous manner. Do other types of chemosensory neurons also undergo mating-state-dependent neuromodulation? If so, is the aforementioned neuropeptidergic modulation the only mechanism for such modulation?

In males, the pheromone-sensing Or47b neurons exhibit age-dependent sensitization under the regulation of juvenile hormone (JH), a sesquiterpenoid lipid-like hormone that regulates reproductive maturity in adult *Drosophila* (Bontonou et al., 2015; Flatt et al., 2005; Moshitzky et al., 1996). Specifically, JH levels increase with age after eclosion (Lee et al., 2017), and treating young males with a JH analogue can mimic the age effect to increase Or47b pheromone responses (Lin et al., 2016). Intriguingly, JH levels increase in females after mating (Reiff et al., 2015). These findings suggest that 1) JH may serve as a signal to indicate mating status; 2) that female Or47b neuronal responses may also be regulated by JH signaling; and that 3) post-mating neuromodulation in the periphery may involve other SPR-independent mechanisms. Given these possibilities, might female Or47b ORNs be sensitized as in males, or might they be desensitized instead? How might such modulation affect female behavior?

In this Chapter's project, I studied the role of Or47b ORN modulation in female mate-choice behavior. An interesting post-mating behavioral phenomenon was first observed by our collaborator, Professor Jean-Christophe Billeter at the University of Groningen, who found that virgin females, when presented with the choice of two different strains of males, do not show preference towards either strain; on the other hand, mated females strikingly prefer the strain with higher levels of cuticular pheromones. The Billeter lab's findings raise the possibility that copulation may modulate the pheromone-sensing neurons in females, underlying their change in mate selectivity. My project aims to test this possibility by examining the responses of these neurons after mating.

Through single-sensillum recording together with pharmacological and genetic manipulations, I found that pheromone-sensing Or47b neurons undergo desensitization in mated females. Mechanistically, this neuromodulation is regulated by JH. Given that desensitized Or47b neurons require higher levels of ligands to be activated, mated females may thus be more attracted to males with higher levels of cuticular pheromones. My study reveals a mechanism for the increased mate

choice selectively of mated females: an SPR-independent mechanism operating at the sensory periphery, a novel and previously unidentified site for post-mating neuromodulation.

## 4.3 Results

### 4.3.1 Mating reduces the pheromone responses of female Or47b ORNs

To test if female Or47b ORN responses are impacted by mating status, I conducted single-sensillum recordings using an identified Or47b ligand, palmitoleic acid (Lin et al., 2016), to compare the Or47b ORN responses from virgin and mated females (Figure 4.1). Recordings were conducted at different time points after copulation. Following 24hrs post-mating, the peak Or47b neuronal responses in mated females were markedly lower than those in virgin females (Figure 4.1A and B), suggesting that Or47b neurons in females indeed undergo post-mating modulation. Furthermore, I found that reduced Or47b responses in mated females were only observed over 16hrs post-mating, while no changes were observed compared to virgins at 6hr or 12hr after mating (Figure 4.1C). For the remaining assays in this study, all mated females were therefore copulated 24hrs before the recordings.

To determine if such post-mating reduction in olfactory response is specific for Or47b neurons, I further recorded the responses of two other pheromone-sensing neurons, expressing the Or67d or Or88a olfactory receptors, to their respective odorant ligands. The Or67d neurons respond to *cis*-vaccenyl acetate (cVA) (van der Goes van Naters and Carlson, 2007; Ha and Smith, 2006; Kurtovic et al., 2007), and their activation increases female sexual receptivity (Kurtovic et al., 2007). Or88a ORNs respond to methyl palmitate (Dweck et al., 2015), but their neuronal inputs does not appear to influence receptivity in virgin females (Sakurai et al., 2013). Unlike Or47b ORNs, the Or67d (Figure 4.2A and B) and Or88a ORNs (Figure 4.2C and D) in mated females did not change their olfactory responses compared to virgins, suggesting that mating status does not affect the sensitivity of these two neuronal types, and that post-mating modulation does not occur in all pheromone-sensing ORNs.

Overall, my findings show that Or47b ORNs undergo post-mating neuromodulation in the form of neuronal desensitization. This reduced sensitivity was absent in the other two pheromone-sensing olfactory neurons, and is thus exclusive to the Or47b ORNs.

### 4.3.2 JH signaling mediates Or47b ORN desensitization in mated females

What are the possible mechanisms for the desensitization of Or47b ORNs in mated females? I first tested if reduced receptor expression affects neuronal responses by examining whether there is a haploinsufficiency phenotype. To this end, I recorded from heterozygous $Or47b^{2/+}$ receptor mutants, and compared their Or47b neuronal responses to wildtype females (Figure 4.3A). The responses from heterozygous mutant females were similar to controls (Figure 4.3B). I further confirmed that ligand-evoked responses were abolished in $Or47b^{2/2}$ homozygous mutants (data not shown). These results suggest that changes in receptor level likely do not underlie Or47b olfactory desensitization, and that these reduced neuronal responses are likely mediated by a mechanism apart from reduced receptor expression. I note that confirmation of reduced Or47b receptor expression in $Or47b^{2/+}$ flies will require qPCR quantification of receptor transcript levels between heterozygous mutants and wildtype controls.

In males, Or47b neurons show age-dependent sensitization mediated through the JH pathway (Lin et al., 2016). Given this result, and also that JH levels rise in mated females, I hypothesized that JH is similarly required for the change in Or47b ORN response in mated females. To test my hypothesis, I treated virgin females with methoprene, a JH analog, approximately 18hrs prior to the recording (Figure 4.4). If JH is indeed required for neuromodulation, methoprene-treated virgins were expected to show desensitized Or47b neuronal responses as observed in mated females. Indeed, this was what I observed: in support of my hypothesis, Or47b ORN responses in virgins were significantly reduced with methoprene treatment (Figure 4.4), suggesting that elevated levels of JH desensitize female Or47b neurons.

To determine whether JH directly targets female Or47 ORNs to modulate their responses, I used the GAL4/UAS system to specifically knock down Methoprene-tolerant (Met), a JH receptor, (Jindra et al., 2013), in the Or47b neurons, and found that this manipulation abolished the desensitization of Or47b neurons in mated females (Figure 4.5A-C). On the other hand, the Or47b neuronal responses of mated parental controls were reduced compared to virgin controls (Figure 4.5D-I), furthering indicating that Met is required for post-mating desensitization. Furthermore, knockdown of Met did not affect Or47b responses in virgins (Figure 4.5C, F, I), suggesting that Met does not impact the Or47b neuronal responses of unmated females. Together, these results suggest that JH signaling is required for the desensitization in Or47b neurons specifically in mated females.

To confirm how the JH-mediated neuromodulation affects females behaviorally, Philip Kohlmeier from the Billeter lab conducted complementary behavior experiments. He found that virgin females treated with methoprene showed a similar shift in mate preference as is found in mated females, that they prefer the strain of males with higher cuticular pheromone level. On the other hand, selective knockdown of Met in Or47b ORNs abolishes the change in selectivity in mated females, which showed no preference towards either strain. These behavioral results are consistent with my recording data, in that JH signaling is required for mate choice in mated females.

Taken together, these experiments show that similarly to males, JH also mediates neuromodulation in females: specifically, JH directly targets Or47b ORNs via Met, and desensitizes their neuronal responses in mated females. This neuromodulation is behaviorally relevant, as knockdown of Met abolished mate preference in mated females, while methoprene treatment conferred mate selectively in virgin females. Taken together, these results indicate that the desensitization in Or47b neurons through JH signaling underlies the enhanced selectivity in mated females, as higher levels of aphrodisiac pheromones are required to activate the desensitized Or47b ORNs.

### 4.3.3 SPR-independent post-mating neuromodulation

Interestingly, subsets of other chemosensory neurons also undergo post-mating neuromodulation (Hussain et al., 2016a). Specifically, calcium imaging in antennal lobe innervated by ORNs expressing both Ir41a and Ir76b receptors show reduced calcium responses in mated females, and this modulation requires the expression of SPR in these neurons (Hussain et al., 2016a). Having established that JH signaling desensitizes Or47b ORN in mated females, I therefore asked if SPRs also play a role to coordinate the mating information with Or47b ORN response.

To address this question, I employed a previously characterized SPR micro RNAi line (Yapici et al., 2008) to specifically knock down SPRs in Or47b neurons , and compared the Or47b neuronal responses from virgin and mated females. If SPRs are indeed required for the post-mating desensitization, post-mating Or47b ORNs should remain unaffected in the absence of SPRs. However, I found that in SPR knockdown flies, the mated females still show reduced Or47b neuronal response (Figure 4.6A & B), similar to the results found in parental controls (Figure 4.6 C-F). These results suggest that the post-mating neuromodulation in Or47b ORN is SPR-independent.

### 4.3.4 Sexually dimorphic neuromodulation by JH signaling in Or47b ORNs

Intriguingly, a comparison of results from Chapter 3 and Chapter 4 shows that JH signaling differentially regulates Or47b ORNs in a sexually dimorphic manner. Specifically in males, JH is upstream of $Fru^{MB}$, and is required for the age-dependent sensitization in Or47b neurons, which grants a courtship advantage to older males (Lin et al., 2016, Figure 3.8B). Females, on the other hand, do not change their Or47b olfactory response with age but rather undergo posting-mating desensitization of their Or47b neurons (Figure 4.1B), which is mediated by the elevated JH level (Figure 4.4). How then does JH signaling differentially modulate Or47b neurons in the two sexes?

To address this question, I focused on the sex-determination gene, *transformer* (*tra*), which yields a female-specific splicing factor. The Tra protein targets the primary RNAs, *doublesex* (*dsx*)

and *fruitless* (*fru*), both of which transcribe into important transcription factors for sexual dimorphism (Auer and Benton, 2016). I therefore hypothesized that Tra differentially modulate Or47b neurons through its downstream targets.

To test my hypothesis, I feminized male Or47b neurons by using the GAL4/UAS system to express Tra, as a result, these neurons only express the female-form of Tra targets. I then treated these males with methoprene to test how JH signaling affects their Or47b neuronal responses. I reasoned that if my hypothesis is correct, methoprene treatment should reduce the responses of feminized Or47b ORNs, as observed in mated females (Figure 4.4). Indeed, through single-sensillum recordings, I found that in Or47b-GAL4 > UAS-Tra males, methoprene treatment significantly decreased their neuronal responses compared to solvent control treatment (Figure 4.7A-B). On the other hand, in parental control flies with non-feminized ORNs, methoprene treatment sensitizes Or47b neurons in males (Figure 4.7C), consistent with published findings (Lin et al., 2016). These results suggest that the female-specific expression of Tra underlies the sexually dimorphic neuromodulation in Or47b neurons.

Given that Dsx is not expressed in adult ORNs (Rideout et al., 2010), the key distinction between male and female Or47b neurons is therefore the differential expression of $Fru^{M}$ (Stockinger et al., 2005), which has three functional variants, $Fru^{MA}$, $Fru^{MB}$, and $Fru^{MC}$ (based on Demir and Dickson, 2005; Song et al., 2002). Critically, in males, $Fru^{MB}$ and $Fru^{MC}$ are both required for the JH mediated sensitization in Or47b ORNs (Figure 3.2E, G); on the other hand, female Or47b ORNs can be sensitized when $Fru^{MB}$ and $Fru^{MC}$ are ectopically expressed (Figure 3.9C). Might JH-mediated desensitization of female Or47b ORNs arise due to the lack of $Fru^{M}$?

To specifically test how JH signaling modulates Or47b ORNs in the absence of $Fru^{M}$, I decided to feed methoprene to $fru^{F}$ males, which do not express any functional $Fru^{M}$ proteins (Demir and Dickson, 2005). I found that methoprene-treatment increases Or47b ORN responses in wild type males as expected (Figure 4.8A-B). In comparison, Or47b neurons in $fru^{F}$ males show JH-mediated

reduction in response (Figure 4.8C-D); consistent with the results observed from Tra-expressing Or47b neurons in JH-treated males (Figure 4.7B). Taken together, these results suggest that in the absence of $Fru^M$, JH signaling desensitizes the Or47b neurons of both sexes.

### 4.4 Discussion

Mated females are more selective in mate choice—specifically preferring males with higher levels of cuticular pheromones—compared to virgins. Here I show that in female flies, Or47b ORNs undergo neuromodulation which decreases their olfactory responses after mating (Figure 4.1). Mechanistically, this desensitization is mediated by JH signaling (Figure 4.4 and 4.5), whereby elevated JH levels in mated females mediates desensitization in their Or47b ORNs, such that higher pheromone levels are likely required for receptor activation, resulting in increased selectivity towards males with greater amounts of cuticular pheromones. Notably, this neuromodulatory mechanism is independent of SPR (Figure 4.6).

Through single-sensillum recording from feminized Or47b neurons in males, I found that in the absence of $Fru^M$, O47b ORNs undergo desensitization by JH signaling (Figure 4.7, 4.8). These findings are consistent with my findings from female Or47b ORNs, which lack $Fru^M$ and are also desensitized by JH. These data suggest that by default, JH signaling desensitizes Or47b neurons. In the presence of $Fru^M$, however, through the regulation of their downstream targets, amplification channels are formed to sensitize the neurons instead (See Chapter 3). The neuromodulation of Or47b neurons in both sexes therefore share the same upstream mechanisms, while sexual dimorphic modulations occur at the level of sex-specific transcription factors.

Intriguingly, another subset of ORNs expressing Ir41a receptors also show reduced sensitivity in mated females (Hussain et al., 2016a), but through a different mechanism from Or47b ORNs. Specifically, it is suggested that the Ir41a ORNs undergo post-mating modulation through SPR and MIPs in a cell-autonomous manner, and SPR expression in Ir41a ORNs is both sufficient and

necessary for their desensitization (Hussain et al., 2016a). In contrast, the desensitization in Or47b ORNs is independent of SPR (Figure 4.6B). These findings suggest that ORNs are important post-mating modulation sites, and different subsets of ORNs may employ different mechanisms to modulate their olfactory responses.

Notably, the MIP-mediated Ir41a desensitization happens rapidly after mating within 6hrs post-mating, and the antennal SPR transcript level also increases within this time period after mating (Hussain et al., 2016a). The rapid neuromodulation in Ir41a ORNs likely corresponds to these neurons' roles in mediating post-mating behaviors: the ORNs respond to polyamines, an important food substrate for reproduction that is likely required immediately after mating for egg production (Hussain et al., 2016b). I found that Or47b desensitization instead occurs 16hrs after copulation (Figure 4.1C), indicating the requirement for multiple levels of transcriptional modulation for JH-mediated neuromodulation.

Or47b neurons respond to fly pheromones to promote courtship in males. It is therefore likely that these neurons mediate mating behaviors in females as well. Indeed, preliminary results from our lab show that activating Or47b ORNs increases the receptivity of mated females but not virgins (data not shown), suggesting that similar to these neurons' courtship-promoting role in males, Or47b ORNs also function in a stimulatory role in females. Our collaborators also showed that mated Or47b receptor mutant females, do not demonstrate increased selectivity (not shown), highlighting the role of Or47b ORNs in female mating behavior. Finally, I found that Met knockdown in Or47b ORNs abolished the change in mate selectivity in females (Figure 4.5B, C), suggesting that Or47b ORN inputs are the key determinants of the post-mating plastic mate choice in females. Taken together, these results support the model whereby mating desensitizes female Or47b ORNs, which in turn leads to a higher selectivity towards males with higher cuticular pheromone content levels.

Why do females show this striking mating-dependent change in mate choice? Being polyandrous, female flies gain various benefits from mating with multiple partners, including securing

against infertility, improving female fertility, and allowing increased genetic diversity among offspring for higher chance of survival (Kvarnemo and Simmons, 2013). Low mate selectivity may yield a higher chance of early mating for virgin females, thus ensuring generation of their offspring; for mated females, on the other hand, higher mate selectivity may provide chances to mate with males with "better" genes or with a higher genetic compatibility (Trivers, 1972), thus improving the genetic quality of offspring. In all, it is likely that plastic mate choice serves as a mechanism which allows female flies to best leverage the benefits of polyandry.

## 4.5 Materials and methods

### *Drosophila* stocks

All flies (*Drosophila melanogaster*) were raised on standard cornmeal medium at 25°C, ~60% relative humidity in an incubator with a 12-hr light/dark cycle. Flies were collected upon eclosion, separated by sex and raised in groups of 10. Female flies 5 days post-eclosion were used in all experiments. Mated females were copulated 24hrs before experiments unless noted otherwise. Specifically, a virgin female (4-day old) and male (7-day old) were allowed to mate for an hour in a food vial. Copulation events were visually confirmed. Mated females were then recollected in groups of 10 and raised in an incubator until the experiments.

### Single-sensillum recordings

A fly was wedged into the narrow end of a truncated plastic 200-µl pipette tip to expose the antenna, which was then stabilized between a tapered glass microcapillary tube and a coverslip covered with double-sided type. Single-unit recordings were performed essentially as described (Ng et al., 2017). Briefly, electrical activity of the ORNs was recorded extracellularly by placing a sharp electrode filled with artificial hemolymph solution (Wang et al., 2003) in the at4 sensillum (Or47b ORN and Or88a recordings). For at1 (Or67d ORN) sensillum recordings, 0.6X sensillum lymph

Ringer solution (Kaissling and Thorson, 1980) was used. The reference electrode filled with the same respective solution was placed in the eye. No more than three sensilla from the same antenna were recorded per fly.

AC signals (100-20k Hz) were recorded on an NPI EXT-02F amplifier (ALA Scientific Instruments) and digitized at 5 kHz with Digidata 1550 (Molecular Devices). ORN spikes were detected and sorted using threshold search under Event Detection in Clampfit 10.4 (Molecular Devices). Spike timing data were exported and analyzed in Igor Pro 6.3 (Wavemetrics). Peri-stimulus time histograms (PSTHs) were obtained by averaging spike activities in 50-ms bins and smoothed using a binomial filter (Igor Pro 6.3, Wavemetrics). For dosage curves and statistical analysis, responses were quantified by subtracting the pre-stimulus spike rate (1 s) from the peak spike response during odorant stimulation (adjusted peak responses).

**Odor stimuli**

Methyl palmitate was diluted in paraffin oil, applied as 100-µl aliquots on filter discs and delivered to the antenna via a 500-ms air pulse at 200 ml $min^{-1}$ through the main airstream (2000 ml $min^{-1}$). Both *c*VA (10 µl per filer disc) and palmitoleic acid (4.5 µl per filer disc), were diluted in ethanol and delivered via a 500-ms air pulse at 250 ml $min^{-1}$ directly to the antenna from a close range, as previously described (Ng et al., 2017). Ethanol was allowed to evaporate for 1 hour in a vacuum desiccator prior to experiments.

**Pharmacological manipulations of juvenile hormone**

Methoprene (33375, Sigma-Aldrich), 15 µl at 0.25% v/v concentration was applied to the surface of fly food. Ethanol was used as a solvent. The fly vials were placed in the fume hood for 2-hr to evaporate the solvent. Flies were flipped to the freshly prepared methoprene-coated food 16-hr before experiments.

**Statistics**

Statistical results (p value and n) are indicated in figure legends corresponding to each experiment. In cases where a dosage curve for odor concentration was performed, two-tailed t tests comparing the experimental and control groups were performed for each concentration and the p-value is indicated on the figure by asterisks (*p < 0.05; **p < 0.01; ***p < 0.001) . All data are presented as mean ± SEM and plotted in Igor Pro 6.32A (https://www.wavemetrics.com/products/igorpro/igorpro). Dosage response curves were fitted with Hill equation for illustration purposes.

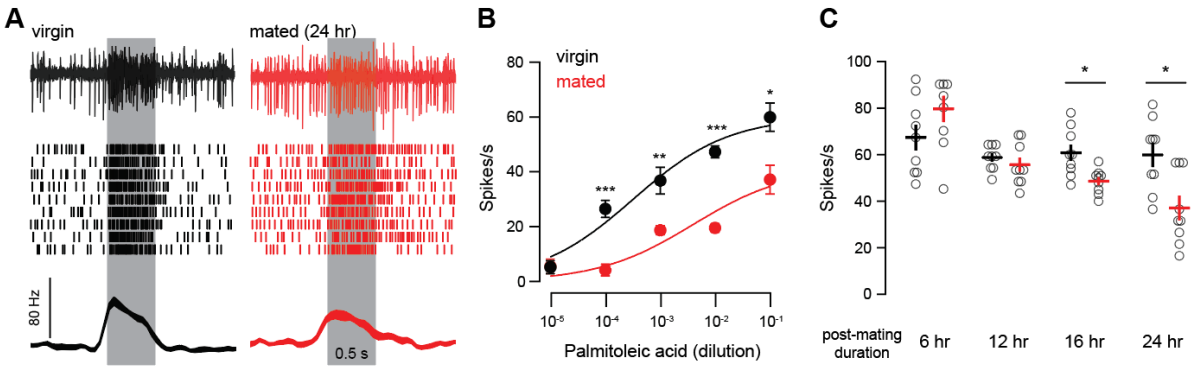


**Figure 4.1. Mating reduces Or47b ORN responses in females.**

**(A)** Single-sensillum recording. Representative traces (top), raster plots (middle), and peri-stimulus time histograms (PSTH, bottom) are shown for Or47b ORN responses in 5d virgin (left panel) or mated females (24 hr post-mating, right panel). Palmitoleic acid: $10^{-1}$. Line width: s.e.m. Gray bar: stimulus duration. **(B)** Dosage curves of Or47b spike responses from virgin and mated females. Dose response relation was fitted with the Hill equation. Adjusted peak responses (pre-stimulus baseline activity subtracted from the peak response). Parallel experiments, mean ± s.e.m. ($n$=9, from 4~5 flies). * $P < 0.05$, ** $P < 0.01$, *** $P < 0.0001$, $t$-test. **(C)** Comparison between the Or47b ORN responses of virgin and mated females to palmitoleic acid ($10^{-1}$). Parallel experiments were conducted for each post-mating duration, mean ± s.e.m. ($n$=9, from 4~5 flies). * $P < 0.05$, $t$-test.

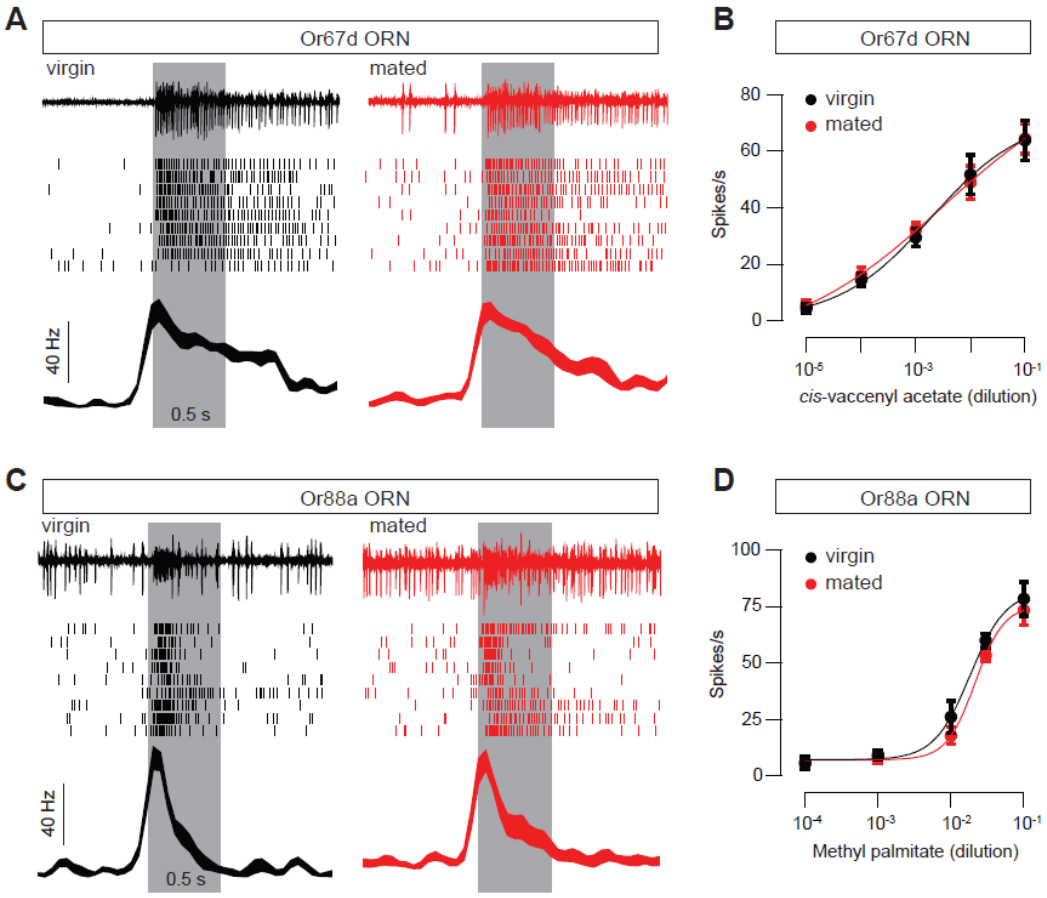


**Figure 4.2. Mating does not reduce olfactory responses of Or67d or Or88a ORNs in females.**

**(A)** Single-sensillum recording. Representative traces (top), raster plots (middle), and peri-stimulus time histograms (PSTH, bottom) are shown for Or67d ORN responses in 5d virgin (left panel) or mated females (24 hr postcopulation, right panel). Palmitoleic acid: $10^{-1}$. Line width: s.e.m. Gray bar: stimulus duration. **(B)** Dosage curves of Or67d spike responses from virgin and mated females. Dose response relation was fitted with Hill equation. Adjusted peak responses (pre-stimulus baseline activity subtracted from the peak response). Parallel experiments, mean ± s.e.m. ($n$=9, from 4~5 flies). **(C-D)** Similar to **(A-B)** except that Or88a ORN responses were recorded in the virgin and mated females.

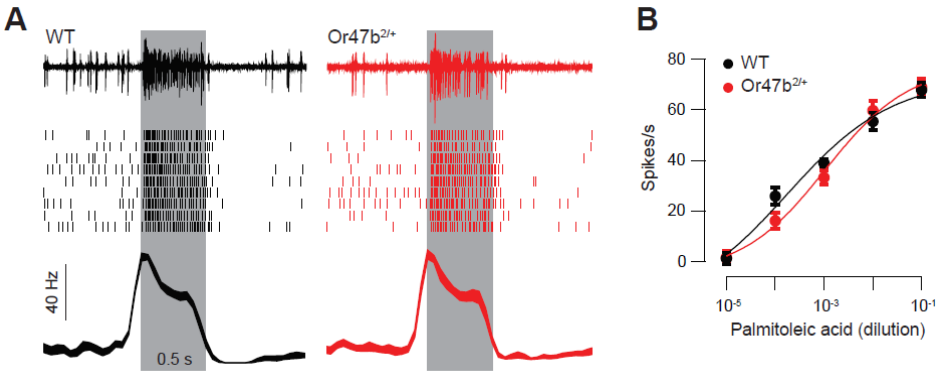


**Figure 4.3. Reduced olfactory responses of Or47 ORNs in mated females are not due to decrease in olfactory receptor expression level.**

**(A)** Single-sensillum recording. Representative traces (top), raster plots (middle), and peri-stimulus time histograms (PSTH, bottom) are shown for Or47b ORN responses in mated 5d WT (left panel) or Or47b heterozygous mutant females ($Or47b^{2/+}$, 24 hr postcopulation, right panel). Palmitoleic acid: $10^{-1}$. Line width: s.e.m. Gray bar: stimulus duration. **(B)** Dosage curves of Or47b spike responses from WT and $Or47b^{2/+}$ females. Dose response relation was fitted with Hill equation. Adjusted peak responses (pre-stimulus baseline activity subtracted from the peak response). Parallel experiments, mean ± s.e.m. ($n$=9, from 4~5 flies).

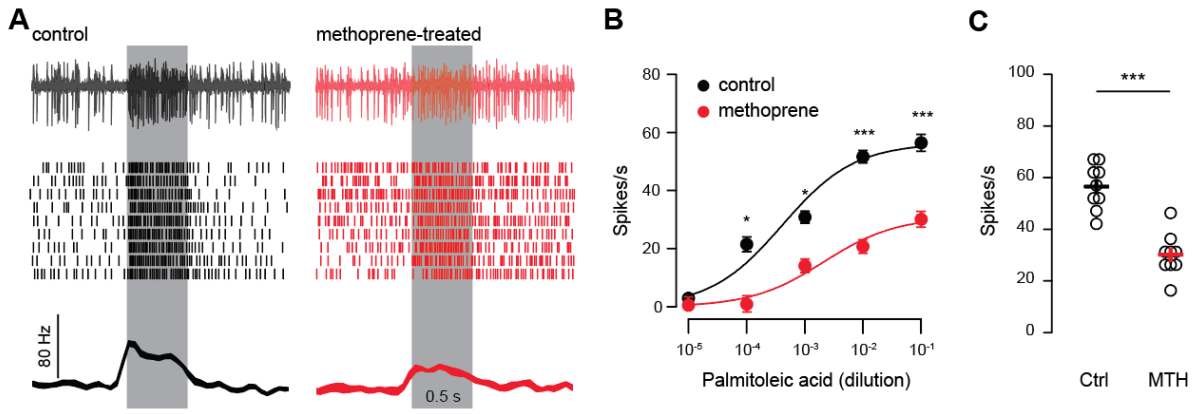


**Figure 4.4. Methoprene treatment reduces Or47b ORN responses in virgin females.**

**(A)** Single-sensillum recording. Representative traces (top), raster plots (middle), and peri-stimulus time histograms (PSTH, bottom) are shown for Or47b ORN responses in 5d virgin treated with ethanol solvent (left panel) or methoprene (18 hr, 15 µl 0.25%, right panel). Palmitoleic acid: $10^{-1}$. Line width: s.e.m. Gray bar: stimulus duration. **(B)** Dosage curves of Or47b spike responses from control and methoprene-treated virgin females. Dose response relation was fitted with Hill equation. Adjusted peak responses (pre-stimulus baseline activity subtracted from the peak response). Parallel experiments, mean ± s.e.m. ($n$=9, from 4~5 flies). * $P < 0.05$, *** $P < 0.001$, $t$-test. **(C)** Comparison between the Or47b ORN responses of control and treated females to palmitoleic acid ($10^{-1}$). Empty circles represent responses from individual ORNs. Filled circles are average responses, mean ± s.e.m. ($n$=9, from 4~5 flies). *** $P < 0.001$, $t$-test.

**Figure 4.5. Or47b ORN responses do not reduce in mated Met-knockdown females.**

**(A)** Single-sensillum recording. Representative traces (top), raster plots (middle), and peri-stimulus time histograms (PSTH, bottom) are shown for Or47b ORN responses in 5d virgin (left panel) or mated (right panel) Met-knockdown females. Palmitoleic acid: $10^{-1}$. Line width: s.e.m. Gray bar: stimulus duration. **(B)** Dosage curves of Or47b spike responses from virgin and mated females. Dose response relation was fitted with Hill equation. Adjusted peak responses (pre-stimulus baseline activity subtracted from the peak response). Parallel experiments, mean ± s.e.m. ($n$=9, from 4~5 flies). **(C)** Comparison between the peak Or47b ORN responses of virgin and mated females to palmitoleic acid ($10^{-1}$). Empty circles represent responses from individual ORNs. Filled circles are average responses, mean ± s.e.m. ($n$=9, from 4~5 flies). **(D-F)** As in **(A-C)** except that recordings were conducted in the Or47b-GAL4/+ parental control line. ** $P < 0.01$ *** $P < 0.001$, $t$-test. **(G-I)** As in **(A-C)** except that recordings were conducted in the UAS-Met-RNAi/+ parental control line. ** $P < 0.01$ *** $P < 0.001$, $t$-test.

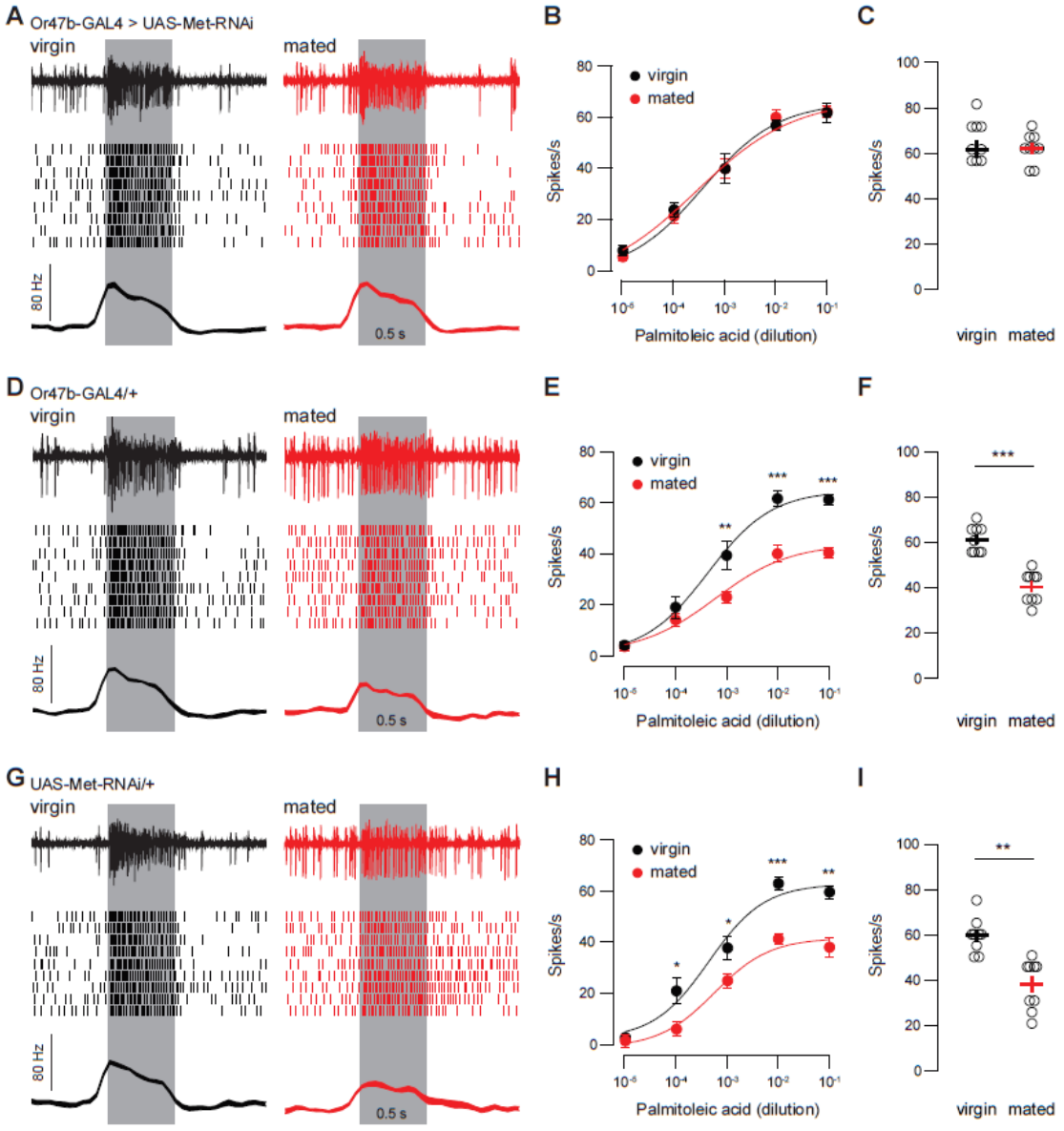
A
Or47b-GAL4 > UAS-Met-RNAi
virgin
mated
80 Hz
0.5 s
B
virgin
mated
Spikes/s
Palmitoleic acid (dilution)
C
Spikes/s
virgin
mated
D
Or47b-GAL4/+
virgin
mated
80 Hz
0.5 s
E
virgin
mated
Spikes/s
Palmitoleic acid (dilution)
F
Spikes/s
virgin
mated
G
UAS-Met-RNAi/+
virgin
mated
80 Hz
0.5 s
H
virgin
mated
Spikes/s
Palmitoleic acid (dilution)
I
Spikes/s
virgin
mated

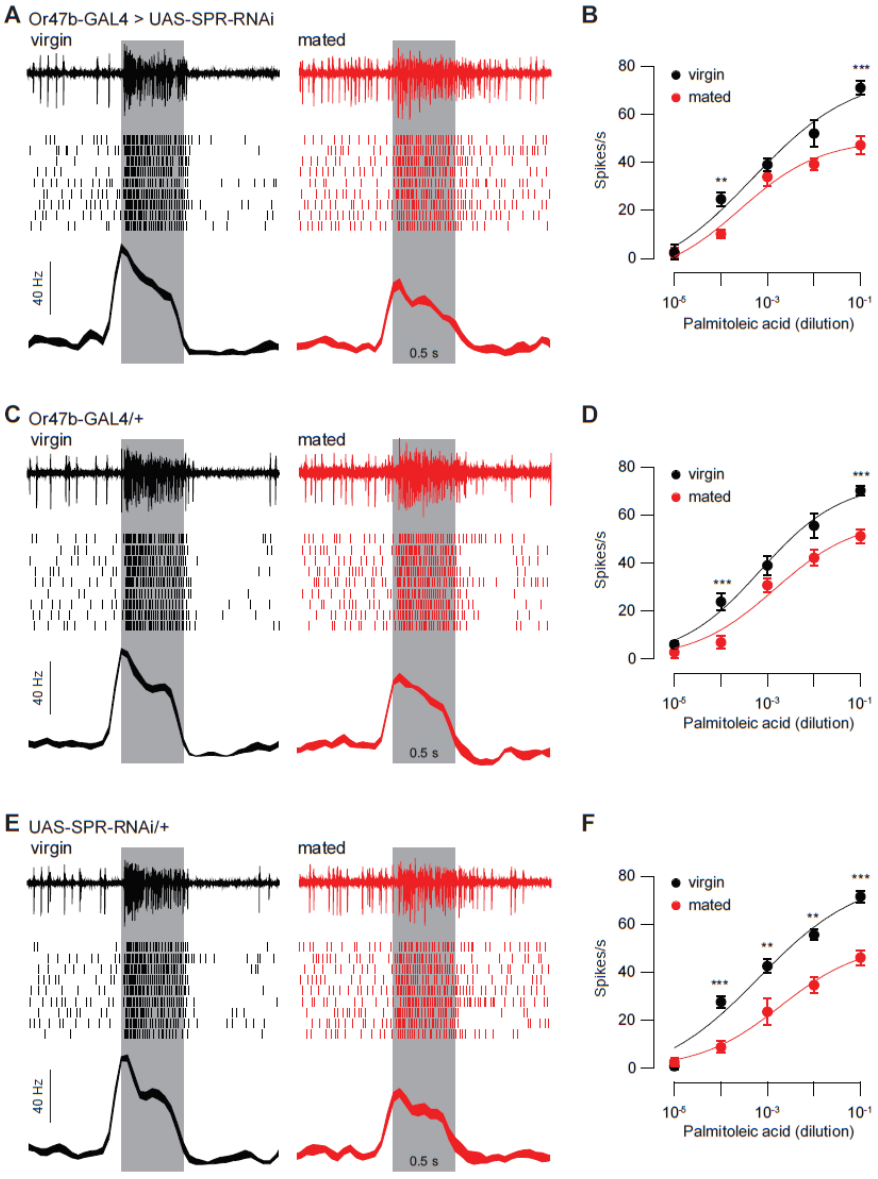


**Figure 4.6. SPR-knockdown does not affect the reduced Or47b ORN responses in mated females.**

**(A)** Single-sensillum recording. Representative traces (top), raster plots (middle), and peri-stimulus time histograms (PSTH, bottom) are shown for Or47b ORN responses in 5d virgin (left panel) or mated (right panel) SPR-knockdown females. Palmitoleic acid: $10^{-1}$. Line width: s.e.m. Gray bar: stimulus duration. **(B)** Dosage curves of Or47b spike responses from virgin and mated females. Dose response relation was fitted with Hill equation. Adjusted peak responses (pre-stimulus baseline activity subtracted from the peak response). Parallel experiments, mean ± s.e.m. ($n$=9, from 4~5 flies). **(C-D)** As in **(A-B)** except that recordings were conducted in the Or47b-GAL4/+ parental control line. **(E-F)** As in **(A-B)** except that recordings were conducted in the UAS-SPR-RNAi/+ parental control line. ** $P < 0.01$ *** $P < 0.001$, $t$-test.

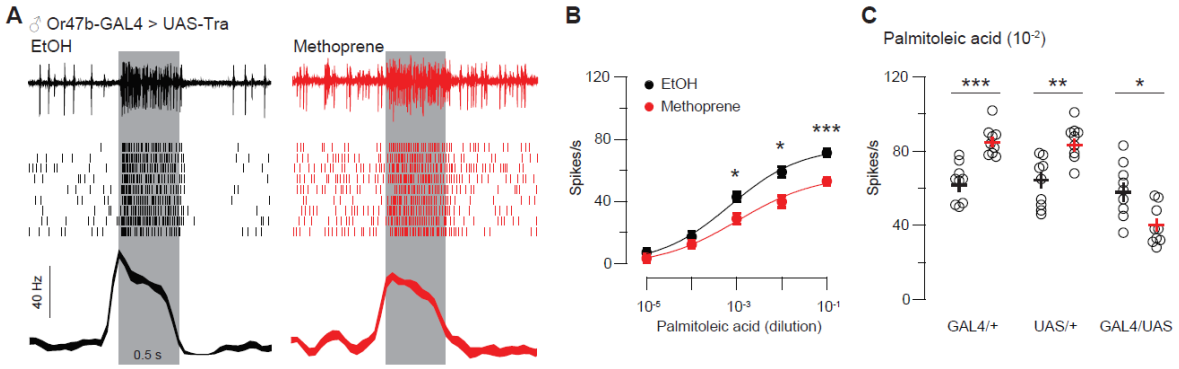


**Figure 4.7. JH signaling decreases feminized Or47b ORN responses in males.**

**(A)** Single-sensillum recording. Representative traces (top), raster plots (middle), and peri-stimulus time histograms (PSTH, bottom) are shown for Or47b ORN responses in 5d virgin females treated with EtOH (left panel) or methoprene (16-hr before experiment, right panel). Palmitoleic acid: $10^{-1}$. Line width: s.e.m. Gray bar: stimulus duration. **(B)** Dosage curves of Or47b spike responses from virgin and mated females. Dose response relation was fitted with Hill equation. Adjusted peak responses (pre-stimulus baseline activity subtracted from the peak response). Parallel experiments, mean ± s.e.m. ($n$=9, from 4~5 flies). * $P < 0.05$, *** $P < 0.0001$, $t$-test. **(C)** Comparison between the Or47b ORN responses of EtOH and methoprene treated experimental and parental control males to palmitoleic acid ($10^{-2}$). Parallel experiments were conducted for each genotypes, mean ± s.e.m. ($n$=9, from 4~5 flies). * $P < 0.05$, ** $P < 0.01$, *** $P < 0.0001$, $t$-test.

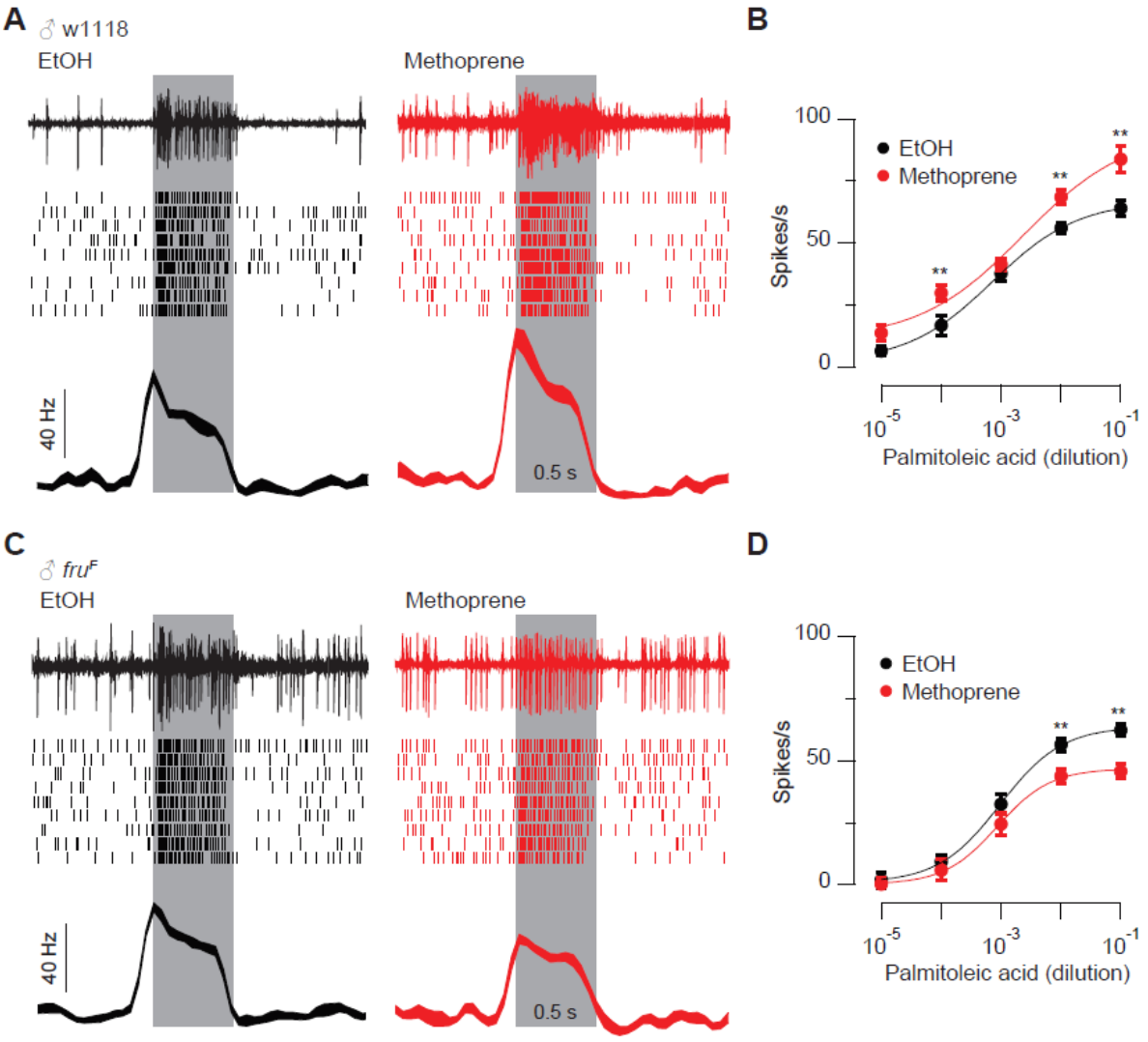


**Figure 4.8. JH signaling decreases OR47b ORN response in feminized males.**

**(A)** Single-sensillum recording. Representative traces (top), raster plots (middle), and peri-stimulus time histograms (PSTH, bottom) are shown for Or47b ORN responses in WT 5d EtOH treated (left panel) or methoprene treated males (16-hr before experiment, right panel). Palmitoleic acid: $10^{-1}$. Line width: s.e.m. Gray bar: stimulus duration. **(B)** Dosage curves of Or47b spike responses from EtOH and methoprene treated males. Dose response relation was fitted with Hill equation. Adjusted peak responses (pre-stimulus baseline activity subtracted from the peak response). Parallel experiments, mean ± s.e.m. ($n$=9, from 4~5 flies). **(C-D)** Similar to **(A-B)** except that Or47b ORN responses in $fru^F$ males were recorded.

**Table 4.1. Fly genotypes.**

| | | |
|---|---|---|
| Figure 4.1 | A-C | Wild-type *Canton-S* |
| Figure 4.2 | A-D | Wild-type *Canton-S* |
| Figure 4.3 | A-B | $w^{1118}$ |
| | | $Or47b^{2/+}$ *(Bloomington #51306, RRID:BDSC_51306)* |
| Figure 4.4 | A-C | Wild-type *Canton-S* |
| Figure 4.5 | A-C | *UAS-Met-RNAi/+; Or47b-GAL4/+ (VDRC #100638) (Bloomington #9984, RRID:BDSC_9984)* |
| | D-F | *+; Or47b-GAL4/+* |
| | G-I | *UAS-Met-RNAi/+; +* |
| Figure 4.6 | A-B | *UAS-SPR-RNAi/+; Or47b-GAL4/+ (VDRC #106804)* |
| | C-D | *+; Or47b-GAL4/+* |
| | E-F | *UAS-SPR-RNAi/+; +* |
| Figure 4.7 | A-C | *UAS-*$tra^F$*/+; Or47b-GAL4/+ (Bloomington #4590, RRID:BDSC_4590)* |
| Figure 4.8 | A-B | $w^{1118}$ |
| | C-D | $fru^F$ *(Bloomington #66873, RRID:BDSC_66873) (Demir & Dickson, 2005, Cell)* |

### 4.6 References


Auer, T.O., and Benton, R. (2016). Sexual circuitry in Drosophila. Curr. Opin. Neurobiol. *38*, 18–26.

Bontonou, G., Shaik, H.A., Denis, B., and Wicker-Thomas, C. (2015). Acp70A regulates Drosophila pheromones through juvenile hormone induction. Insect Biochem. Mol. Biol. *56*, 36–49.

Demir, E., and Dickson, B.J. (2005). fruitless Splicing Specifies Male Courtship Behavior in Drosophila. Cell *121*, 785–794.

Dweck, H.K.M., Ebrahim, S.A.M., Thoma, M., Mohamed, A.A.M., Keesey, I.W., Trona, F., Lavista-Llanos, S., Svatoš, A., Sachse, S., Knaden, M., et al. (2015). Pheromones mediating copulation and attraction in Drosophila. Proc. Natl. Acad. Sci. U. S. A. *112*, E2829-35.

Feng, K., Palfreyman, M.T., Häsemeyer, M., Talsma, A., and Dickson, B.J. (2014). Ascending SAG neurons control sexual receptivity of Drosophila females. Neuron *83*, 135–148.

Flatt, T., Tu, M.-P., and Tatar, M. (2005). Hormonal pleiotropy and the juvenile hormone regulation ofDrosophila development and life history. BioEssays *27*, 999–1010.

van der Goes van Naters, W., and Carlson, J.R. (2007). Receptors and Neurons for Fly Odors in Drosophila.

Ha, T.S., and Smith, D.P. (2006). A Pheromone Receptor Mediates 11-cis-Vaccenyl Acetate-Induced Responses in Drosophila. J. Neurosci. *26*.

Häsemeyer, M., Yapici, N., Heberlein, U., and Dickson, B.J. (2009). Sensory Neurons in the Drosophila Genital Tract Regulate Female Reproductive Behavior. Neuron *61*, 511–518.

Hussain, A., Üçpunar, H.K., Zhang, M., Loschek, L.F., and Grunwald Kadow, I.C. (2016a). Neuropeptides Modulate Female Chemosensory Processing upon Mating in Drosophila. PLOS Biol. *14*, e1002455.

Hussain, A., Zhang, M., Üçpunar, H.K., Svensson, T., Quillery, E., Gompel, N., Ignell, R., and Grunwald Kadow, I.C. (2016b). Ionotropic Chemosensory Receptors Mediate the Taste and Smell of Polyamines. PLOS Biol. *14*, e1002454.

Isaac, R.E., Li, C., Leedale, A.E., and Shirras, A.D. (2010). *Drosophila* male sex peptide inhibits siesta sleep and promotes locomotor activity in the post-mated female. Proc. R. Soc. B Biol. Sci. *277*, 65–70.

Jang, Y.H., Chae, H.S., and Kim, Y.J. (2017). Female-specific myoinhibitory peptide neurons regulate mating receptivity in Drosophila melanogaster. Nat. Commun. *8*, 1–12.

Jindra, M., Palli, S.R., and Riddiford, L.M. (2013). The Juvenile Hormone Signaling Pathway in Insect Development. Annu. Rev. Entomol. *58*, 181–204.

Kaissling, K.E., and Thorson, J. (1980). Insect olfactory sensilla: structure, chemical and electrical aspect of the functional organization. In Receptors for Neurotransmitters, Hormones, and Pheromones in Insects: Proceedings of the Workshop on Neurotransmitter and Hormone Receptors in Insects Held in Cambridge, pp. 261–282.

Kim, Y.J., Bartalska, K., Audsley, N., Yamanaka, N., Yapici, N., Lee, J.Y., Kim, Y.C., Markovic, M.,

Isaac, E., Tanaka, Y., et al. (2010). MIPs are ancestral ligands for the sex peptide receptor. Proc. Natl. Acad. Sci. U. S. A. *107*, 6520–6525.

Kubli, E. (2003). Sex-peptides: Seminal peptides of the Drosophila male. Cell. Mol. Life Sci. *60*, 1689–1704.

Kubli, E. (2010). Sexual behavior: Dietary food switch induced by sex. Curr. Biol. *20*, R474–R476.

Kurtovic, A., Widmer, A., and Dickson, B.J. (2007). A single class of olfactory neurons mediates behavioural responses to a Drosophila sex pheromone. Nature *446*, 542–546.

Kvarnemo, C., and Simmons, L.W. (2013). Polyandry as a mediator of sexual selection before and after mating. Philos. Trans. R. Soc. B Biol. Sci. *368*.

Lee, S.S., Ding, Y., Karapetians, N., Rivera-Perez, C., Noriega, F.G., and Adams, M.E. (2017). Hormonal Signaling Cascade during an Early-Adult Critical Period Required for Courtship Memory Retention in Drosophila. Curr. Biol. *27*, 2798-2809.e3.

Lin, H.-H., Cao, D.-S., Sethi, S., Zeng, Z., Chin, J.S.R., Chakraborty, T.S., Shepherd, A.K., Nguyen, C.A., Yew, J.Y., Su, C.-Y., et al. (2016). Hormonal Modulation of Pheromone Detection Enhances Male Courtship Success. Neuron *90*, 1272–1285.

Moshitzky, P., Fleischmann, I., Chaimov, N., Saudan, P., Klauser, S., Kubli, E., and Applebaum, S.W. (1996). Sex-peptide activates juvenile hormone biosynthesis in the Drosophila melanogaster corpus allatum. Arch. Insect Biochem. Physiol. *32*, 363–374.

Ng, R., Lin, H.H., Wang, J.W., and Su, C.Y. (2017). Electrophysiological Recording from Drosophila Trichoid Sensilla in Response to Odorants of Low Volatility. J. Vis. Exp. e56147.

Poels, J., Van Loy, T., Vandersmissen, H.P., Van Hiel, B., Van Soest, S., Nachman, R.J., and Vanden Broeck, J. (2010). Myoinhibiting peptides are the ancestral ligands of the promiscuous Drosophila sex peptide receptor. Cell. Mol. Life Sci. *67*, 3511–3522.

Reiff, T., Jacobson, J., Cognigni, P., Antonello, Z., Ballesta, E., Tan, K.J., Yew, J.Y., Dominguez, M., and Miguel-Aliaga, I. (2015). Endocrine remodelling of the adult intestine sustains reproduction in Drosophila. Elife *4*, e06930.

Rideout, E.J., Dornan, A.J., Neville, M.C., Eadie, S., and Goodwin, S.F. (2010). Control of sexual differentiation and behavior by the doublesex gene in Drosophila melanogaster. Nat. Neurosci. *13*, 458–466.

Shao, L., Chung, P., Wong, A., Siwanowicz, I., Kent, C.F., Long, X., and Heberlein, U. (2019). A Neural Circuit Encoding the Experience of Copulation in Female Drosophila. Neuron *102*, 1025-1036.e6.

Song, H.J., Billeter, J.C., Reynaud, E., Carlo, T., Spana, E.P., Perrimon, N., Goodwin, S.F., Baker, B.S., and Taylor, B.J. (2002). The fruitless gene is required for the proper formation of axonal tracts in the embryonic central nervous system of Drosophila. Genetics *162*, 1703–1724.

Stockinger, P., Kvitsiani, D., Rotkopf, S., Tirián, L., and Dickson, B.J. (2005). Neural Circuitry that Governs Drosophila Male Courtship Behavior. Cell *121*, 795–807.

Trivers, R.L. (1972). Parental Investment and Sexual Selection (London: Heinemann).

Wang, J.W., Wong, A.M., Flores, J., Vosshall, L.B., and Axel, R. (2003). Two-photon calcium

imaging reveals an odor-evoked map of activity in the fly brain. Cell *112*, 271–282.

Yang, C. hui, Rumpf, S., Xiang, Y., Gordon, M.D., Song, W., Jan, L.Y., and Jan, Y.N. (2009). Control of the Postmating Behavioral Switch in Drosophila Females by Internal Sensory Neurons. Neuron *61*, 519–526.

Yapici, N., Kim, Y.J., Ribeiro, C., and Dickson, B.J. (2008). A receptor that mediates the post-mating switch in Drosophila reproductive behaviour. Nature *451*, 33–37.